LOAN DOCUMENT

PHOTOGRAPH THIS SHEET

DTIC ACCESSION NUMBER

LEVEL

INVENTORY

0

Heat Transfer Evaluation of HFC-236EA and CFC-114 in Condensation & Evaporation

DOCUMENT IDENTIFICATION

Jun 96

DISTRIBUTION STATEMENT A
Approved for public release
Distribution Unlimited

DISTRIBUTION STATEMENT

ACCESSION FOR

NTIS	GRA&I	☑
DTIC	TRAC	☐
UNANNOUNCED		☐
JUSTIFICATION		

BY

DISTRIBUTION/

AVAILABILITY CODES

DISTRIBUTION	AVAILABILITY AND/OR SPECIAL	
A-1		

DISTRIBUTION STAMP

DATE ACCESSIONED

DATE RETURNED

19980710 086

DATE RECEIVED IN DTIC

REGISTERED OR CERTIFIED NUMBER

PHOTOGRAPH THIS SHEET AND RETURN TO DTIC-FDAC

DTIC FORM 70A JUN 90

DOCUMENT PROCESSING SHEET

PREVIOUS EDITIONS MAY BE USED UNTIL STOCK IS EXHAUSTED.

LOAN DOCUMENT

HANDLE WITH CARE

REPORT DOCUMENTATION PAGE

Form Approved
OMB No. 074-0188

1. AGENCY USE ONLY (Leave blank)	2. REPORT DATE June 1996	3. REPORT TYPE AND DATES COVERED Final Report, Oct 1992 - March 1995

4. TITLE AND SUBTITLE

Heat Transfer Evaluation of HFC-236ea and CFC-114 in Condensation and Evaporation

5. FUNDING NUMBERS

CR820755-01-4

6. AUTHOR(S)

W.W. Huesbach, & M.B. Pate

7. PERFORMING ORGANIZATION NAME(S) AND ADDRESS(ES)

Iowa State University
2088 H.M. Black Engineering Building
Ames, Iowa 50011-2160

8. PERFORMING ORGANIZATION REPORT NUMBER

N/A

9. SPONSORING / MONITORING AGENCY NAME(S) AND ADDRESS(ES)

EPA, Office of Research & Development
Air Pollution Prevention & Control Division
Research Triangle Park, NC 27711

SERDP
901 North Stuart St. Suite 303
Arlington, VA 22203

10. SPONSORING / MONITORING AGENCY REPORT NUMBER

EPA/600/R-96-070

11. SUPPLEMENTARY NOTES

APPCD project officer is Theodore G. Brna, Mail Drop 63, 919/541-2683. This work was supported in part by Contract/Grant No. CR820755-01-4.

12a. DISTRIBUTION / AVAILABILITY STATEMENT

Approved for public release: distribution is unlimited

12b. DISTRIBUTION CODE

A

13. ABSTRACT ***(Maximum 200 Words)***

The report gives results of a heat transfer evaluation of the refrigerants hexafluoropropane and 1, 1, 2, 2-dichloro-tetrafluoroethane. This research focuses on comparing refrigerants not only in condensation and pool boiling, but also with various tube surfaces. The test facility used in this study was initially used for spray evaporation testing; however, it was redesigned and modified for use with condensation, pool boiling, or spray evaporation testing. During pool boiling or spray evaporation, the test facility was capable of testing pure refrigerants or refrigerant/lubricant mixtures. The test facility is described in detail in the full report. The tow refrigerants produced similar performance characteristics in condensing vapor on integral-fin tubes so that the transition to HFC-236ea should be accomplished without major modifications to existing condensers.

14. SUBJECT TERMS

SERDP, Pollution, Refrigerant, Halohydrocarbons, condensing, spraying, evaporation

15. NUMBER OF PAGES

140

16. PRICE CODE N/A

17. SECURITY CLASSIFICATION OF REPORT	18. SECURITY CLASSIFICATION OF THIS PAGE	19. SECURITY CLASSIFICATION OF ABSTRACT	20. LIMITATION OF ABSTRACT
unclass.	unclass.	unclass.	UL

United States
Environmental Protection
Agency

EPA-600/R-96-070

June 1996

46 - 1996

EPA

Research and Development

HEAT TRANSFER EVALUATION
OF HFC-236EA AND CFC-114 IN
CONDENSATION AND EVAPORATION

Prepared for

National Risk Management Research Laboratory

Prepared by

National Risk Management
Research Laboratory
Research Triangle Park, NC 27711

FOREWORD

The U.S. Environmental Protection Agency is charged by Congress with protecting the Nation's land, air, and water resources. Under a mandate of national environmental laws, the Agency strives to formulate and implement actions leading to a compatible balance between human activities and the ability of natural systems to support and nurture life. To meet this mandate, EPA's research program is providing data and technical support for solving environmental problems today and building a science knowledge base necessary to manage our ecological resources wisely, understand how pollutants affect our health, and prevent or reduce environmental risks in the future.

The National Risk Management Research Laboratory is the Agency's center for investigation of technological and management approaches for reducing risks from threats to human health and the environment. The focus of the Laboratory's research program is on methods for the prevention and control of pollution to air, land, water, and subsurface resources; protection of water quality in public water systems; remediation of contaminated sites and groundwater; and prevention and control of indoor air pollution. The goal of this research effort is to catalyze development and implementation of innovative, cost-effective environmental technologies; develop scientific and engineering information needed by EPA to support regulatory and policy decisions; and provide technical support and information transfer to ensure effective implementation of environmental regulations and strategies.

This publication has been produced as part of the Laboratory's strategic long-term research plan. It is published and made available by EPA's Office of Research and Development to assist the user community and to link researchers with their clients.

E. Timothy Oppelt, Director
National Risk Management Research Laboratory

EPA REVIEW NOTICE

EPA-600/R-96-070
June 1996

HEAT TRANSFER EVALUATION OF HFC-236EA AND CFC-114 IN CONDENSATION AND EVAPORATION

by

W.W. Huebsch
M.B. Pate
Iowa State University
Ames, IA 50011

EPA Cooperative Agreement No. CR820755-01-4

Project Officer

Theodore G. Brna
U.S. Environmental Protection Agency
National Risk Management Research Laboratory
Air Pollution Prevention and Control Division
Research Triangle Park, NC 27711

Prepared for:

U.S. ENVIRONMENTAL PROTECTION AGENCY
OFFICE OF RESEARCH AND DEVELOPMENT
WASHINGTON, DC 20460

ABSTRACT

With the mandatory phase-out of CFCs (chlorofluorocarbons) as dictated by the Montreal Protocol and the Clean Air Act Amendments, it is imperative for the Navy to find a replacement that is environmentally safe and possesses similar performance characteristics to CFC-114 (1,1,2,2 - dichlorotetrafluoroethane). Currently, one of the leading candidates to replace CFC-114 is HFC (hydrofluorocarbon)-236ea (1,1,1,2,3,3 - hexafluoropropane). This research focuses on comparing the refrigerants not only in condensation and pool boiling, but also with various tube surfaces.

The test facility used in this study was initially used for spray evaporation testing, however it was redesigned and modified for use with either condensation, pool boiling, or spray evaporation testing. During condensation, the rig was capable of producing saturated or superheated vapor. During pool boiling or spray evaporation, the test facility was capable of testing pure refrigerants or refrigerant / lubricant mixtures. The test facility is described in detail in the final report.

The two refrigerants, namely HFC-236ea and CFC-114, produced similar performance characteristics in condensing vapor on integral-fin tubes, so that the transition to HFC-236ea should be accomplished without major modifications to the existing condensers. The results also showed that the condensation of superheated vapor had negligible effects on the shell-side heat transfer coefficient as compared to condensation of saturated vapor results. The superheated vapor data for the 26 fpi (fins per inch) and 40 fpi tubes were within 5% and 3%, respectively, of the saturated vapor results for the same tube surface.

HFC-236ea produced higher boiling coefficients than CFC-114 for all tubes tested. In addition, the 26 fpi tube outperformed the 40 fpi by 18% and the plain tube by 41% for HFC-236ea. The maximum increase in boiling with HFC-236ea was 39% for the 26 fpi tube, and 34% for the 40 fpi tube.

The mineral oil used with CFC-114 showed a general improvement in the heat transfer performance, while the polyol-ester oil consistently degraded the performance of HFC-236ea. Even then the boiling performance of HFC-236ea was either equal to, or greater than, the performance of CFC-114 for all tested parameters.

This report was sumitted in fulfillment of CR820755-01-4 by Iowa State University under the sponsorship of the U.S. Environmental Protection Agency through the EPA/DoD/DOE Strategic Environmental Research and Development Program (SERDP). This report covers a period from October 1992 to March 1995.

CONTENTS

LIST OF FIGURES

LIST OF TABLES

LIST OF ABBREVIATIONS AND SYMBOLS

ABBREVIATIONS

A -- area (m^2)

A_{ef} -- effective finned-tube surface area (m^2)

A_b -- outside area used in Equation 5.14 (m^2)

A_p -- profile area of fin (m^2)

C -- tube geometry function used in Equation 4.12

C_{sf} -- dimensionless proportionality constant used in Equation 5.1

C_p -- specific heat of fluid at constant pressure (J/kg·K)

d_b -- bubble diameter used in Equation 5.7 (m)

D -- tube diameter (m)

D_b -- boiling diameter defined in Equation 5.5 (m)

D_{eq} -- equivalent diameter defined in Equation 4.4

f -- bubble frequency defined in Equation 5.7

F -- forced convection multiplier defined in Equation 5.13

fpi -- fins per inch

fpm -- fins per meter

g -- acceleration due to gravity (m/s^2)

G -- condensate mass flow rate in half of fin channel (Equation 4.7)

h_{fg} -- enthalpy of vaporization (J/kg)

h -- heat transfer coefficient ($W/m^2 \cdot K$)

h_f -- heat transfer coefficient along the fin surface ($W/m^2 \cdot K$)

h_r -- heat transfer coefficient on the unfinned surface ($W/m^2 \cdot K$)

h_b -- heat transfer coefficient in flooded region of a finned tube ($W/m^2 \cdot K$)

h_{nb} -- nucleate boiling coefficient used in Equation 5.13 ($W/m^2 \cdot K$)

h_{fc} -- forced convection coefficient used in Equation 5.13 ($W/m^2 \cdot K$)

k -- thermal conductivity (W/m·K)

k_{wall} -- thermal conductivity of tube wall (W/m·K)

L -- tube length (m)

LMTD -- log-mean-temperature difference (C)

M -- molecular weight

$\dot{m}$ -- mass flow rate (kg/s)

P -- pressure (Pa)

P_c -- critical pressure (Pa)

P_f -- fin pitch (m)

q -- heat transfer rate (W)

q'' -- heat flux (W/m^2)

R -- thermal resistance of tube wall

R_o -- radius to the outside of the fin tips used in Equation 4.8 (m)

R_p -- surface roughness parameter (mm)

R_f -- radius of tube to tip of fin (m)

s -- fin spacing (in. or m)

S -- maximum length of the convex condensate surface along a fin (m)

SF -- suppression factor used in Equation 5.13

STC -- Sieder-Tate coefficient

t -- fin thickness (m)

T -- temperature (C)

ΔT -- excess temperature (C) (= $T_{sat} - T_w$ for condensation and = $T_w - T_{sat}$ for evaporation)

ΔT_w -- temperature difference between the water inlet and water outlet

U -- overall heat transfer coefficient ($W/m^2 \cdot K$)

WP -- wetted perimeter (m)

y -- fin height (m)

SYMBOLS

μ -- dynamic viscosity ($N \cdot s/m^2$)

ρ -- density (kg/m^3)

π -- pi

σ -- surface tension (N/m)

β -- contact angle (degrees)

θ -- fin-tip half angle (degrees)

θ_m -- maximum rotation angle of the normal to the convex condensate surface (degrees)

υ -- kinematic viscosity (m^2/s)

η -- efficiency

α -- thermal diffusivity (m^2/s)

ϕ -- volume fraction of pure refrigerant used in Equation 5.15

ϕ_f -- flooding angle measured from the top of the tube shown in Figure 4.1 (degrees)

ψ -- flooding angle measured from the bottom of the tube (degrees)

ζ -- condensate shape parameter used in Equation 4.11

ω_f -- two-phase friction multiplier

SUBSCRIPTS

b -- bulk; boiling; base

f -- film; fin

g -- saturated gas

i -- tube-side; inside; inlet

l -- saturated liquid

o -- shell-side; outside; outlet

p -- refrigerant pool

r -- root

ref -- refrigerant

s -- surface

sat -- saturation condition

v -- vapor

w -- water

DIMENSIONLESS GROUPS

Nu -- Nusselt number, $\left(\frac{h D}{k}\right)$

Pr -- Prandtl number, $\left(\frac{c_p \mu}{k}\right)$

Re -- Reynolds number, $\left(\frac{4\dot{m}_w}{\pi D \mu}\right)$

ACKNOWLEDGMENTS

This work was sponsored by the Environmental Protection Agency (EPA) in cooperation with the United States Navy as EPA Contract # CR820755-01-4 and Project Category IV. Funding for this work was provided by the Department of Defense's Strategic Environmental Research and Development Program through the EPA, and this support is gratefully acknowledged.

The authors would like to express their appreciation to EPA's project officer, Theodore Brna, for his guidance and support in completing this work. They also thank the Ketema Company and the Wolverine Tube Company for their generous contributions towards the completion of this project.

CHAPTER 1

INTRODUCTION

There is continued interest in every aspect of the refrigerant industry to discontinue the use of chlorofluorocarbons (CFCs) as the refrigerant of choice. The movement is to incorporate refrigerants, which are termed HFC's or hydrofluorocarbons, that do not contribute to ozone depletion and minimize global warming. This project has been initiated by the U.S. Navy and the Environmental Protection Agency (EPA). The United States Navy presently uses CFC-114 (also designated as R-114) as the working refrigerant in shipboard and submarine chiller units. With the mandatory phase-out of CFCs as dictated by the Montreal Protocol and national policy, it is imperative for the Navy to find a replacement that is environmentally safe and possesses similar performance characteristics to CFC-114. The circumstances unique to the Navy are that the replacement be non-toxic due to the confined quarters that are common to a military ship. Also, the replacement refrigerant should perform similar to that of the present refrigerant so that an easy transition can be accomplished.

BACKGROUND

The research needs required in the effort to replace CFC-114 with a similar performing refrigerant include:

- Heat transfer evaluation
- Solubility, miscibility, and viscosity of refrigerant / lubricant mixtures study
- Thermodynamic property study of alternative refrigerant
- Modeling study
- Design analysis

This project focuses on the heat transfer evaluation of the condenser and evaporator performance. In particular, this project conducted a comparative study of single-tube condensation and pool boiling between CFC-114 and an alternative refrigerant (i.e., HFC-236ea, also designated R-236ea) in order to determine its viability as a replacement for the CFC refrigerant.

Currently, one of the leading candidates to replace CFC-114 is HFC-236ea (hexafluoropropane). This alternative refrigerant is the focus of the results presented herein. There are several reasons for choosing this particular refrigerant to replace CFC-114. First, there is currently a commercial production route available for

acquiring the refrigerant. Of special importance, the operating capacities, pressures, and temperatures are very similar to that of CFC-114 [1].

For a refrigerant to be considered for use on a ship or submarine, certain requirements must be met in addition to the performance requirements. The EPA, in cooperation with the U.S. Navy, has shown that HFC-236ea would have favorable characteristics with respect to naval applications [1]. Some of the characteristics that may potentially meet the naval requirements are that HFC-236ea is not flammable, material compatibility testing shows it is compatible with currently available materials, HFC-236ea has a lower acute toxicity than CFC-114, and HFC-236ea is miscible with a synthetic ester refrigerant oil.

The published data using CFC-114 in either condensation or evaporation is limited because the Navy is the primary user of this refrigerant. Industry, in general, has not opted to use it in large refrigeration systems. The Navy's decision to use CFC-114 was based on advantages specific to their needs. Several of these advantages are of great importance when considering potential refrigerant leaks. The refrigerant that escapes from submarine cooling systems is circulated through a high temperature air purification system. Therefore, the absence of toxic breakdown products is a primary concern to the Navy. The main advantages of CFC-114 are that it is: (1) a moderate-pressure refrigerant, (2) more stable with temperature than other refrigerants, (3) more stable when exposed to water vapor than other refrigerants, and (4) low in toxicity. These same advantages are also inherent in the use of HFC-236ea

This research focuses on comparing the refrigerants not only in condensation and pool boiling, but also with various tube surfaces. Horizontal, integral finned tubes have been in service for over 40 years. These tubes are widely used in condensation applications because of their higher performance compared to plain tubes. In addition, condensation testing of integral-fin tubes in a single-tube test facility accurately models the performance of a tube bundle. Webb and Murawski [2] have shown that integral-fin tubes have negligible inundation effects during condensation within a tube bundle and, therefore, have similar performance characteristics to those found for a single-tube test.

Flooded evaporators use smooth or finned tubes in a majority of the current refrigeration systems. However, there also have been recent advances in the tube surfaces for flooded nucleate boiling. The data from an enhanced surface test could prove invaluable to naval applications where the size and weight of the evaporators could be significantly reduced by their application.

OBJECTIVES

The research described within this report was sponsored by the U.S. Environmental Protection Agency with cooperation of the U.S. Navy. The overall objective of the project was to evaluate all aspects of the alternative refrigerant HFC-236ea as a near term substitute for CFC-114 with respect to naval applications. The objective

specific to this report was to conduct an experimental heat transfer evaluation comparing the performance of CFC-114 and HFC-236ea in the condensation and evaporation environments.

RESEARCH PROGRAM

The main goal of the research effort described here was to evaluate heat transfer with HFC-236ea and determine whether it is a viable replacement for CFC-114. Baseline data were also obtained for CFC-114 to provide an accurate measure of comparison for the two refrigerants.

Scope

The scope of this project was as follows:

- Modify an existing spray evaporation test facility so it could perform condensation and pool boiling tests using a two-pass single-tube setup.
- Test CFC-114 as the reference fluid and compare the performance with the alternative refrigerant HFC-236ea.
- Evaluate the plain, 26 fpi (fins per inch), and 40 fpi tubes for condensation.
- Evaluate the plain, 26 fpi, and 40 fpi tubes for flooded evaporation.
- Investigate oil effects in pool boiling on the shell-side heat transfer performance by varying the oil concentration from 0% - 3%.
- Compare results with published correlations for condensation and pool boiling.

Refrigerants of Interest

HFC-236ea is considered as a possible environmentally favored alternative refrigerant for CFC-114. The thermodynamic and transport properties of HFC-236ea are very similar to those of CFC-114, which would aid in the transition for systems presently using CFC-114. Appendix D contains property information for both refrigerants. Condensation and pool boiling tests were conducted on CFC-114 to provide a baseline for an accurate comparison to HFC-236ea.

Lubricants of Interest

Miscibility and solubility testing for CFC-114 and HFC-236ea were performed prior to this research in another portion of the project. As expected, the data from that research verified that the miscibility and solubility

of mineral oil was acceptable for use with CFC-114. The mineral oil used was York "C" with a viscosity of 315 SUS (68 centistokes at 40°C).

This data also showed that a synthetic ester refrigerant oil performed satisfactorily with HFC-236ea, while mineral oil did not. This acceptable lubricant is a polyol-ester oil with a viscosity of 340 SUS at 37.8°C. The trade name is Castrol Icematic SW-68. The two lubricants, York "C" and Castrol SW-68, were miscible with the corresponding refrigerants, CFC-114 and HFC-236ea, respectively, over the entire range of conditions tested in this research.

CHAPTER 2

CONCLUSIONS

The main objective of this study was to conduct an experimental heat transfer evaluation comparing the performance of CFC-114 and HFC-236ea in the condensation and pool boiling environments. The condensation testing included an investigation of saturated and superheated vapor on finned-tube surfaces. The pool boiling research involved nucleate boiling of pure refrigerant and refrigerant / lubricant mixtures on finned-tube surfaces.

All of the tubes used in this study had a nominal outside diameter of 19.1 mm (0.75 in.) and a length of 838.2 mm (33 in). The shell-side heat transfer coefficients that were presented in this study were based on the outside surface area of a corresponding smooth tube, with the outer diameter measured over the surface enhancement. Therefore, the calculated heat transfer coefficient takes into account the area enhancement, fin efficiency, and surface enhancement of the tubes tested.

Condensation Heat Transfer

The refrigerants CFC-114 and HFC-236ea were evaluated in the condensation environment on a plain, 26 fpi, and 40 fpi tube surface. In addition, the effects on the heat transfer performance from condensing superheated vapor were investigated with CFC-114. During saturated vapor testing, the saturation temperature was held constant at 40°C. For condensation of superheated vapor, the saturation temperature was also 40°C, but the incoming vapor was 3°C to 5°C higher than T_{sat}.

For condensation of both refrigerants, the integral-fin tubes yielded heat transfer coefficients approximately four times those produced with the plain tube. In addition, all combinations of the finned tubes and refrigerants produced similar shell-side condensation coefficients in the heat flux range tested, with a maximum deviation of 9%.

The results also showed that the condensation of superheated vapor had negligible effects on the shell-side heat transfer coefficient with respect to the saturated vapor results. The superheated vapor data for the 26 fpi and 40 fpi tubes were within 5% and 3%, respectively, of the saturated vapor results for the same tube surface.

The correlation comparison made with the plain tube results showed excellent agreement with the Nusselt correlation. The CFC-114 and HFC-236ea data were predicted within ±3% and ±10%, respectively. The Beatty and Katz correlation was able to predict the 26 fpi tube data for both refrigerants with a maximum deviation of

15%. The predictions for the 40 fpi tube resulted in larger deviations. The Beatty and Katz correlation predicted the 40 fpi tube data within 18% and 21% for CFC-114 and HFC-236ea, respectively.

Overall, the above information shows that HFC-236ea is a valid replacement for CFC-114 in the condensation environment. Since the two refrigerants produced similar performance characteristics in condensing vapor on integral-fin tubes, the transition to HFC-236ea from CFC-114 should be accomplished without major modifications to the existing condensers.

Pool Boiling Heat Transfer

The refrigerants CFC-114 and HFC-236ea were evaluated in the pool boiling environment on a plain, 26 fpi, and 40 fpi tube surface. In addition, this study investigated the effects of small concentrations of oil on the heat transfer performance. The concentrations tested were 1% and 3% by mass using a 315-SUS mineral oil for CFC-114 and a 340-SUS polyol-ester oil for HFC-236ea. During pool boiling, data were taken at a constant saturation temperature of 2°C for both pure refrigerant and refrigerant / lubricant mixtures.

The pool boiling results for the pure refrigerants show that the tube performance for CFC-114 and HFC-236ea fall in the following order from high to low: 26 fpi, 40 fpi, and plain tube. The 26 fpi tube produced boiling coefficients for CFC-114 that were 12% and 30% higher than the 40 fpi tube and the plain tube, respectively. For HFC-236ea, the 26 fpi tube outperformed the 40 fpi tube by 18% and the plain tube by 41%. In addition, HFC-236ea produced higher boiling coefficients than CFC-114 for all tubes tested. The maximum coefficient increase in boiling with HFC-236ea was 39% for the 26 fpi tube, and 34% for the 40 fpi tube.

The lubricant addition with CFC-114 produced enhancements in the boiling heat transfer coefficients for the three tubes tested with oil. The maximum enhancement occurred at a 3% oil concentration for each tube. The addition of oil at a 1% concentration improved the heat transfer coefficients for the 26 fpi tube by 27%, while the 3% oil concentration showed only a minor improvement over the 1% results. The 40 fpi tube produced similar trends to the 26 fpi tube at both oil concentrations.

Pool boiling of HFC-236ea with the polyol-ester oil produced consistent decreases in the heat transfer performance at both concentrations. The 26 fpi tube showed a decrease in performance of 6% and 17% at oil concentrations of 1% and 3%, respectively. The 40 fpi tube had only a 10% decrease in the boiling coefficients at a 3% concentration with respect to the pure refrigerant. At an oil concentration of 1%, the 40 fpi tube showed negligible oil effects on heat transfer in the low heat flux range. It is evident that the oil enhancement gained from the turbulent mixing within the foaming layer is dependent upon the type of oil. The mineral oil used with CFC-114 showed a general improvement in the heat transfer performance, while the polyol-ester oil consistently degraded the performance of HFC-236ea.

It is also worth noting that even though the pure HFC-236ea results are higher than those for pure CFC-114, the oil effects on CFC-114 cause the boiling coefficients to be higher than the HFC-236ea results for the 26 fpi

tube. In addition, the boiling coefficients for both refrigerants are within 12% for the this tube at an oil concentration of 3%. Therefore, the addition of oil decreased the deviation in the heat transfer coefficients between the two refrigerants.

A review of the above information shows that HFC-236ea is a valid replacement for CFC-114 in the nucleate boiling environment. The boiling performance of HFC-236ea was either equal to or greater than the performance of CFC-114 for all tested parameters. With the similar boiling characteristics, transition to HFC-236ea in a flooded evaporator would be relatively simple.

CHAPTER 3

RECOMMENDATIONS

This section offers a listing of recommendations for future research needed in the area of heat transfer evaluation of alternative refrigerants in all modes of heat transfer (e.g., pool boiling, condensation, etc.).

1. Perform condensation and pool boiling testing with HFC-236ea at multiple saturation temperatures for accurate development of heat transfer correlations. A variable temperature component in a correlation would offer a much wider range in which the correlation is valid. Correlations could be developed for each specific tube, or a general correlation with a surface enhancement factor.
2. Evaluate the heat transfer performance of enhanced pool boiling surfaces with HFC-236ea.
3. Evaluate the heat transfer performance of enhanced condensation surfaces with HFC-236ea. Also investigate the effects of vapor shear and noncondensible gases in the condensation environment.
4. Use refrigerant as the working fluid on the water-side to investigate the heat flux range of 5 kW/m^2 to 15 kW/m^2. There has been recent interest by the refrigeration industry in studying the heat transfer performance in this low heat flux range.
5. Perform spray evaporation testing with HFC-236ea on condensation and boiling surfaces and compare the heat transfer coefficients with the pool boiling coefficients. Spray evaporation has the ability of reducing the required refrigerant charge, which corresponds to a weight and size reduction. This would be particularly important to naval applications where the size and weight are such critical parameters.

CHAPTER 4

LITERATURE REVIEW OF CONDENSATION

OVERVIEW

Condensation occurs when a vapor is cooled when it comes in contact with a surface that has a lower wall temperature than the saturation temperature of the vapor. The impinging vapor is transformed to its liquid phase by losing its latent heat to the cooler surface. Filmwise condensation is the most common mode of condensing a vapor. The vapor condenses on the tube surface forming a continuous film and leaves the tube by gravity.

The film that is formed in filmwise condensation has a certain thickness depending on the rate of vapor condensation and the rate of condensate removal from the surface of the tube. As the film thickness increases, so does the thermal resistance, which decreases the heat transfer performance of the tube. Therefore, any means by which the film thickness can be reduced will enhance the heat transfer.

There are four major factors that affect the heat transfer performance in condensation on a single horizontal tube.

- Tube geometry
- Vapor shear
- Superheated vapor
- Noncondensible gas

These factors can either enhance or degrade the heat transfer performance of a given fluid.

The tube geometry factor includes the size and type of tube surface. When a horizontal smooth tube surface is being used to condense vapor, the top of the tube has a very thin film of condensate. The film thickness steadily increases as it moves downward around the tube periphery, thus steadily decreasing the heat transfer performance at specific radial tube locations. Therefore, an enhancement to the tube surface that would reduce the film thickness around the periphery of the tube would increase the heat transfer performance. One method of achieving this is to incorporate finned surfaces or enhanced condensation surfaces. Typically, these enhanced surfaces are only used to condense refrigerants, which have a relatively low surface tension. High surface-tension fluids, such as water and ammonia, use plain tube surfaces for condensation.

The vapor shear effect in condensation occurs when the vapor impinges on the tube with a significant velocity. The vapor velocity exerts a shear stress on the film, and when this velocity is relatively high, there is a

significant amount of drag at the liquid-vapor interface. If the vapor flow is in the upward direction, it adds to the shearing force from the viscosity and increases the film thickness. If the vapor flow is in the downward direction, it couples with gravity to decrease the film thickness. When the velocity is negligible, the condensate flows primarily by gravity, with the viscosity of the fluid resisting the gravity force.

Superheated vapor is formed when energy is added to a saturated vapor without a change in the pressure. Therefore, the temperature of the inlet vapor will be above the saturation temperature of the pressure existing in the condenser. If the vapor is superheated, the sensible heat content of the vapor must be removed and transferred to the cooling water before the vapor can be condensed on the tube surface. If the tube wall is above the saturation temperature of the vapor, the heat is removed by single-phase convective heat transfer and condensation does not occur. However, if the outside tube wall is below the saturation temperature of the vapor at the existing pressure, vapor will condense upon contact with the surface.

The same saturation temperature exists during condensation of either saturated vapor or superheated vapor. However, during condensation of saturated vapor, the incoming vapor has the same temperature as T_{sat}, whereas the superheated vapor has a higher temperature. It has been shown that in condensation of superheated vapor, calculating the average heat transfer coefficient using the temperature difference between the saturation temperature and the surface temperature results in little error [3]. In addition, a study by Goto et al. [4] for condensation of CFC-113 superheated vapor showed that heat transfer coefficients for superheated vapor were only slightly higher (5%) than those for saturated vapor.

The final factor that can affect the condensation heat transfer coefficients on single horizontal tube tests is the presence of noncondensible gases, most notably air. Noncondensible gases cause an increase in the thermal resistance at the condensing surface and reduce the overall heat transfer coefficient. The most common causes of noncondensible gases being introduced into the system are leaks resulting from operating the evaporator with a refrigerant that has a pressure below atmospheric and performing insufficient evacuation prior to charging the system. Care must be taken to avoid having noncondensible gases present in the test facility.

The above factors that affect the heat transfer performance during condensation does not include lubricant contamination or the effects of multiple tubes as in a bundle. When bundle work is performed, additional factors such as inundation effects and bundle geometry effects can alter the performance. Inundation is the term used for the condensate that drips from tube-to-tube within the bundle.

These are factors that can influence the heat transfer performance in condensation for a specific refrigerant (or working fluid). In addition to these factors, each refrigerant possesses unique characteristics in condensation. In particular, the thermodynamic and transport properties of refrigerants have different effects on condensation heat transfer performance. For example, the viscosity and surface tension are major contributors to the heat transfer characteristics. The surface tension is especially important when condensing vapor on a finned surface where it acts to retain liquid condensate between the fins, which thickens the film and increases the resistance to heat transfer.

HEAT TRANSFER

This section describes past work in the area of condensation heat transfer. It covers published results, observations, and correlations from research completed that is pertinent to this report. The experimental results are first reviewed, followed by published theoretical results from research in condensation.

Experimental Results

In 1948, Beatty and Katz [5] performed experiments to measure the condensation heat transfer coefficients for various fluids using a 16-fins per inch (fpi) tube. The fluids included methyl chloride, sulfur dioxide, HCFC-22, propane, and n-pentane, all of which are low surface tension fluids. For HCFC-22, additional tubes were also tested. Their results showed that the overall heat transfer coefficient increased by a factor of up to 2.3 for the finned tubes over that of the smooth tube.

Karkhu and Borovkov [6] conducted experiments on condensing CFC-113 and steam on four different tubes with trapezoidal fins. The measured heat transfer coefficients were between 50 and 100 % higher than for a smooth tube. In 1980, Carnavos [7] measured condensation heat transfer coefficients for CFC-11 on a wide variety of augmented tubes as well as a smooth tube. The augmented tubes included flat-sided finned surfaces, fluted surfaces, and knurled surfaces. The reported heat transfer enhancements (i.e.,, enhancement factors) were 3 to 4 times that of a smooth tube.

Rudy [8] performed condensation testing with CFC-11 on four copper integral-fin tubes. Three of the tubes were commercially available with 748, 1024, and 1378 fpm (19, 26, and 35 fpi). The fourth tube was a 748 fpm tube that was altered to reduce the fin height from 1.53 to 0.85 mm. The results showed that the 1378 fpm tube had higher heat transfer coefficients than the 1024 fpm and 748 fpm tubes by 49% and 71%, respectively. In 1983, Honda et al. [9] tested four low-fin tubes with different fin geometries using methanol and CFC-113. Based on a constant vapor-to-wall temperature, the best performing tube produced enhancement factors of 8.8 for CFC-113 and 4.9 for methanol over that of the smooth tube.

The effects of fin density and fin height have also been studied. In 1984, Yau et al. [10] tested 13 tubes with rectangular fins with the only variable being fin spacing. Comparing the finned-tube results with the smooth tube, an enhancement factor of four was obtained for steam condensing at atmospheric pressure. Kabov [11] tested several groups of tubes having different fin densities and fin heights with CFC-12 and R-21. It was determined that fin spacing is one of the principal parameters controlling heat transfer. Sukhatme et al. [12] varied fin density, fin height, and fin-tip half angle of integral-fin tubes during condensation of CFC-11. The fin density that produced the highest heat transfer coefficients was 1417 fpm with an enhancement ratio of about 10 over that found on the smooth tube.

In 1988, Marto et al. [13] conducted condensation testing on a variety of finned tubes using CFC-113 as the working fluid. The thickness and height of the fins was kept constant at 1.0 mm, while the fin spacing was varied: 0.25, 0.5, 1.0, 1.5, 2.0, and 4.0 mm. The results showed that 0.5 mm was the optimum fin spacing for condensing CFC-113. Masuda and Rose [14] also condensed CFC-113 on multiple finned tubes. The fin spacings used were between 0.25 mm and 20 mm. These tests gave a maximum enhancement of 7.3 at a fin spacing of 0.5 mm. Yau et al. [15] condensed steam on similar finned surfaces and found the optimum fin spacing to be 1.5 mm with a maximum enhancement of 2.4.

Masuda and Rose [14] performed tests on ethylene glycol in addition to CFC-113. These results showed that the maximum enhancement was 4.7 at a spacing of 1.0 mm. The three fluids (CFC-113, ethylene glycol, and steam) used above were chosen because they offered a wide range in the surface tension-to-density ratio, σ/ρ. The results indicate that the maximum heat transfer enhancement increases and the optimum fin spacing decreases as the ratio σ/ρ decreases.

Recently, Huber et al. [16,17,18] conducted condensation testing of HFC-134a, CFC-12, HCFC-123, and CFC-11 on multiple tube surfaces, including 26 fpi and 40 fpi tubes. The data were taken on tube bundles (25 total tubes), with the refrigerant saturation temperature and the heat flux range being 35°C and 18 to 40 kW/m^2, respectively. The 40 fpi tube outperformed the 26 fpi tube for all four refrigerants. The results from Huber et al. also showed that the condensation coefficient increased as the heat flux was increased for all four tube bundles tested with CFC-11. The other three refrigerants performed as expected by producing a decrease in the heat transfer coefficient as the heat flux was increased.

A Turbo-Cii tube bundle was also evaluated by Huber et al. [16, 17, 18], and it outperformed all other bundles for the four refrigerants tested. The greatest difference between the Turbo-Cii bundle and the other bundles was found in the heat flux mid-range (18 to 40 kW/m^2). The Turbo-Cii surface showed the smallest enhancement in condensing CFC-11 as compared with the Turbo-Cii performance with the other three refrigerants tested.

Condensation testing by Webb and Murawski [2] showed that the Turbo-C tube had the highest single-tube performance, but it produced poor row effects in the bundle, which substantially decreased its performance. The row effect in a tube bundle is defined as the specific performance of a given row with respect to the top row. Inundation effects cause the lower rows to experience a thicker film of condensate than the top row, which decreases the heat transfer performance within these rows. Therefore, a tube surface that produces only minor inundation, will have a improved heat transfer performance in the lower rows of the bundle, and thus a greater overall performance. The study conducted by Webb and Murawski showed that the integral-fin tube bundles have negligible inundation effects. The GEWA-SC tube, which was also tested, produced single-tube heat transfer coefficients that were 80% less than that for the Turbo-C, but provided greater row effect.

Theoretical Results

Even though the plain tube is rarely used for industrial applications, it is useful to include this surface as a base reference. Nusselt developed an equation to calculate the shell-side heat transfer coefficient for laminar film condensation on a plain tube [19]. The average heat transfer coefficient is found from

$$h = C\left[\frac{g\,\rho_l(\rho_l - \rho_v)\,k_l^3\,h'_{fg}}{\mu_l(T_{sat} - T_s)\,D}\right]^{1/4}, \tag{4.1}$$

where

$$h'_{fg} = h_{fg} + 0.68\,c_{p,l}(T_{sat} - T_s) \tag{4.2}$$

and C = 0.729 for a smooth single horizontal tube. The assumptions made in this equation are:

- The liquid film is only acted upon by gravity.
- The condensate film is laminar.
- The condensing surface is a single smooth horizontal tube.
- Saturated vapor is being condensed.
- The temperature drop across the film is constant around the tube.

Several of these assumptions are very limiting in modeling realistic condensation, but the equation offers an adequate first approximation of the condensation heat transfer coefficients. Webb [20] gives corrections to this equation for vapor superheat and vapor shear effects.

The integral-fin tube was not developed specifically for use in condensation; however it was found to significantly outperform the surface being used in condensation at that time, which was the plain tube. The primary advantage of the finned tube over the plain tube is the increased surface area on the outside surface. Presently, integral-fin tubes are used for condensation of refrigerants, which possess low surface tension characteristics. They are not beneficial in use with higher surface tension fluids, such as ammonia and water, because capillary forces act to flood the spaces between the fins with condensate. Condensate retention is discussed in the following section.

Beatty and Katz [5] developed the first model for condensation on integral-fin tubes. The assumption in their model is that gravity is the driving force behind the condensate drainage on the fin surface as well as the fin-root tube surface. The Nusselt theories for a vertical plate and a horizontal tube were used to model the fin-flank and tube-surface contributions, respectively. The resulting equation for the average condensation coefficient is

$$h = 0.689\left[\frac{k^3\,\rho_l^2\,g\,h_{fg}}{\mu\,\Delta T\,D_{eq}}\right]^{1/4} \tag{4.3}$$

where

$$\left(\frac{1}{D_{eq}}\right)^{1/4} = 1.30\,\eta_f \frac{A_f}{A_{ef}} \frac{1}{L^{1/4}} + \frac{A_o}{A_{ef}} \frac{1}{D_o^{1/4}}, \tag{4.4}$$

$$L = \frac{\pi\,(D_f^2 - D_o^2)}{4D_f}, \text{ and} \tag{4.5}$$

$$A_{ef} = A_o + \eta_f A_f \tag{4.6}$$

The equivalent diameter, D_{eq}, accounts for the fin efficiency, η_f, and A_{ef} is an effective total surface area.

This model does not take into consideration any surface tension effects and assumes that no condensate is retained within the fins. Beatty and Katz [5] based this model on experimental measurements of condensation heat transfer for various fluids and tubes, all of which were low surface tension fluids and low fin-density tubes. Therefore, the model should only be implemented under these circumstances.

The effect of surface tension on condensation heat transfer contains two parts. The first effect is the retention of condensate between fins, which leads to a decrease in heat transfer. Secondly, surface tension helps to thin the condensate film on the fin flanks in the unflooded region of the tube, which leads to increased heat transfer. Marto [21] makes the observation that with surface tension effects ignored in the above model, the trends tend to cancel one another out, thus extending the range in which the equation is applicable. However, the model overpredicts the heat transfer coefficient as surface tension and fin density are increased.

In 1954, Gregorig [22] investigated film condensation on vertical fluted surfaces and noted that surface tension effects can produce large pressure gradients, many times larger than those produced by gravity. Physically, these pressure gradients accelerate the condensate flow, thus thinning the condensate film and increasing the heat transfer performance.

Karkhu and Borovkov [23] were the first to analyze the importance of surface tension effects on horizontal finned tubes. The study involved condensing steam on tubes with fins of trapezoidal cross section. The analysis assumed two different regions:

- the fin flanks where the vapor condensed and the resulting condensate flowed toward the fin root under the influence of surface tension only
- the channel between the fins where the condensate from the fin flanks flowed around the tube under the influence of gravity only

The heat transfer within the channel was neglected because it was assumed that the film thickness was large. It was also assumed that the fin temperature is constant over the entire length. The resultant equation for the average heat transfer coefficient is as follows:

$$h = \frac{G\, h_{fg}}{A_s(T_s - T_o)} \tag{4.7}$$

where:

$$A_s = \left(\frac{t}{2} + \frac{t_h}{2} + \frac{2y}{\cos\theta}\right)\pi R_o \tag{4.8}$$

The variable G represents the condensate mass flow rate in half of the channel as a function of angular position around the tube. The model was compared to their experimental data with the agreement being within ± 5%.

Rudy and Webb [24] were also interested in accounting for surface tension effects in condensation. They proposed making a modification to the Beatty and Katz [5] model which would account for condensate flooding by neglecting the heat transfer in the flooded portion of the tube. This was accomplished by multiplying the heat transfer coefficient found from Equation 4.3 by the ratio of the unflooded area of the tube to the total area, which produced

$$h = 0.689\left(\frac{k^3 \rho^2 g\, h_{fg}}{\mu\, \Delta T\, D_{eq}}\right)^{1/4}\left(\frac{\phi_f}{\pi}\right). \tag{4.9}$$

Comparing this model to their CFC-11 data on a 1378 fpm tube, it was found that the model underpredicted the heat transfer coefficients by 35%.

Work continued by various researchers in an attempt to include the influences of heat transfer through the flooded region, surface tension drainage on the fin flanks, and gravity drainage between the fins. In 1985, Webb et al. [25] developed a model accounting for these phenomena through the following equation:

$$h = \frac{\phi_f}{\pi}\left(\eta_f h_f \frac{A_f}{A_{ef}} + h_r \frac{A_r}{A_{ef}}\right) + \left(1 - \frac{\phi_f}{\pi}\right) h_b \tag{4.10}$$

where:

$$h_f = 2.149\,\frac{k}{S}\left[\frac{\rho\,\sigma\, h_{fg}\,\theta_m\, S}{\mu\, k\, \Delta T}\,\frac{(\zeta + 1)}{(\zeta + 2)^3}\right]^{1/4}. \tag{4.11}$$

The equation for the flooding angle ϕ_f can be seen in Equation 4.15. The variable h_r represents a modified Nusselt expression (Equation. 4.1) to account for the heat transfer on the tube surface between the fins. This expression includes the effect of additional condensate from the fin flanks. The variable h_b characterizes the heat transfer coefficient in the flooded part of the tube. Using this model, their predicted heat transfer coefficients were within ±20% of the experimental values for CFC-11.

Honda and Nozu [26] developed a comprehensive numerical model to predict the heat transfer performance of finned tubes. The tube was divided into an unflooded and flooded region. It was assumed that surface tension and gravity were the forces behind the condensate flow on the fins, whereas gravity was the only force acting on the condensate flow on the tube surface between the fins. The fin surface was also divided into two regions: a thin film region on the upper part of the fin and a thick film region on the lower part of the fin. The heat transfer in the thick film region was neglected, and the heat transfer in the thin film region was solved numerically by a fourth-order differential equation. The final model included separate terms for the wall temperatures in the flooded regions and unflooded regions, which must be considered because of the large difference in heat transfer rates between the two regions. This model predicted heat transfer coefficients that were compared to experimental results for 11 fluids and 22 tubes with the agreement being within ± 20%.

Adamek and Webb [27] recently improved some previous work to predict condensation coefficients on horizontal integral-fin tubes. Additional factors incorporated into their model were condensation at the bottom of the unflooded part of the channel, condensation on a small length of the fin flank in the flooded part of the tube, and condensation on the fin tip. The predicted results from this model were compared to various sources of experimental steam data. The results fell within ±15% of the experimental data over the full range of fin spacings.

CONDENSATE RETENTION

When a horizontal finned tube is being used in condensation, the surface tension forces inherent with the working fluid will cause the liquid to be retained between the fins on the bottom portion of the tube. This is referred to as condensate retention or flooding. The result is a film build-up that increases the resistance to heat transfer and reduces the effective surface area for condensation.

During condensation, a finned tube surface has two distinct regions: a flooded region and an unflooded region. The flooded portion of the tube is defined by an angle from the bottom of the tube up to the highest position on the tube where the interfin space is filled with condensate. This angle is termed the retention angle and is designated by ψ. If the angle is measured from the top of the tube down to the point of flooding, then it is designated by ϕ_f. Decreasing the retention angle increases the heat transfer performance. Figure 4.1 presents a schematic of the condensate retention.

Experimental Results

The condensate retention angle (ϕ_f or ψ) was first measured by Katz et al. [28] for water, aniline, acetone, and carbon tetrachloride under static conditions on various integral-fin tubes with fin densities ranging from 276 to 984 fpm and fin heights of 1.2 to 5.7 mm. Static conditions refer to the absence of condensation, while dynamic conditions refer to the active condensation of vapor. This study showed that condensate retention is

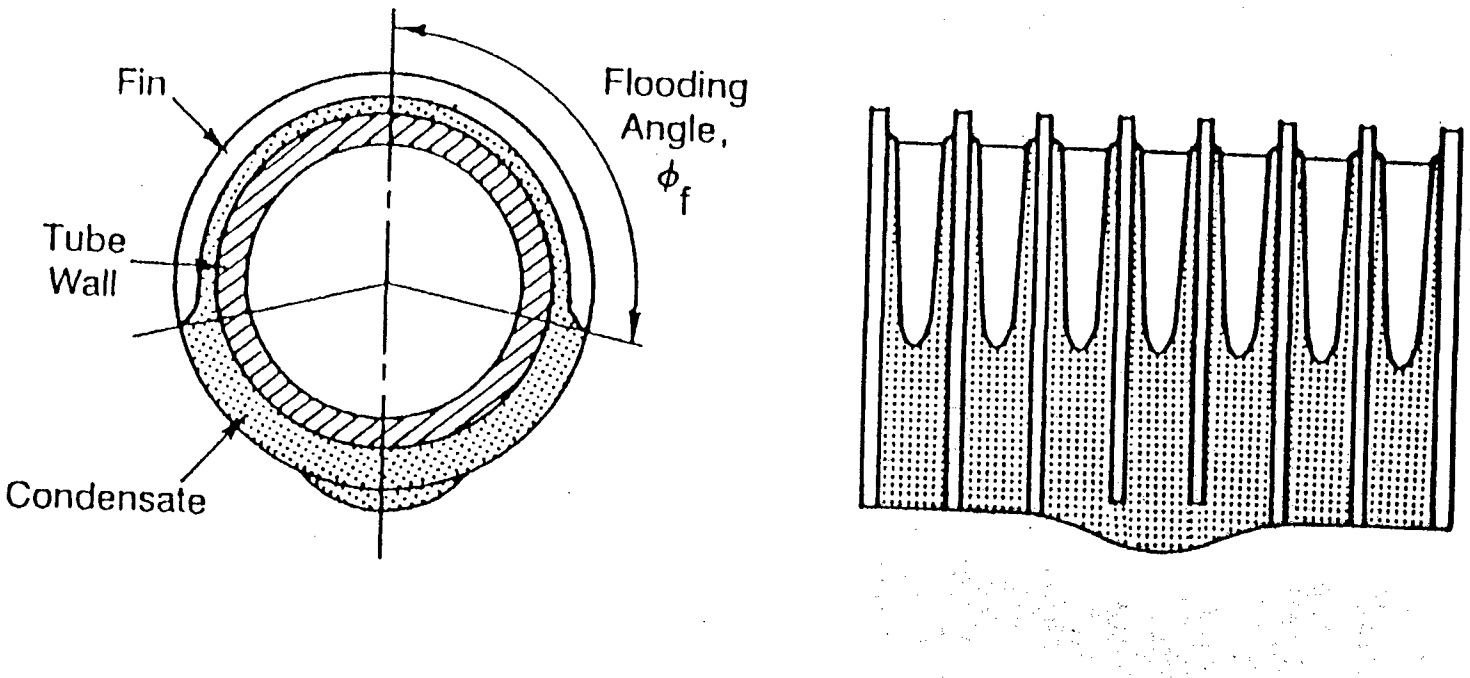

Figure 4.1 Schematic of condensate retention

very dependent upon the ratio of surface tension to liquid density and on the fin spacing. It also showed that retained condensate could completely flood the tube surface in some circumstances.

More recently, the condensate retention angle has been investigated in both static and dynamic modes. In 1981, Rudy and Webb [24] made condensate retention measurements on finned tubes with three different fin densities: 748, 1024, and 1378 fpm. The test fluids were water, CFC-11, and n-pentane under static and dynamic conditions. They found that the retention angle increases with an increase in the ratio of surface tension to density (σ_f / ρ_f). It was also found that there is little difference between the static and dynamic conditions. Honda et al. [9] reported measurements on finned tubes with ethanol and CFC-113 under static and dynamic conditions. Their results verified many of the conclusions found by Rudy and Webb [24].

In 1987, Masuda and Rose [29] observed the effects of tube flooding using static liquid retention on finned tubes. Their results showed that the liquid condensate is not only retained on the bottom portion of the tube, but also on the upper portion in the form of a small liquid "wedge" between the fin flanks and the tube surface between the fins.

There also has been numerous investigations into the idea of thinning the film thickness by incorporating longitudinal condensate drainage strips placed at the bottom of the tube. Marto et al. [30] produced results which showed that the strips significantly reduce the amount of flooding on the finned tube.

Theoretical Results

The condensate retention angle was first modeled by Katz et al. [28] with the following equation:

$$\frac{\psi}{\sin\psi} = C \frac{\sigma_f}{\rho_f}\left[\frac{(4D_f - 2D_o + 2s)}{(\pi/4)\,(D_f^2 - D_o^2)\,t}\,\frac{180}{980}\right], \tag{4.12}$$

where C is only a function of the tube geometry. The major contribution in the calculation of the retention angle comes from the tube geometry function, C, and the ratio of surface tension to density term, σ_f/ρ_f.

In 1983, Rudy and Webb [31] developed a theoretical model for calculation of the condensate retention angle on finned tubes that have rectangular fins. The model was based on capillary equations for condensate rise of a liquid in a vertical U-shaped channel. The equation that resulted was

$$\psi = \cos^{-1}\left(1 - \frac{2\sigma_f(2y - t)}{\rho_f g\, y\, s\, R_f}\right). \tag{4.13}$$

The model assumes that the flooded portion of the tube does not contribute to the heat transfer. In addition, the model does not account for vapor shear effects. The model was able to predict most of their test data to within ±

10%. Equation 4.13 shows that the retention angle is a function of the surface tension-to-density ratio and the fin density. For example, the heat transfer coefficient will decrease as either the fin density or the surface tension-to-density ratio increase. This can be observed by noting that ψ refers to the angle measured from the bottom of the tube. An increase in this angle results in a greater portion of the tube being flooded.

In the same year, Honda et al. [9] conducted an analysis to model the condensate retention angle. Their approach was based on the analysis of the static meniscus between low trapezoidal-shape fins. One of the assumptions made for this model was that the meniscus went from fin tip to fin tip and had a zero contact angle at both tips. The expression that resulted from their analysis was

$$\psi = \cos^{-1}\left(1 - \frac{2\sigma_f \cos\theta}{\rho_f g s R_o}\right). \tag{4.14}$$

Measuring the condensate retention angle from the top of the tube, the expression is given by:

$$\phi_f = \cos^{-1}\left(\frac{2\sigma_f \cos\theta}{\rho_f g s R_o} - 1\right). \tag{4.15}$$

This model showed good agreement with their own experimental data and the data of Rudy and Webb [24]. Both equations show that an increase in the fin density and/or an increase in the surface tension-to-density ratio will produce more flooding, and thus a decrease in heat transfer.

Rudy and Webb [32] modified their previous model, given by Equation 4.13, in 1985. They expanded the range of the equation by allowing for an arbitrary shape in the fin geometry. This modified model was also based on capillary rise in a vertical U-shaped channel. They suggest using the following equation to predict the condensate retention angle:

$$\psi = \cos^{-1}\left(1 - \frac{2\sigma_f (WP - t_h)}{D_o \rho_f g (P_f y - A_p)}\right). \tag{4.16}$$

It can be shown that this equation will reduce to Equation 4.14 for a finned tube with rectangular fins.

SUMMARY

The literature review presented in this chapter shows that the integral-fin tubes produce higher condensation coefficients than the plain tube surface. The importance of the surface tension of the fluid was also highlighted. The results indicated that the maximum heat transfer enhancement increases and the optimum fin

spacing decreases as the surface tension-to-density ratio (σ/ρ) decreases. Correlations were also presented to predict the shell-side heat transfer coefficient for both the smooth tube and integral-fin tube.

The studies that focused on condensate retention were reviewed as well. It was shown that the integral-fin tube is prone to condensate flooding or retention. As the fin density is increased to create more total surface area, more liquid condensate is retained between the fins which results in more of the condensing surface becoming ineffective. Correlations were presented that predict the condensate retention angle as a function of fin density, fin height, and fluid properties.

CHAPTER 5

LITERATURE REVIEW OF POOL BOILING

OVERVIEW

Pool boiling is an important mode of heat transfer to the refrigeration industry. This literature review will concentrate on the flooded evaporator and the nucleate boiling process. Boiling is the term to describe evaporation occurring at a solid-liquid interface. When the boiling surface temperature exceeds the saturation temperature (T_{sat}) of the liquid, vapor bubbles will be formed.

Boiling heat transfer has two main modes. The first is pool boiling where fluid flow and heat transfer are due primarily to free convection, bubble growth, and detachment induced by a buoyancy force from the density difference. The other type of boiling is forced convection boiling, where flow is due to a bulk motion of the fluid in addition to the buoyancy effects. A single-tube boiling test focuses solely on the nucleate boiling mode, while a tube-bundle test is a combination of nucleate boiling and forced convection boiling.

There are different modes of pool boiling, which are a function of the excess temperature. The excess temperature is defined by the difference between the tube-wall temperature and the saturation temperature of the liquid ($T_w - T_{sat}$). It is also termed wall superheat and is expressed as ΔT. When ΔT is still relatively small, there exists only free convection boiling. In this mode, the excess temperature is not large enough to have bubble formation. The fluid motion is controlled only by free convection effects. Eventually, the excess temperature will increase to a point where bubble formation is initiated and the fluid enters the nucleate boiling mode.

There are two different levels of nucleate boiling. The first level only produces isolated bubbles from nucleation sites on the tube surface. The bubble separation causes substantial fluid mixing near the surface, which results in a higher heat transfer performance than free convection boiling. If the excess temperature continues to increase, there is additional bubble formation and more nucleation sites become active. This causes the bubbles to escape as columns of vapor.

As ΔT is increased further, the surface reaches a critical heat flux and transition boiling begins. The bubble formation is so rapid that a vapor film begins to form on the surface. In this mode, the heat transfer performance begins to degrade because of the low thermal conductivity of vapor. If the excess temperature continues to increase, film boiling will be present. Heat is transferred from the surface to the liquid by conduction through the vapor, with the heat transfer performance continuing to decrease.

Pool boiling can also be classified by saturated or subcooled boiling. In saturated boiling, the pool temperature slightly exceeds the saturation temperature. Bubbles are formed on the surface and escape to the liquid-vapor interface through buoyancy. During subcooled boiling, the pool temperature is below that of T_{sat} and bubbles formed at the surface may condense in the liquid before reaching the vapor space. In the nucleate boiling mode, the effect of subcooled boiling is considered to be negligible [19].

There are several important factors that can influence the heat transfer characteristics in pool boiling. These factors include boiling pressure, fluid properties, tube-surface conditions, excess temperature, and the type and amount of impurities. One fluid property that has a large effect on pool boiling is the surface tension of the fluid. The impurity in pool boiling is usually the presence of oil, but could also include noncondensible gas within the system. Variations in these factors can significantly affect pool boiling heat transfer.

One aspect of the surface condition factor is the tube geometry. Many flooded refrigerant evaporators use integral-fin tubes, which have a higher performance than a smooth tube. Recently, enhanced tube geometries have become available for pool boiling applications. The tube surface provides a stable enhancement of nucleate boiling. The two main types of enhanced surfaces are reentrant grooved surfaces (e.g., the Turbo-B tube) and porous coated surfaces. These enhanced tube geometries have a higher nucleate boiling performance than the integral-fin tube. The enhanced surfaces that are presently available were reviewed by Webb [33].

This chapter concentrates on a review of available literature for nucleate pool boiling. The parameters that are of interest to this particular research are as follows:

1) Single tube testing
2) Shell-side evaporation of refrigerants
3) Finned-tube results as well as enhanced surface results
4) Boiling of pure refrigerant and refrigerant / lubricant mixtures

The experimental results for pure refrigerants, containing the above parameters, are first reviewed. This is followed by presenting existing models that predict boiling heat transfer coefficients. The literature on refrigerant / lubricant mixtures is also reviewed and experimental results are presented, including a developed correlation for prediction of the boiling coefficient with the presence of oil.

POOL BOILING OF PURE REFRIGERANT

There has been a great amount of research conducted in the area of nucleate pool boiling with pure refrigerants. This includes many different refrigerants as well as various tube surfaces. A large portion of the data were taken on copper tubes with a nominal outer diameter of 19.1 mm (0.75 in). The literature also shows a wide range of saturation temperatures that were used in conducting the experiments.

Experimental Results

The integral-fin tube was the industry standard for use in flooded evaporators until the early 1970's, when the enhanced boiling surfaces were introduced. A survey on the evolution of enhanced surface geometries is presented by Webb [33]. These enhanced surfaces were specifically designed to promote high-performance nucleate boiling and they show significant improvement in the boiling coefficients over the integral-fin tubes. As witnessed in the literature, it is still customary to present the plain tube performance as a reference for the finned and enhanced surfaces.

Experimental results have been published for both single-tube work and for tube bundles. This literature review concentrates mainly on single-tube results. In a tube bundle, vapor bubbles rise, especially from the lower tube row, causing a convective component to enhance the heat transfer in the upper rows. Webb [33] reported that the boiling coefficient of enhanced surfaces in a tube bundle is approximately equal to that measured in a single-tube test. This is due to the fact that nucleate boiling dominates the heat transfer with enhanced tube bundles. It was also reported that plain or integral-finned tubes have a higher boiling coefficient when measured in a tube bundle as compared to a single-tube test. Apparently, the convective component in a tube bundle provides a much greater improvement for finned or plain tubes than for the enhanced surfaces.

In 1981, Yilmaz and Westwater [34] investigated the performance of four enhanced surfaces. The test was single-tube pool boiling of p-xylene. The highest performance was provided by the HIGH-FLUX tube and the Turbo-B tube, which are porous coated and reentrant grooved surfaces, respectively.

Nakayama et al. [35] investigated the boiling heat transfer performance on porous surface structures using CFC-11 as the working fluid. The system pressure was varied in three steps, 0.04, 0.1, and 0.23 MPa. At a system pressure of 0.23 MPa (T_{sat} = 50°C), the porous tube, with pore size of 150 μm, showed the highest performance. This tube outperformed tubes with pore sizes of 50, 100, and 200 μm. Similar trends were found in the other two system pressures. With the 150 μm pore tube and a system pressure of 0.23 MPa, nucleate boiling continued even when the wall superheat was reduced to 0.1 K. They also observed that when boiling with a porous surface, rapid bubble formation does not necessarily guarantee high heat transfer performance.

Experiments were performed on special finned tubes and a plain tube by Gorenflo and Fath [36] in 1987. The special finned tubes consisted of a trapezoid-shaped fin and a T-shaped fin, with trade names of GEWA-K and GEWA-T, respectively. The experiment used HCFC-22 as the working fluid with a testing pressure range of 6 to 93% of the critical pressure, which is 4.99 MPa. At 93% of the critical pressure, the plain tube boiling coefficient matched the boiling coefficient for the trapezoid-shaped fin tube at heat fluxes greater than 5 kW/m^2. In addition, the T-shaped fin tube had the highest performance throughout the pressure range. It was also concluded that the differences in the relative increase of the boiling coefficient with heat flux and pressure between the plain and finned tubes tend to vanish at high heat fluxes and at pressures higher than approximately 50% of the critical pressure.

Ayub and Bergles [37] conducted pool boiling tests with CFC-113 and water on a 19 fpi, 26 fpi, and a T-shaped fin tube. By varying the gap spacing at the fin tip, it was found that an optimum gap spacing exists. The optimum gap width is 0.25 mm (0.0098 inch) for the 19 fpi tube with CFC-113 and 0.35 mm (0.0138 inch) for water.

In 1991, Webb and Pais [38] tested five refrigerants on three tube geometries for pool boiling heat transfer. The tubes used in the research were the 26 fpi tube, Turbo-B tube, and the GEWA-SE tube, with a nominal outside diameter of 19.1 mm (0.75 inch). Data were taken with refrigerants CFC-11, CFC-12, HCFC-22, CFC-113, HCFC-123, and HFC-134a at a saturation temperature of 27°C (80°F). Tests performed on the 26 fpi tube showed that the boiling coefficients for HCFC-123 and CFC-11 were very similar, as were the boiling coefficients for HFC-134a and CFC-12. But, with the other two enhanced surfaces, the pool boiling coefficients for HCFC-123 and HFC-134a fell considerably below those values for CFC-11 and CFC-12, respectively. At a heat flux of 70 kW/m^2, the Turbo-B and GEWA-SE had a higher performance than the 26 fpi tube by 35% for HCFC-123 and 30% for HFC-134a. For HCFC-123, the Turbo-B tube had the highest heat transfer coefficient, which at 70 kW/m^2 was 20% below that of CFC-11 for the same tube. For HFC-134a, the GEWA-SE had the highest heat transfer coefficient. At 70 kW/m^2, the boiling coefficient was approximately 10% below that of CFC-12 for the same tube.

Webb and Pais [39] extended the above research by including two additional tubes and a different saturation temperature. A plain tube and a GEWA-TX19 were added to the matrix and data were taken at a saturation temperature of 4.44°C (40°F). This work showed that the boiling heat transfer coefficients for the alternative refrigerants HCFC-123 and HFC-134a were within 10% of the values for CFC-11 and CFC-12, respectively. This held true for all tubes except the Turbo-B with CFC-11/HCFC-123. It also showed that an increase in the saturation temperature causes an increase in the boiling coefficient at a given heat flux and tube geometry.

Theoretical Results

Presently, there does not exist a generalized correlation or model that is reliable in predicting boiling heat transfer coefficients for different refrigerant / tube surface combinations. This is partly due to the lack of complete understanding in the nucleate pool boiling regime and the tube-surface effects in this area.

In 1952, Rohsenow [40] proposed a predictive equation for nucleate boiling that has been incorporated in many studies as a comparison to experimental results. The equation is as follows:

$$Nu = Re^{2/3} (Pr)_l^{-0.7} / C_{sf} \qquad (5.1)$$

where C_{sf} is a dimensionless proportionality constant, which is dependent upon the solid / liquid combination. For CFC-11 and copper, the C_{sf} value is 0.022. The dimensionless parameters in Equation 5.1 are defined below.

$$Nu = \frac{h D_b}{k_l}, \tag{5.2}$$

$$(Pr)_l = \left[\frac{\mu c_p}{k}\right]_l, \tag{5.3}$$

$$Re = \frac{q D_b}{A h_{fg} \mu_l}, \text{ and} \tag{5.4}$$

$$D_b = \sqrt{\frac{\sigma}{(\rho_l - \rho_v) g}}. \tag{5.5}$$

The surface tension term, σ, was incorporated because of the significant effect this fluid property has on bubble formation and development. The above correlation can only be applied to a plain tube surface.

Another early model for plain tubes was proposed by Mikic and Rohsenow [41] in 1969. The correlation assumes that the main mechanism of heat transfer in nucleate boiling is transient heat conduction. When the bubble departs from the boiling site, it pumps superheated liquid away from the surface. In the time interval between bubble departures, the transient heat conduction is found by

$$\frac{q}{(T_w - T_{sat})} = h = \frac{2 k_l f^{1/2}}{(\pi\alpha)^{1/2}}. \tag{5.6}$$

The bubble frequency, f, is calculated with the following equation:

$$f d_b = 0.59 \left[\frac{\sigma g (\rho_l - \rho_v)}{\rho_l^2}\right]^{1/4} \tag{5.7}$$

where d_b is the bubble diameter as it departs from the surface.

In 1980, Stephan and Abdelsalam [42] presented a plain tube correlation to calculate the heat transfer coefficient in natural convection boiling (i.e.,, single-tube nucleate boiling). The correlation is empirical and based on 12 data sets. The resulting equation is only for use with refrigerants.

$$Nu = 207 X_1^{0.745} X_2^{0.581} X_3^{0.533} \tag{5.8}$$

where

$$X_1 = \frac{0.146\, q''\, \beta \left[\frac{2\sigma}{g\,(\rho_l - \rho_v)}\right]^{1/2}}{k_l\, T_{sat}}, \tag{5.9}$$

$$X_2 = \frac{\rho_v}{\rho_l}, \text{ and} \tag{5.10}$$

$$X_3 = \frac{\upsilon_l}{\alpha_l}. \tag{5.11}$$

The above correlation is valid within a working pressure range of $0.003 \le P/P_c \le 0.78$, and the contact angle, β, is assumed to be 35°. The RMS error of this correlation was 10.6%.

In 1984, Cooper [43] developed an empirical correlation for a plain tube surface, which is valid for all fluids, and is given by

$$h = 90\,(q'')^{0.67} M^{-0.5} \left(\frac{P}{P_c}\right)^m \left[-\log_{10}\frac{P}{P_c}\right]^{-0.55} \tag{5.12}$$

where $m = 0.12 - 0.2 \log_{10} R_P$.

The Cooper correlation contains a surface roughness parameter, R_P, which has a value in the range of 0.3 to 0.9. This term accounts for the micro-roughness of the tube surface and is expressed in μm. Stephan and Abdelsalam [42] reported that commercial-finish copper tubes have an R_P value approximately equal to 0.4 μm. Webb and Pais [39] found that a value of $R_P = 0.3$ μm produced good agreement with their experimental results.

In common industrial chiller units, the evaporator contains a tube bundle instead of a single tube. In shell-side boiling of a tube-bundle arrangement, the mechanism is one of combined nucleate boiling and forced convection. In 1963, Chen [44] proposed a model to predict the boiling heat transfer coefficient by

$$h_o = SFh_{nb} + Fh_{fc}. \tag{5.13}$$

The term h_{nb} is for the nucleate boiling coefficient on a single tube. This term can be found by using a pool boiling correlation for the surface geometry and refrigerant of interest. If a plain surface tube bundle is being tested, one of the above correlations can be used; however, no correlations exist for predicting h_{nb} as a function of

temperature and refrigerant type for other tube surfaces. Therefore, it is necessary to have actual pool boiling data for the refrigerant, temperature, and tube type of interest.

The term h_{fc} is the forced convection coefficient for the liquid phase flowing alone in the bundle. The suppression factor (SF) and the forced convection multiplier (F) are functions of the two-phase Reynolds number. The F term is a function of the two-phase friction multiplier, ω_f^2, which relates to the two-phase friction pressure gradient. Webb et al. [45] present correlations for the four component terms in Equation 5.13.

In 1989, Chen et al. [44] proposed a model for pool boiling on an integral-fin tube bundle. The model retained the same basic form as Equation 5.13 with contributions coming from nucleate boiling and forced convection. However, this model eliminated the generic components of S and F and replaced them with terms specific to a finned tube bundle. The proposed equation is as follows:

$$h_o = h_{nb}\left(\frac{A_b}{A_o}\right) + h_{fc}\left(1 - \frac{A_b}{A_o}\right). \qquad (5.14)$$

The definition of A_b is the area influenced by nucleate boiling. The term A_b/A_o is the fraction of the total finned surface area influenced by nucleate boiling. Webb et al. [45] present a detailed description of incorporating the Chen model [44] to predict tube bundle performance. The present research is on single tube pool boiling. However, given the analysis by Webb et al. [45], it is possible to use the single tube results and predict how this particular combination of refrigerant, temperature, and tube type would perform in tube-bundle evaporators.

POOL BOILING OF REFRIGERANT / LUBRICANT MIXTURES

The investigation of lubricant effects on heat transfer performance is important because refrigeration compressors require lubrication. The lubricants used in these compressors are miscible with the working refrigerant, which results in oil being mixed and circulated with the refrigerant. Depending on the concentration of oil in the system, the refrigerant / lubricant mixture has different performance characteristics than a pure refrigerant. This section concentrates on the present state of knowledge in reference to lubricant effects on heat transfer performance, both experimentally and theoretically.

Experimental Results

Experiments performed by Stephan [46] and Dougherty and Sauer [47] have shown that the addition of oil can significantly affect the refrigerant heat transfer performance. There are various phenomena that occur once oil is introduced, including an increase in the boiling temperature as compared to the pure refrigerant temperature at the same pressure (see Chapter 7 for solubility analysis). The thermodynamic properties are altered through an

increase in viscosity and surface tension with the addition of oil. Increased surface tension makes it more difficult for vapor bubbles to develop, which results in an added resistance to boiling heat transfer.

A refrigerant / lubricant mixture can also produce a layer of foam at the top of the pool when there is a low concentration of oil present. This foaming action can act to enhance the heat transfer process. Generally, the heat transfer performance decreases with increasing concentrations of oil. The only exception that has been noted is at oil concentrations of 3% or lower where the foaming action can increase the heat transfer coefficient.

Dougherty and Sauer [47] performed pool boiling experiments with CFC-11 and CFC-113 mixed with a paraffin-base lubricant at concentrations up to 10% by weight. The tests were performed on single copper tube surfaces with diameters of 15.9 mm and 28.6 mm. The results of these tests showed that oil concentrations greater than 3% always decreased the boiling coefficient, while concentrations less than 3% produced slight increases in the heat transfer performance.

Sauer et al. [48] conducted heat transfer experiments on a single-tube apparatus with CFC-12 and three paraffin-base oils having viscosities of 155, 290, and 515 SUS. The experimental results showed that the heat transfer performance was consistently decreased with oil concentrations greater than 7%, while concentrations below 7% sometimes significantly increased the heat transfer performance. The peak boiling performance occurred at an oil concentration of 3%. In addition, Chongrungreong and Sauer [49] showed that the heat transfer coefficient in pool boiling decreases with an increase in oil viscosity.

Stephan and Mitrovic [50] also performed testing on an CFC-12-oil mixture. Their results showed that the heat transfer coefficient decreased by 20% for an increasing oil concentration of 3% to 9%. However, increases in the boiling coefficient, with respect to the pure refrigerant values, were found at the highest heat flux (21.75 kW/m^2) with oil concentrations of up to 6%.

In 1986, Wanniarachchi et al. [51] conducted boiling tests with CFC-114 refrigerant / lubricant mixtures on a porous-coated surface. This experiment showed the maximum heat transfer enhancement, with respect to lubricant addition, occurred at oil concentrations of 3% to 6% with a heat flux of 1 kW/m^2. At heat fluxes greater than 5 kW/m^2, the lubricant addition always decreased the heat transfer performance relative to the pure refrigerant case. The authors also suggest that the performance of the enhanced boiling surfaces (such as the porous-coated tube) could be much more severely affected by the presence of oil than the plain tube, or even an integral-fin tube. This is a result of the numerous reentrant cavities present on an enhanced surface. These cavities can experience a much larger concentration of oil than is present within the pool. Specifically, it is possible that the oil is trapped in the cavities, with the refrigerant being boiled off and the oil remaining on the tube surface.

Webb and McQuade [52] conducted experiments in which no enhancement in the boiling performance was observed with the addition of oil. The tests involved CFC-11 and HCFC-123 with a mineral oil on various enhanced boiling surfaces. The findings revealed that the enhanced surfaces experience a much greater performance degradation than the plain surface tube. All of the data showed no increase in heat transfer

performance over that found for pure refrigerant boiling. Jensen and Jackman [53] showed similar trends with their tests of CFC-113 refrigerant / lubricant mixtures. Jensen concluded that the decrease in heat transfer performance was related to the oil-rich boundary layer at the vapor-liquid interface of the nucleate bubble which causes an increase in the resistance to diffusion of the more volatile component. In a binary mixture of refrigerant and lubricant, the saturation pressure of pure refrigerant is lower than that of pure oil; so the refrigerant is termed the more volatile component.

Sauer et al. [54] performed nucleate boiling tests with CFC-11 and a napthene-based oil of two different viscosities. The results were similar to his previous study [48], in that they showed small lubricant concentrations could produce small improvements in the shell-side heat transfer coefficient. The authors note that this trend is related to foaming which occurs in the upper rows of flooded evaporator tube bundles.

In 1977, Arai et al. [55] tested an enhanced surface tube bundle with CFC-11 and oil concentrations of 3.4% or less. A foam layer was observed at the top of the bundle during testing. The results showed an increase in the heat transfer coefficient when the top of the bundle was in the foaming region. If the top of the bundle was not in the foaming region, the oil concentration reduced the boiling coefficient less than 10%.

It is evident that in some instances a small concentration of oil can enhance the heat transfer performance. It is also evident that the foaming phenomenon from the addition of oil is a factor in the enhancement of the boiling coefficient. In reference to a tube bundle, the foaming region is only found in the upper rows of the bundle. Therefore, single-tube experimentation with refrigerant / lubricant mixtures basically models the top row of a tube bundle.

Theoretical Results

In 1980, Chongrungreong and Sauer [49] performed a study to develop a general correlation equation for predicting the heat transfer coefficient of a refrigerant / lubricant mixture under pool boiling conditions. Two correlations were produced from this study. The first is to be used when the fluid properties of the refrigerant / lubricant mixture are known. The other correlation can be used without knowledge of the thermodynamic and transport properties of the mixture. The second correlation was developed considering only wall heat flux, the volume fraction of pure refrigerant (ϕ), and the boiling pressure. Since property data for refrigerant / lubricant mixtures is very limited, the following equation can be used without that data known.

$$h = 6.17\,[q'']^{0.55}\,[\phi]^{3.65}\,P^{0.24} \qquad (5.15)$$

This equation predicts the following: 1) h increases as P_{sat} increases, 2) h decreases with an increase in viscosity, 3) h increases as q" increases, and 4) h increases as ϕ increases. One limitation of Equation 5.15 is that it cannot account for the foaming effects on the boiling heat transfer coefficient.

It is a difficult process to develop a generic correlation to predict heat transfer coefficients for multiple refrigerants, various tube geometries, and different saturation temperatures. The boiling of refrigerant / lubricant mixtures is a very complicated process, which further inhibits the development of a general boiling correlation. More accurate fluid properties of mixtures are needed before an accurate model of heat transfer performance can be made.

SUMMARY

The review presented in this chapter shows that the enhanced boiling surfaces significantly outperform the integral-fin tubes, as well as the plain tube. The measured heat transfer performance of these enhanced surfaces on a single-tube test facility are consistent with the performance that will be found in a tube bundle. Fairly accurate correlations have been developed for a plain tube in nucleate pool boiling, but no correlation exists for a finned or enhanced tube surface.

Studies on pool boiling of refrigerant / lubricant mixtures are also of great importance. This chapter has shown that a small concentration of oil (i.e., 3% or less) can sometimes enhance the heat transfer performance with the onset of foaming. The heat transfer coefficient is always decreased, with respect to the pure refrigerant values, at oil concentrations greater than 3%.

CHAPTER 6

EXPERIMENTAL APPARATUS

The test facility used in this study was initially used for spray evaporation testing; however, it was redesigned and modified for use with either condensation, pool boiling, or spray evaporation testing. During condensation, the rig was capable of producing saturated or superheated vapor. During pool boiling or spray evaporation, the test facility was capable of testing pure refrigerants or refrigerant / lubricant mixtures.

CONDENSATION TEST FACILITY

A test facility was constructed to study shell-side film condensation on a single, horizontal tube and was capable of either producing saturated vapor or superheated vapor. The test facility was comprised of several major components, including a test section, the test tubes, the refrigerant loop, the closed water loop, the glycol flow loop, and the data acquisition system. A schematic drawing of the test facility can be seen in Figure 6.1, and a detailed description is presented below.

Test Section

The test section was constructed of stainless steel with a diameter of 101.6 mm (4 in.) and a length of 406.4 mm (16 in.). There were two glass view ports (one per side) in the middle of the test section. Offset from top-dead center and, along opposite sides were the two refrigerant vapor inlets. Two liquid outlets lie along the bottom-dead center of the test section. There is a stainless steel tube sheet attached to each end of the test section, each having two threaded ports. Each threaded port contained a compression fitting which allowed the insertion of the copper test tube. A drip-deflector was also installed in the test section. This consisted of a thin aluminum sheet placed directly below each vapor inlet port. The test section was equipped with two thermistors, one per side placed on opposite ends, which measured the refrigerant vapor temperature. A pressure transducer connected to a pressure tap was also installed. This allowed for measurement of the saturation pressure within the test section, which was used to determine a saturation temperature. A schematic of the test section is presented in Figure 6.2.

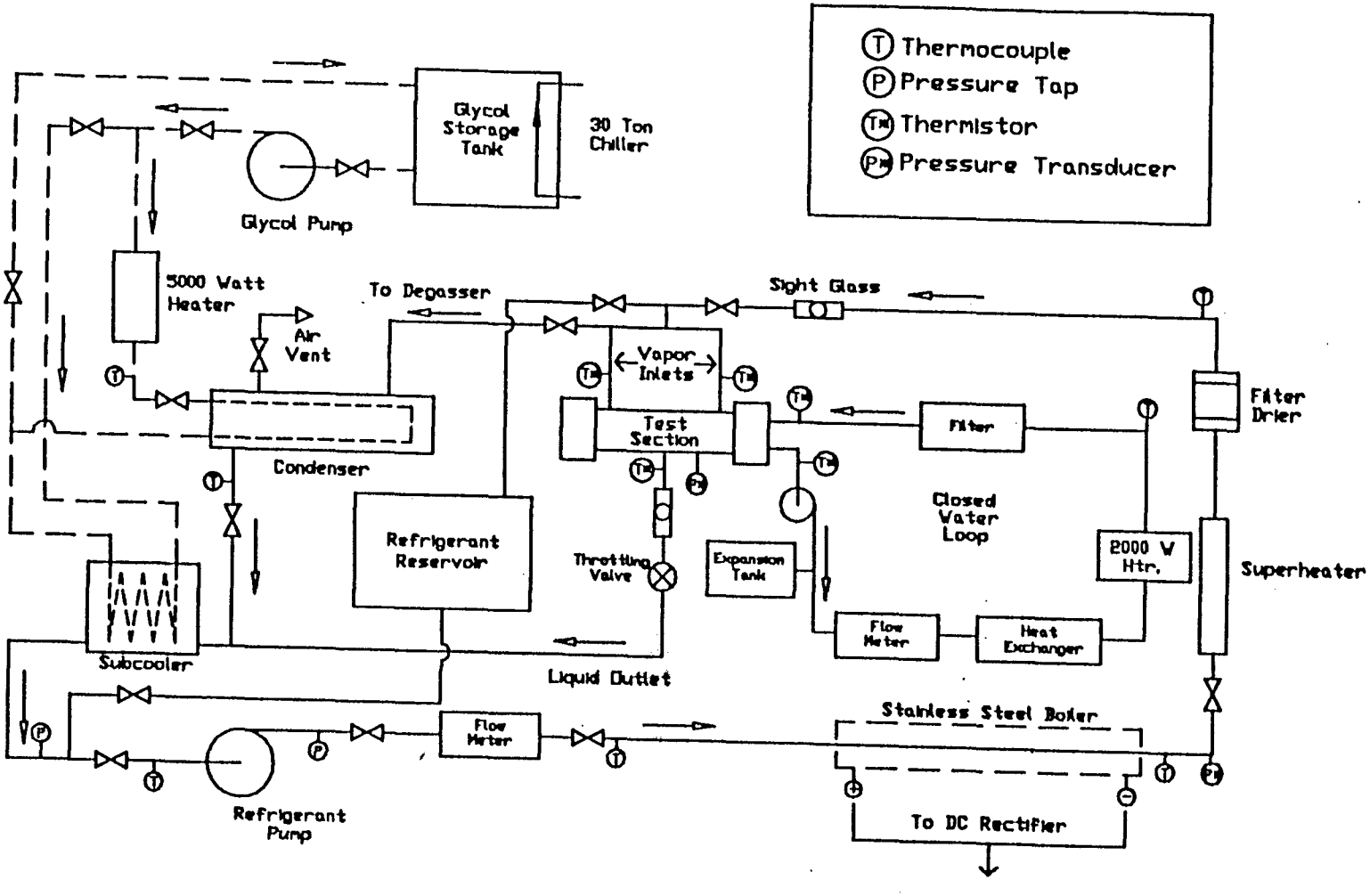

Figure 6.1 Schematic of condensation test facility

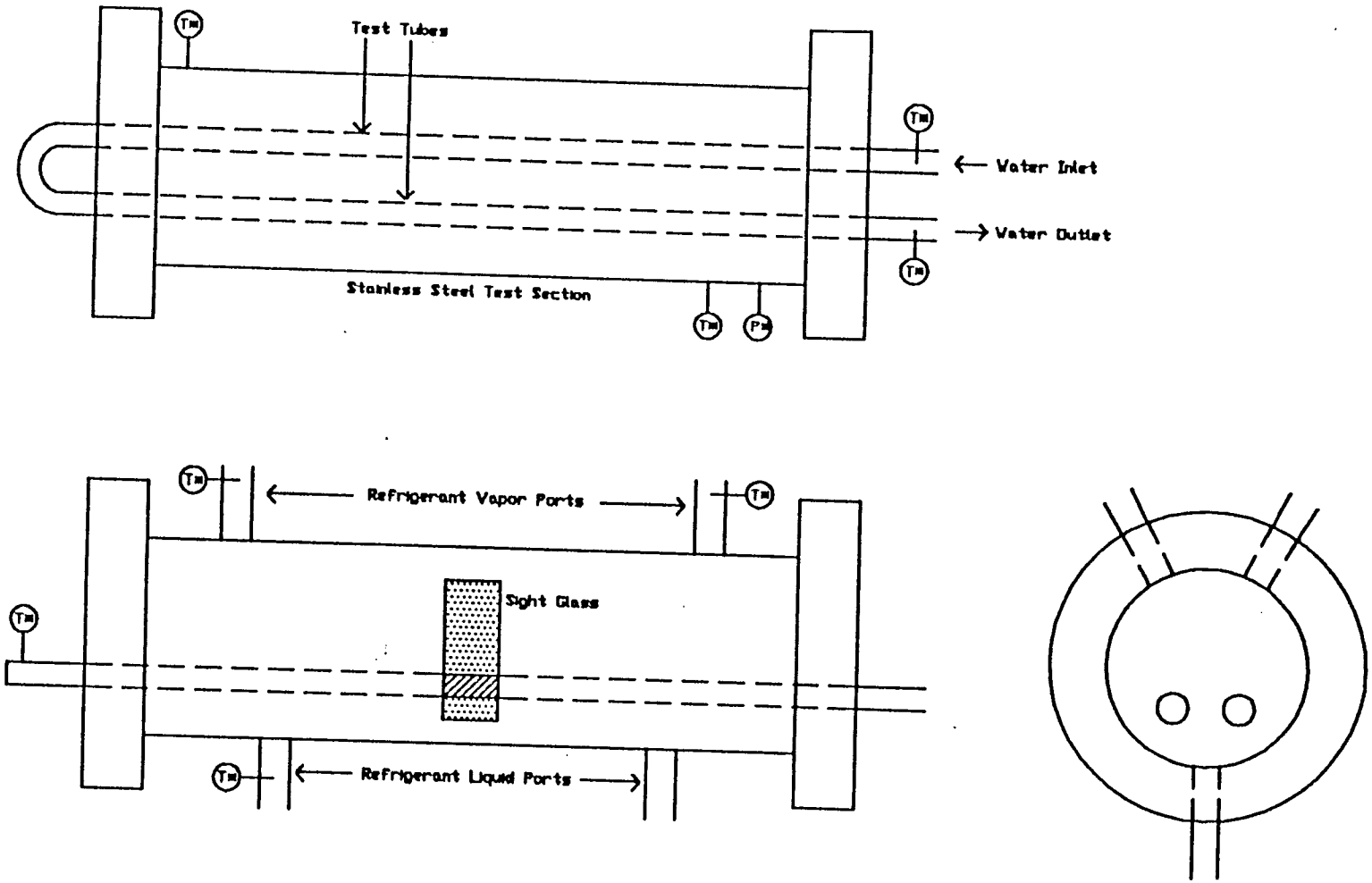

Figure 6.2 Schematic of test section

Test Tubes

There were three different tube surfaces tested: plain, 26 fpi, and 40 fpi. The copper tubes had a nominal outer diameter (OD) of 19.1 mm (0.75 in.) and an enhancement length of 838.2 mm (33 in.). There was a 101.6 mm (4 in.) length of plain tube on each end, which was located outside of the test section. These plain-tube sections made up the water inlet, outlet, and turn-around. The 40 fpi tube had a fin height of 0.86 mm (0.034 in.), while the 26 fpi tube had a fin height of 1.45 mm (0.057 in.). There were two test tubes (each 419.1 mm in length) contained in the test section at the same height and with a spacing of 23.8 mm (0.938 in.). One end of the test section contained the water inlet and outlet. The other end contained a U-shaped copper tube, which acted as the water turn-around. With this two-pass configuration, the test tube was 838.2 mm long (not including the U-bend tube portion). The tube specifications are provided in Appendix C.

The tube-side (i.e., water-side) was enhanced for each test tube by installing spring-type turbulators. The turbulator is a copper spring which is placed on the inside of the tube and held stationary by a friction fit between the coils of the turbulator and the inner tube wall. Installation techniques allowed the turbulators to be installed with a consistent spacing between spring coils. These turbulators were used to increase the tube-side Nusselt number by continuously tripping the boundary layer to maintain turbulence. It should be noted that these turbulators are also used in several industrial chiller applications [56].

Refrigerant Flow Loop

The refrigerant loop is used to circulate refrigerant and deliver it to the test section at the desired conditions. The refrigerant was circulated by a diaphragm-type positive displacement pump through a closed-flow loop. This type of pump is self lubricated with an oil sump that is sealed from the refrigerant side of the pump. After the pump, the refrigerant was circulated through a mass flow meter and then into the boiler. The boiler was a stainless steel tube that was 2.44 m (8 ft) long with a 19.1 mm (0.75 in.) OD. The boiler was operated by passing electric current through the tube wall, which heated the stainless steel to boil the liquid refrigerant. The current to the boiler wall was supplied by a silicon-controlled rectifier (SCR) with an output of 0-12 VDC and 500 amps. A temperature control device was connected to thermocouples on the boiler wall and to the current control of the rectifier. If the boiler wall temperature exceeded a certain value, a relay switch would open and the rectifier would be shut down automatically. There was also a pressure transducer placed at the end of the boiler tube to determine the exiting vapor pressure.

After leaving the boiler, the refrigerant vapor flowed through a 19.1 mm (0.75 in.) ID copper pipe that was 1.52 m (5 ft) in length. The pipe contained heat tapes that were used as the superheater. The vapor would then pass through a filter/dryer and a sight glass before entering the vapor ports at the top of the test section, where it was condensed on the test tube. The condensed vapor would exit the test section through the two liquid outlet

ports. The refrigerant liquid would then flow through another sight glass into a throttling valve. After passing through the throttling valve, the liquid continued through a subcooler before returning to the pump.

The refrigerant loop also contained a seven-ton condenser that acted as a degassing facility for the test rig. The vapor could be directed into the condenser where the refrigerant vapor would condense to liquid and the noncondensible gas would remain at the top of the condenser. A charge valve was installed in a port on top of the condenser where the noncondensible gases could be purged.

Water Loop

Water was circulated through the inside of the test tube by two diaphragm-type positive displacement pumps. The water flowed through the test tube in a two-pass configuration. Inlet and outlet temperatures were measured by thermistors placed at the water inlet and outlet ports. After exiting the test section, the water flowed to the pumps. The water leaving the pumps passed through a mass flow meter followed by a heat exchanger. The heat exchanger removed the energy from the water that was gained in the test section. The water then flowed through an immersion heater that was connected to an automatic temperature control device. This allowed for accurate control of the water temperature before it entered the test section. A water reservoir tank was also connected to the water loop. This was used to aid in the contraction and expansion that the water experienced due to the large temperature changes.

Glycol Flow Loop

A 30-ton chiller unit was used to cool a glycol/water mixture that was circulated with a 2.5 hp centrifugal pump to several components of the test rig, namely, the degasser, the refrigerant subcooler, and the water heat exchanger. The glycol/water mixture was a 60/40 mixture by volume. The chiller was a 141 kW packaged unit capable of supplying 35 kW at an evaporator temperature of -17.8^{o}C (0^{o}F). The water/glycol storage tank has a capacity of 1,140 L (300 gal). After the coolant has circulated through the various components, it passed through a three-way valve. This valve controlled the amount of glycol/water mixture that was either returned to the chiller unit to be cooled, or that bypassed the chiller and returned directly to the test rig components. This allowed the test facility to operate when the chiller unit was running at a lower temperature than needed.

Data Acquisition System

The data acquisition system consisted of a digital multimeter and a switch/control unit controlled by a personal computer. The FORTRAN data acquisition program controls the scanner and multimeter. The program allowed the user to input whether the computer should scan the desired channels when a key was pressed (manual

mode) or at inputted time intervals (auto mode). It also allowed the user to choose which scans were to be written to a file on the hard disk for later post-processing. The program displayed current and previous values for temperature, pressure, energy, and heat flux, with these values being updated after each scan. The occupied channels that were scanned consisted of the following: nine thermocouples, two pressure transducers, two mass flow meters, and eight thermistors.

POOL BOILING TEST FACILITY

A test facility was constructed to study shell-side nucleate pool boiling on a single horizontal tube. The facility was capable testing pure refrigerants or refrigerant / lubricant mixtures. This test facility was comprised of several major components, including a test section, the test tubes, the refrigerant loop, the closed water loop, the glycol flow loop, the oil sampling/injection system, and the data acquisition system. A schematic drawing of the test facility can be seen in Figure 6.3, and a detailed description is presented below.

Test Section

The test section used in the pool boiling tests was the same as the one used in the condensation study described earlier, except with several minor differences. The specifications of the test section are identical to those presented previously. For pool boiling, the two vapor ports were used for the exiting vapor and the two liquid ports were used for the incoming liquid refrigerant. A small amount of liquid was also introduced into the test section through five ports located at top dead center of the test section. The test section was equipped with two thermistors, one per side placed on opposite ends, which measured the refrigerant pool temperature. A pressure transducer was also installed and connected to a pressure tap for the purpose of measuring the saturation pressure, which was then used to determine a saturation temperature.

Test Tubes

The pool boiling tests also used the two integral-fin tubes and the plain tube that were used in condensation. Figure 6.4 shows a schematic drawing of the integral-fin tube. All other specifications that were previously listed above also apply to the tubes used in pool boiling. The exact dimensions on each test tube are shown in Appendix C.

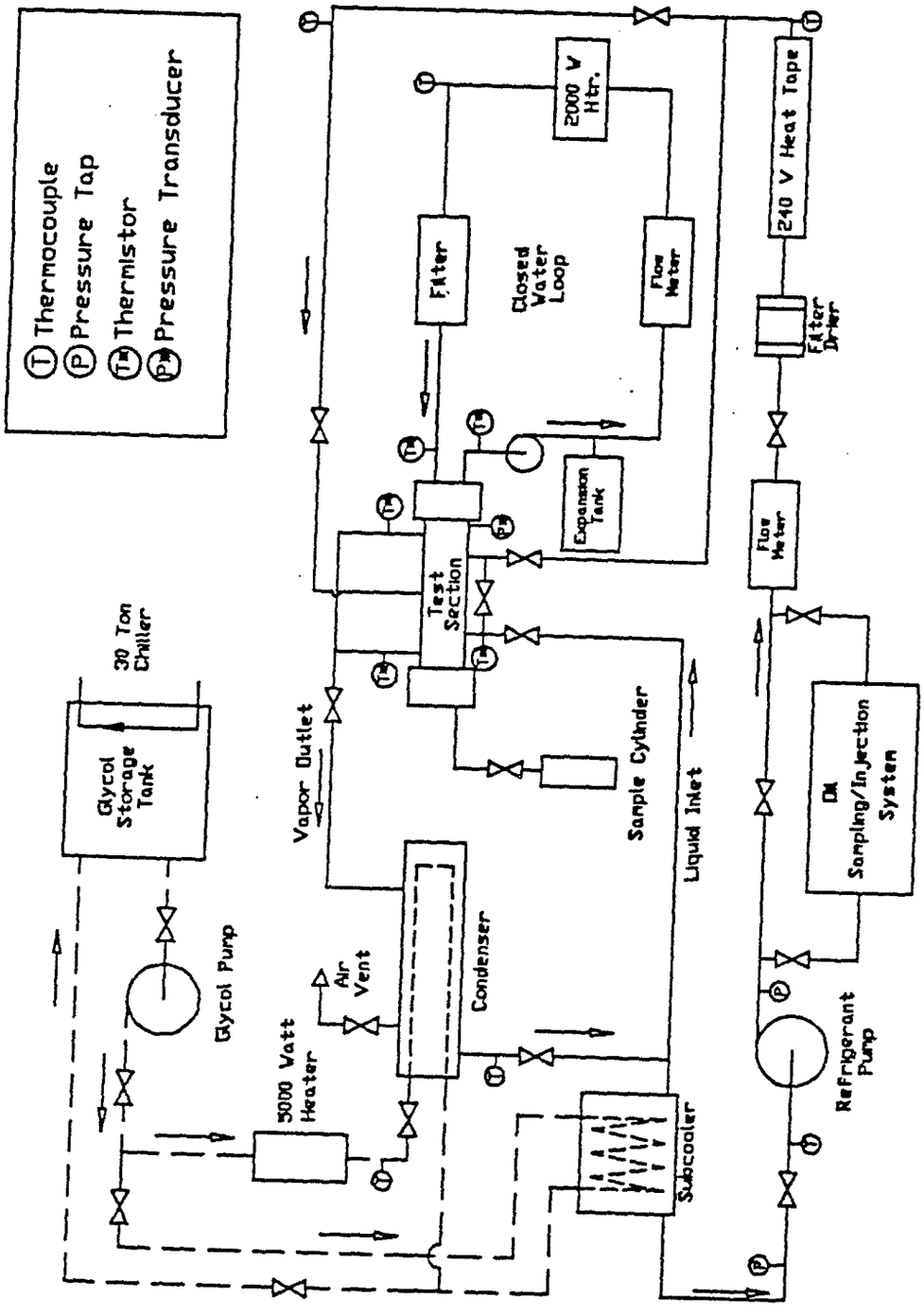

Figure 6.3 Schematic of pool boiling test facility

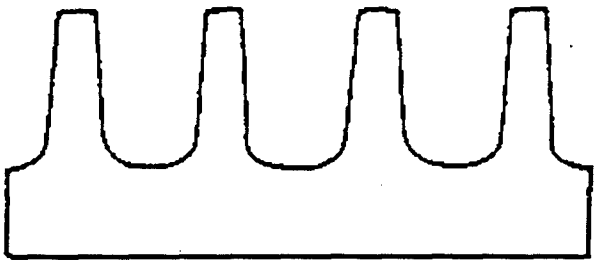

Figure 6.4 Cross-sectional schematic of integral-fin tube surface

Refrigerant Flow Loop

The refrigerant loop was used to circulate refrigerant and deliver it to the test section at the desired conditions. The refrigerant was circulated by a gravity-feed from the condenser and a diaphragm-type positive displacement pump. The refrigerant that was passed through the pump flowed through a mass flow meter and then into a refrigerant filter / dryer. The refrigerant then flowed into pipe that was wrapped with two 240-V heat tapes before entering the test section through the five top liquid ports. The heat tapes were used to increase the temperature of the liquid when it was in a subcooled condition.

A portion of the liquid refrigerant also entered the test section through the two bottom ports. This refrigerant came from the condenser and was fed to the test section by gravity. The condenser was equipped with a purging valve at the top to bleed out any noncondensible gases that were present within the system.

The test tubes were immersed in liquid refrigerant within the test section, where the tube wall temperature was increased beyond the liquid saturation temperature causing the refrigerant to boil into vapor bubbles. The refrigerant vapor escaped through the liquid / vapor interface and traveled out of the two vapor ports at the top of the test section. The vapor then flowed to the condenser where the energy, gained in the test section, was removed and the vapor was changed to its liquid state. The refrigerant exited the condenser through the liquid outlet and returned to the test section via the pump or directly to the liquid inlet ports of the test section by gravity. It should be noted that the condenser pressure controlled the test-section saturation temperature.

Water Loop

The outer tube wall was heated by circulating water through the inside of the test tube with two diaphragm-type positive displacement pumps. The water flowed through the test tube in a two-pass configuration. Thermistors were placed on water inlet and outlet ports. After exiting the test section, the water flowed into the pumps. The water leaving the pumps entered a mass flow meter followed by an immersion heater. The immersion

heater was controlled by an automatic power control device. This allowed for accurate control of the heat flux within the test section. A water reservoir tank was also connected to the water loop. This was used to aid in the contraction and expansion which the water experienced due to the large temperature changes.

Glycol Flow Loop

A 30-ton chiller unit was used to cool a glycol/water mixture that was circulated to several components of the test rig, namely, the condenser and the refrigerant subcooler. The chiller specifications that were discussed in the condensation section are also applicable to the pool boiling testing.

The coolant mixture that circulated through the condenser was first passed through a 5-kW circulation heater, which was controlled by an automatic temperature control device. This was used for accurate control of the condenser pressure and, consequently, the test section saturation temperature.

Data Acquisition System

The data acquisition system that was used during pool boiling was the same system used in the condensation work. The only difference was in the post-processor program. The equations used to calculate the shell-side heat transfer coefficient are slightly different for pool boiling than for condensation. Chapter 6 presents the specific equations used for both condensation and pool boiling.

Oil Sampling/Injection System

Modifications were made to the test rig to allow testing of refrigerant / lubricant mixtures. As seen in Figure 6.3, the oil sampling/injection system was installed in the discharge line of the pump. The sampling system consisted of a stainless steel cylinder that was 50.8 mm (2 in.) in diameter. A bypass line was installed in the pump discharge line that allowed the flow to be diverted through the sampling cylinder. A sampling system was also installed in the test section. This system consisted of a double-actuating stainless steel cylinder with a 31.8 mm (1.25 in.) diameter and a 101.6 mm (4 in.) piston stroke length. This sampling cylinder was installed in one of the test section thermistor ports located on the side of the test section.

As stated previously, the use of the positive displacement pump for the refrigerant loop allowed exact lubricant concentrations to be injected into the system for testing. The oil injection was accomplished by using a stainless steel double-actuating cylinder with a piston / diaphragm configuration. The cylinder had a 50.8 mm (2 in.) diameter with a 152.4 mm (6 in.) stroke length. The top port of the cylinder was used to introduce nitrogen gas and the bottom port was used to inject the oil into the system. Accommodations were made on all three sampling/injection systems to evacuate the air from the lines prior to using the equipment.

CHAPTER 7

EXPERIMENTAL PROCEDURE

OPERATING PARAMETERS

During condensation and pool boiling testing, several parameter ranges were fixed during rig operation. The heat flux range used in both modes of testing was 15 to 40 kW/m^2. The heat transfer rate was allowed to vary ± 0.30 kW while recording data values. The temperature difference between the water inlet and outlet (ΔT_w) was set at 2°C. This was allowed to vary ± 0.1°C during steady-state conditions. The value of 2°C was used for ΔT_w because lowering this value increased the uncertainty in the shell-side heat transfer coefficient to an unacceptable level. The operating saturation temperature in the test section for condensation was 40°C (103°F); for evaporation the saturation temperature was 2°C (35°F). This value was also allowed to vary ± 0.1°C.

Additional parameters that were set prior to taking data were the required heat fluxes and the corresponding mass flow rates. It was decided to take data at six different heat fluxes. Using the aforementioned heat flux range, data were obtained at 5 kW/m^2 intervals. The required water mass flow rate, $\dot{m}_w$, was calculated using Equation 7.1.

$$\dot{m}_w = \frac{q}{C_p \Delta T_w} \tag{7.1}$$

where ΔT_w is the temperature difference between the water inlet and outlet (set at 2°C). The required refrigerant mass flow rate, $\dot{m}_{ref}$, was found from

$$\dot{m}_{ref} = \frac{q}{h_{fg}}. \tag{7.2}$$

With these two equations, the required mass flow rates could be calculated for each heat flux. Table 7.1 illustrates these test parameters.

After steady-state conditions were reached, the system was allowed to run for 15 minutes prior to taking data. At each heat flux, ten data scans were taken (at one minute intervals) and written to the hard disk. When ten scans were obtained, the experiment was moved to the next heat flux setting and the procedure was repeated.

TABLE 7.1 Operating parameters for the test facility.

Heat Flux (kW/m^2)	Heat Transfer Rate (kW)	CFC-114 Mass Flow Rate (kg/min)	HFC-236ea Mass Flow Rate (kg/min)	Water Flow Rate (kg/min)
15	0.752	0.38	0.31	5.40
20	1.003	0.51	0.41	7.20
25	1.254	0.64	0.52	8.99
30	1.505	0.77	0.62	10.79
35	1.756	0.90	0.73	12.59
40	2.007	1.03	0.83	14.39

WILSON PLOT ANALYSIS

A Wilson plot analysis was conducted for each tube that was tested. This analysis was a necessary step prior to taking any condensation or pool boiling data so that the inside (tube-side) heat transfer coefficient could be determined. Chapter 6 shows that the shell-side heat transfer coefficient is determined through the LMTD approach. The use of this method requires that the water-side heat transfer coefficient be known. As mentioned in Chapter 4, the tubes that were used in this research were equipped with internal enhancements, and therefore, the tube-side heat transfer coefficients had to be determined experimentally.

The internal tube enhancements were necessary because in the low heat flux range, the required water mass flow rates were small, which caused the Reynolds number to be low and prevented the flow from being fully turbulent. This in turn resulted in a large tube-side heat transfer resistance compared to the shell-side resistance, which inhibited an accurate determination of the shell-side heat transfer coefficient. As a result, a spring-type turbulator was installed on the inside of each tube to provide the internal enhancement. The turbulators caused the flow to be continuously tripped to the turbulent region, thus enhancing the inner heat transfer coefficient, h_i. This produced the necessary Reynolds numbers for the water mass flow rates at the low end of the heat flux range. As stated previously, the tube-side resistance becomes much larger than the shell-side resistance at low Reynolds numbers which introduce large experimental error.

The procedure used to determine the tube-side heat transfer coefficient was to boil HFC-134a on the outside of the tube being tested [57]. This method required a constant heat flux and constant saturation

temperature throughout the test. The heat flux was held constant by controlling the immersion heater in the water loop. The test section saturation temperature was maintained by controlling the glycol temperature to the condenser, which resulted in keeping the pressure in the condenser constant (i.e., constant T_{sat}). While holding these values constant, the water flow rate on the inside of the tube was varied.

The saturation temperature was set at 2°C and was allowed to deviate no more than ± 0.1°C. The heat transfer rate was also held constant at 1.5 kW (30 kW/m^2), varying no more than ± 3%. The water flow rate was varied from 2 to 18 kg/min, or 0.033 to 0.30 kg/sec.

Data were recorded at each water mass flow rate while the system was at steady-state conditions. Ten data points were written to the disk in one minute intervals. The flow rate was increased by an increment of 0.5 kg/min from 2 to 12 kg/min. From 12 to 18 kg/min, data were taken at increments of 1 kg/min. The system was allowed to come to steady-state and remain there for 15 minutes before writing values to a file. Ten scans were taken at each point. The test run was repeated on the following day for each tube tested. During the repeat run, the water flow rate was increased in increments of 1 kg/min throughout the range. This repeat run was used to verify the validity of the data.

The governing equations for the Wilson Plot method were:

$$q = \dot{m}_w C_p (T_{wi} - T_{wo}) = U_o A_o LMTD \tag{7.3}$$

where

$$LMTD = \frac{T_{wi} - T_{wo}}{\ln\left[\frac{T_{wi} - T_{sat}}{T_{wo} - T_{sat}}\right]}, \tag{7.4}$$

$$\frac{1}{U_o} = \frac{A_o}{A_i}\frac{1}{h_i} + \frac{1}{h_o} + A_o R_w , \tag{7.5}$$

$$R_w = \frac{\ln(D_o/D_i)}{2\pi k_{wall} L}, \text{ and} \tag{7.6}$$

$$h_i = STC \frac{k_w}{D_i} Re^{0.8} Pr^{0.33} \left(\frac{\mu}{\mu_w}\right)^{0.14} . \tag{7.7}$$

When Equation 7.7 is substituted into Equation 7.5, it results in

$$\frac{1}{U_o} - A_o R_w = \frac{1}{h_o} + \frac{1}{STC} \frac{A_o/A_i}{\frac{k}{D_i} Re^{0.8} Pr^{0.33} \left(\frac{\mu}{\mu_w}\right)^{0.14}} . \quad (7.8)$$

Equation 7.8 can be put in the form of $Y = mX + b$, which is the equation for a straight line, where

$$X = \frac{A_o/A_i}{\frac{k}{D_i} Re^{0.8} Pr^{0.33} \left(\frac{\mu}{\mu_w}\right)^{0.14}} \text{ and} \quad (7.9)$$

$$Y = \frac{1}{U_o} - A_o R_w . \quad (7.10)$$

Therefore, the slope of the line (m) is the inverse of the required Sieder-Tate coefficient (STC), and the inverse of the intercept (b) is the shell-side heat transfer coefficient (h_o). The general equation used in the Wilson Plot analysis can be written as

$$Y = \frac{1}{STC} X + \frac{1}{h_o} . \quad (7.11)$$

At each specific water mass flow rate, data were recorded so X and Y could be calculated for each point. These values were then plotted on a linear scale, with m and b determined by fitting a line through the X-Y pairs. Ideally, the slope would remain constant over the entire range of the X parameter, which would produce a constant STC over the same range. For this method to be successful, the intercept of the line must be constant for all X-Y pairs. This was accomplished by maintaining a constant shell-side heat transfer coefficient throughout the test (h_o is the inverse of b). In pool boiling, the heat transfer coefficient is a function of heat flux and fluid properties, which is why care was taken during testing to hold the heat flux and the saturation temperature constant.

All tubes were tested with a water mass flow rate range of 2-18 kg/min. The X-Y pairs plotted for the plain, 26 fpi, and 40 fpi tubes remained linear throughout this range. The use of the STC requires that the Wilson plot data be linear. Therefore, to ensure that linearity was maintained throughout the heat flux range, the lower limit on the water flow rate was set at 5 kg/min. For consistency in the graphical presentation of the data, pool boiling and condensation tests were performed at flow rates above 5 kg/min for all tubes. With this limit, the low end of the heat flux range was constrained to 14 kW/m^2. As shown in Table 7.1, the heat flux range was set at 15 to 40 kW/m^2, which is consistent with industry standards.

The plain tube was tested with and without the inner enhancement (i.e., a turbulator). This was done to check the results without a turbulator against industry specifications. The plain tube without a turbulator insert produced a STC of 0.0247, which is within 8% of the manufacturer's value [57]. Figure 7.1 shows the plain tube results with and without a turbulator installed. The STC for the three tubes that were investigated in this research are summarized in Table 7.2.

TABLE 7.2 Sieder-Tate coefficient data for the four tubes of interest.

Tube Type	Sieder-Tate Coefficient
Plain tube without turbulator	0.0247
Plain tube with turbulator	0.0582
26 fpi tube with turbulator	0.0471
40 fpi tube with turbulator	0.0514

Figures 7.2 and 7.3 show the STC determination for the 26 fpi and 40 fpi tubes, respectively. The Reynolds number range for testing was 2,800 to 19,000. The STC appears to remain constant over the specified flow rate range for all of the tubes. The repeatability data during the Wilson plot analysis are also included in these plots.

GENERAL RIG OPERATION

This section covers the general procedures that were common to both condensation and pool boiling testing. Before charging the system with refrigerant, it was evacuated with a vacuum pump for 8 hours. In addition, the system was known to be free from leaks based on a thorough leak-check procedure when the facility was first built. Leak checks were repeated periodically by charging the rig with compressed air to 75 psig and monitoring the pressure loss in a 24-hour period. This check was also repeated if a component was added to the facility by isolating the specific section where a modification was made and charging it with nitrogen. Leak testing was performed by spraying soapy water (Snoop) which produces bubbles on the solder joint, compression fitting, etc. These areas where then observed for the presence of bubbles. There were several instances were leaks were detected by the loss of pressure, but no bubbles could be found. In these cases, a portable halogen leak detector was used to pin-point the leak.

For the procedure of changing the test tube, the test section was first isolated and the refrigerant was transferred into the condenser. The condenser valve was then closed and the test tube was removed. When the installation of a test tube was complete, the test section was charged with 75 psig of nitrogen. The leak detecting

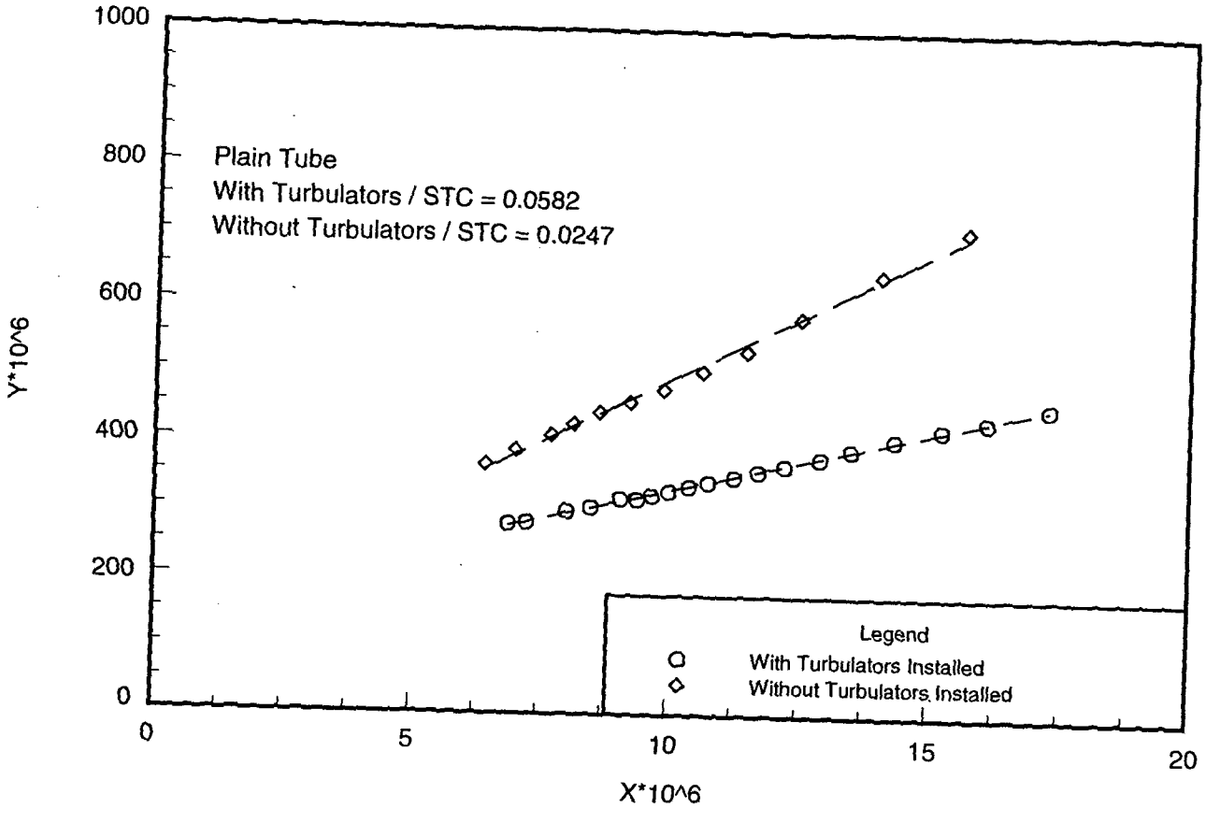

Figure 7.1 Wilson plot data for the plain tube with and without a turbulator installed

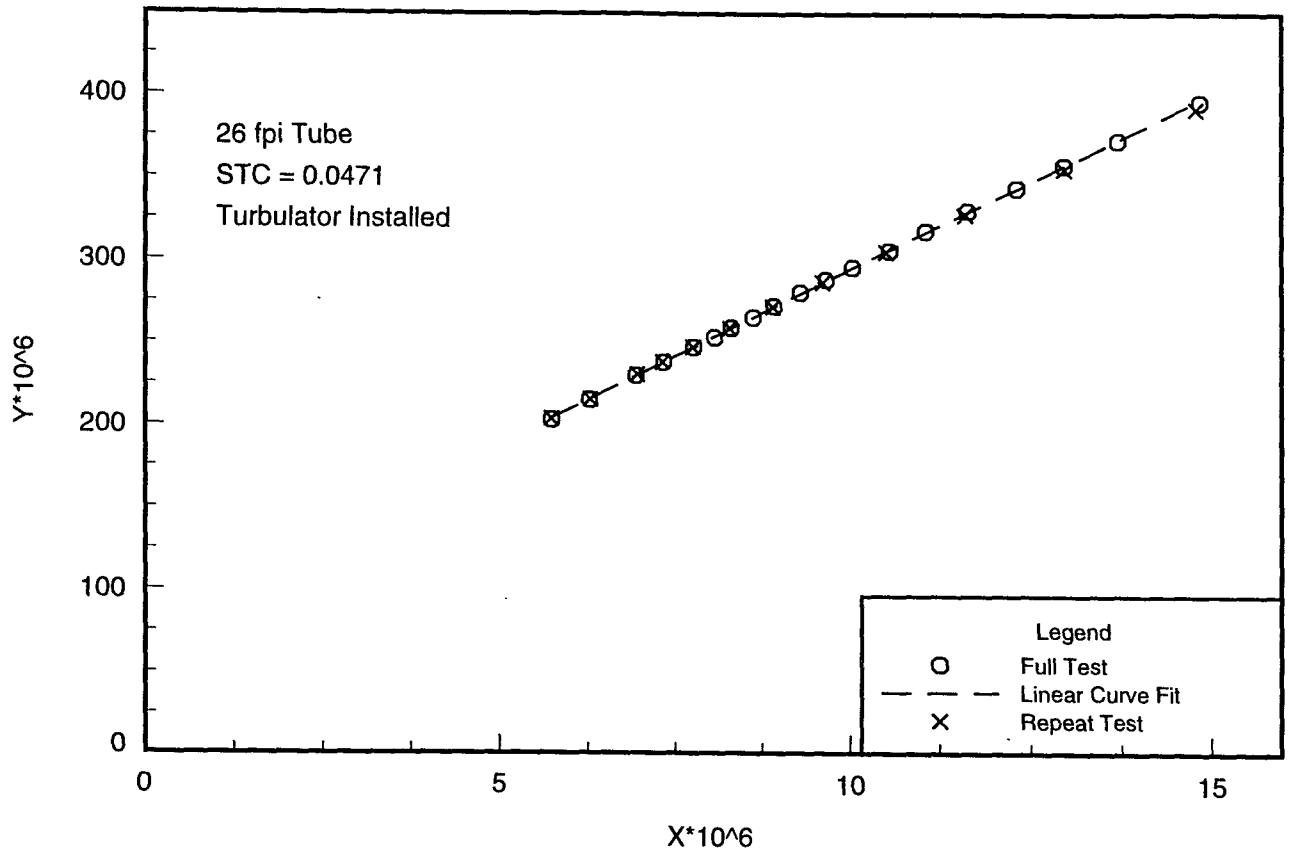

Figure 7.2 Wilson plot data for the 26 fpi tube with a turbulator installed

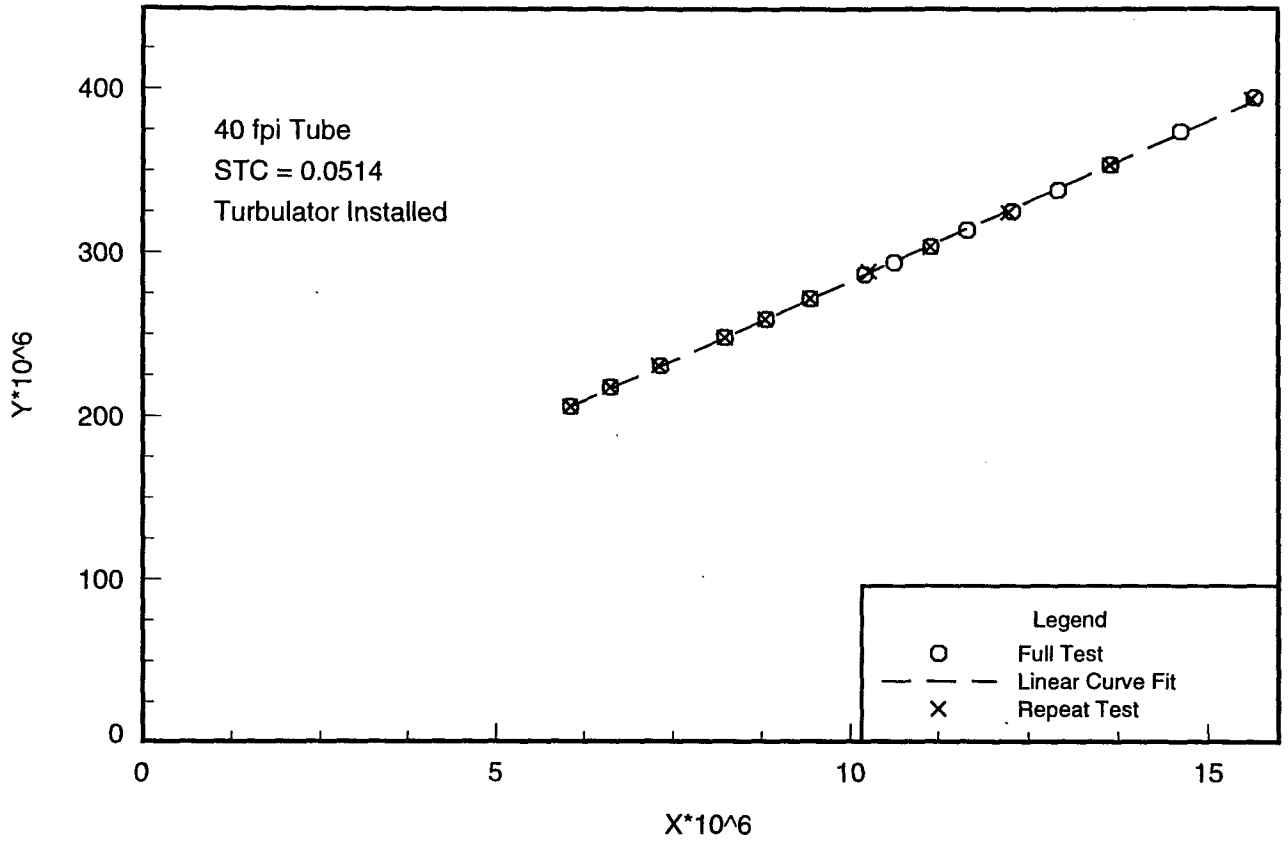

Figure 7.3 Wilson plot data for the 40 fpi tube with a turbulator installed

fluid was then sprayed on the compression fittings that sealed the tubes from the atmosphere. If no bubbles were present, the vacuum pump was attached, and the test section was evacuated for 4 hours. After the evacuation, the vacuum level was checked with the pressure transducer attached to the test section to ensure that all non-condensible gases were purged from the system.

After evacuation, the refrigerant was released back into the test section in preparation for condensation or pool boiling testing. When testing was completed, the system was shut down and allowed to sit overnight. Periodically, the saturation temperature, determined at the saturation pressure, was checked with the pool temperature of the test section after sitting idle for at least 12 hours. This was used as a check for the presence of noncondensible gases. If the deviation was more than $\pm$ 0.1°C, the system was degassed to eliminate the noncondensible gases.

The degassing cycle consisted of bringing the level of refrigerant over the tubes and boiling refrigerant on the outside of the tubes. The refrigerant was boiled at a T_{sat} of 10°C and the vapor was boiled off into the condenser. Once in the condenser, the refrigerant vapor would condense to liquid and fall to the bottom of the condenser, eventually being returned to the test section (evaporator) by gravity. The noncondensible gases (e.g. air) would remain at the top of the condenser. This procedure was continued for 4 hours to ensure that any air present in the system was now trapped in the top of the condenser. At this point, the system was shut down and the condenser was isolated by closing the vapor inlet and liquid outlet valves. A needle valve was attached to a port located at the top of the condenser on the opposite side of the vapor inlet. A reclaimer unit was hooked up to the degassing port and to a refrigerant cylinder and allowed to run for 15 minutes. When the reclaimer was in operation, it removed vapor from the condenser and expelled it into the refrigerant can. This process was used to purge all noncondensible gases from the system.

CONDENSATION PROCEDURES

Saturated Vapor Testing

At the beginning of a condensation test, the two water pumps were started and the water immersion heater was energized and set at the desired temperature. Then, prior to starting the refrigerant pump, glycol was allowed to circulate through the subcooler. Once the refrigerant started circulating, the boiler was turned on and the glycol valves to the water heat exchanger were opened. When the refrigerant began to enter the test section as vapor, the water and refrigerant mass flow rates were set for the first heat flux point as given in Table 7.1. The boiler power input was also set to correspond to the required energy transfer rate at that particular heat flux point.

After condensation began, the water inlet temperature at the test section was adjusted until the desired saturation temperature was obtained. T_{sat} was dictated by the inlet water temperature, which was controlled by the water immersion heater and the water heat exchanger. The outlet water temperature was set at 2°C above the inlet

temperature. A sight glass was placed in the vapor line before the test section to observe if the flow was fully vaporous. As stated in Chapter 4, a drip deflector was placed in the test section to block any liquid droplets carried with the vapor from striking the tube surface. The sight glass and the drip deflector ensured that only vapor was coming in contact with the test tube.

During saturated vapor testing, the vapor temperature was set such that the two thermistor probes in the test section agreed with the saturation temperature within $\pm$ 0.2°C. There was also a sightglass placed in the liquid outlet line of the test section. This was used to visually inspect if all of the refrigerant vapor was being condensed on the tube surface. If vapor was leaving the test section, a throttling valve after the sightglass was closed to correct the problem. Closing of the throttling valve would cause a slight change in the saturation temperature, which was corrected by changing the water temperature.

There was also a refrigerant reservoir installed within the loop. This was used to add additional refrigerant into the system at the higher heat fluxes. A valve attached to the incoming vapor line provided a high pressure in the top of the reservoir and a bottom valve was attached to the pump suction where refrigerant was added to the loop. The level was monitored through a plastic sight tube located on the outside of the reservoir.

After all adjustments were complete, the system was brought to a steady-state condition. The system was allowed to remain at steady-state for 15 minutes, after which 10 data scans were written to a file on the hard disk. When the required data were obtained for the heat flux point, the data acquisition control that writes data to the hard disk was turned off, and the system was moved to the next heat flux point. This was done by increasing the water and refrigerant mass flow rates, increasing boiler power, decreasing the water temperature, and increasing the glycol flow rate to the water heat exchanger. The data readings were recorded in order of increasing heat flux from 15 to 40 kW/m^2 in 5 kW/m^2 increments. The refrigerant saturation temperature in the test section was held constant throughout the heat flux range at 40°C $\pm$ 0.1°C.

During the recorded data scans, the parameters that were required in order to calculate the shell-side heat transfer coefficient were:

- the temperature of the refrigerant vapor entering the test section and the refrigerant liquid leaving the test section,
- the temperature of the water entering and exiting the test section,
- the refrigerant pressure within the test section, and
- the refrigerant and water mass flow rates.

Various other parameters were also measured during a data scan and displayed on the computer screen to aid in bringing the system to a steady-state condition.

After the data run was completed, the rig was shut down. A second test run was conducted the following day for both refrigerants and all tubes to demonstrate the repeatability in the test facility and the data gathering technique.

Superheated Vapor Testing

Data were also collected while condensing superheated vapor on the tube surfaces. During superheated vapor testing, there were only minor procedural changes as compared to the saturated vapor testing methods. Saturated vapor leaving the boiler exit entered the 19.1 mm (0.75 in.) ID copper pipe that contained two heat tapes wrapped on the outside. These heat tapes provided the additional energy to the vapor to superheat it. Once the vapor was condensing on the test tube, the superheater was energized and adjusted to give approximately 4°C of superheat to the vapor entering the test section. The energy transfer rate present in the test section was set by the energy output of both the boiler and the heat tapes. In addition, the two thermistor probes in the test section read approximately 4°C above the saturation temperature. The superheated vapor was allowed to enter the test section at 3°C to 5°C above T_{sat}.

POOL BOILING PROCEDURES

Pure Refrigerant Testing

Before pool boiling tests began, the test facility was charged with refrigerant. A larger refrigerant charge was required for pool boiling than for the condensation testing, and therefore, refrigerant was added until the level was at the top of the test section which ensured that the test section would act as a flooded evaporator.

To start up the pool boiling facility, the circulating of water around the closed loop was first initiated. The automatic temperature control unit for the water circulation heater was then set to the manual mode, which allowed the user to input the percentage of power required from the heater. At the same time, the glycol heater was energized and set for 3°C, while a three-way valve on the glycol return line was moved to 90% recirculation. These steps were taken so the refrigerant pressure would not drop drastically once the cold glycol was introduced into the condenser and refrigerant subcooler. Allowing the system to cool down slowly made it possible to achieve a positive flow rate from the refrigerant pump. If the system was cooled too quickly, a positive flow rate could not be acquired.

Once the positive flow rate was established, the pump speed control was set to output a 0.5 kg/min flow rate through the refrigerant mass flow meter. The refrigerant that passed through the pump then entered the test section at the top inlet ports. Liquid refrigerant also entered through the two liquid inlet ports located at the bottom of the test section. The refrigerant in the test section was vaporized, and traveled through the vapor outlets of the test section and into the condenser. The liquid refrigerant exiting the condenser was eventually split up into two streams. A portion of the refrigerant flowed through the subcooler and into the pump suction line, where it was circulated to the top of the test section. The remaining refrigerant returned directly up to the bottom of the test section. A portion of the incoming refrigerant to the test section was introduced at the top because it aided in maintaining a steady-state condition during data recording.

Glycol was pumped from the chiller unit through the condenser. The temperature of the glycol was controlled by the circulation heater and an automatic temperature control device before it entered the condenser. The flow rate was controlled by adjusting throttling valve. The temperature and flow rate of the glycol through the condenser set the pressure of the condenser on the refrigerant side. This condenser pressure subsequently controlled the test section saturation pressure, which was used to determine the saturation temperature.

During the initial start-up procedures, the saturation temperature was approximately 15°C. After flow into the test section had been established, T_{sat} was decreased to the working temperature of 2°C. This was accomplished by three procedures: 1) decreasing the temperature setting on the glycol circulation heater, 2) closing the three-way valve so a majority of the glycol was sent back to the chiller, and 3) increasing the glycol flow rate to the condenser. The saturation temperature was decreased slowly while at the same time adjusting the water flow rate and water heater to bring the system to the first heat flux point.

During pool boiling, data collection began at the highest heat flux point, 40 kW/m^2, and decreased in increments of 5 kW/m^2 throughout the data runs. This procedure was used to avoid any hysteresis effects in the data. It has been shown in the past that hysteresis effects are present when taking data with increasing heat flux [38]. Starting at a high heat flux ensures that full nucleate boiling will be present throughout the run. When starting at a low heat flux, the variation in the onset of nucleate boiling can affect the results.

Testing of pure refrigerants in pool boiling involved certain restrictions on the allowable variation in testing parameters during data recording. The restricted or controlled parameters were q, T_{sat}, ΔT_w, and the pool temperature (T_p). The first three parameters are outlined above. The pool temperature was found by averaging the readings from the two thermistors in the test section. During the rig's operation, this pool temperature was maintained at a deviation of no more than $\pm$ 0.2°C from the saturation temperature. This was to ensure that there was saturated boiling occurring in the test section.

When the system had reached a heat flux of 40 kW/m^2 and a saturation temperature of 2°C, steady-state conditions were obtained and allowed to remain in this state for 15 minutes before data were recorded. Data were obtained by the same method as the condensation procedures stated above. Once 10 data scans were obtained, adjustments were made to decrease the heat flux to the next point and acquire a steady-state condition again.

When the data runs were completed, the glycol pump and refrigerant pump were shut down. The water was allowed to remain circulating as a precaution against freezing the water in the test section. Once the test section temperature reached 10°C, the entire test facility was shut down.

Repeatability testing was also performed for pool boiling. A random selection of a tube for each oil concentration (0%, 1%, and 3%), and each refrigerant was conducted and the test was repeated the following day. The repeatability performance can be seen in Chapter 9.

Refrigerant / lubricant Mixture Testing

In addition to pure refrigerant testing in pool boiling, refrigerant / lubricant mixtures were also investigated. There were two modifications made to the boiling procedures when oil was present in the system. The procedures used for adding oil and sampling the mixture are presented in the section following this one.

The presence of oil mixed with the refrigerant changes the saturation temperature. For a desired saturation temperature, the required pressure is lower when a refrigerant / lubricant mixture is present than when there is only pure refrigerant (see Chapter 7 for detailed discussion of the solubility analysis). The data acquisition system calculated a saturation temperature for a given refrigerant from the test-section pressure using a two-degree polynomial equation that was fitted to pure refrigerant saturation data. Therefore, the calculated saturation temperature could not be used. Instead, the average pool temperature was used as a reading of the test-section saturation temperature. Most of the published research on boiling of refrigerant / lubricant mixtures states that data were obtained either at a constant saturation pressure, or using the pool temperature as T_{sat}. Using constant saturation pressure data would be equivalent to using the saturation temperature curve-fit equation for both pure and lubricant work without any solubility analysis incorporated into the calculation of T_{sat}.

The other alteration to the procedure for refrigerant / lubricant mixture work was verifying that the proper oil concentration was present. As stated in the following section, the amount of oil added was with respect to the mass of refrigerant in the test section only. In pool boiling, the refrigerant is boiled off and the oil remains in the test section. So, only enough oil was added to the system to bring the concentration in the test section to 1% or 3%. Prior to recording data values, the system was operated for 1 hour to ensure that all of the oil had migrated into the test section.

After testing was completed with a given oil, the refrigerant / lubricant mixture was distilled in preparation for testing of a different refrigerant / lubricant mixture. The distilling procedure consisted of allowing the system to operate long enough so all of the oil was in the test section. The test section was then isolated and the refrigerant / lubricant mixture was drawn out through a charge valve in the liquid outlet line. The mixture was then transferred to a second refrigerant can through the vapor ports. This would allow only the refrigerant to be transferred, with the oil being left in the original can. The pure refrigerant was then charged back into the system.

This procedure was repeated five times and then a sample was drawn to verify that all of the oil was out of the rig. The refrigerant in the test facility was considered pure when the sample produced an oil concentration of 0.05% or less. Great care was taken to distill all of the oil out of the system so that it would not affect any future tests of pure refrigerant.

Lubricant Injection/Sampling

The lubricant was injected with the piston / cylinder described in Chapter 4. The oil was brought into the cylinder and evacuated with a vacuum pump for 4 hours to remove all of the air. When this was completed, the cylinder was attached to the port on the pump discharge line. Initially, only a small amount of oil was added and a sample was drawn from the test section. This defined the additional amount of oil needed to bring the test section concentration to 1%. The exact amount of oil to be injected was found by dividing the mass of oil in the cylinder by the length of displacement of the piston shaft. This offered a value in gm/cm for the piston injection. Nitrogen gas was used to provide the pressure for injecting the oil into the system.

When the proper amount of oil had been injected, a sample was drawn from the test section. The procedure for drawing a sample was to bring the system to a heat flux of 25 kW/m^2 and allow it to operate for 1 hour to ensure that all of the oil had migrated to the test section. During pool boiling, only the refrigerant experiences a phase change. The refrigerant is boiled off as vapor, while the oil remains in the test section. For this reason, the amount of oil added to the system for the desired concentration was with respect to the mass of the refrigerant in the test section only.

When the system had been operated for one hour, the test section was isolated with a pool of refrigerant / lubricant mixture. The double actuating cylinder was attached to a port on the test section, and nitrogen gas was used to apply a back-pressure to the piston. The water heater was set to 30°C and the water continued to circulate. This was continued until the test section temperature was at steady-state and 30°C. The higher temperature of the refrigerant / lubricant mixture and the fact that the nitrogen gas was bled off slowly allowed the sample to be drawn without it flashing into a two-phase mixture.

The average sample size was approximately 75 grams of the refrigerant / lubricant mixture. When it was thought that the proper concentration existed in the test section, two samples were drawn from the mixture to verify the correct oil concentration.

After the samples were taken, the sampling cylinder was weighed and the value recorded. The refrigerant was then bled off slowly from the mixture using a throttling valve. For added protection, the refrigerant leaving the throttling valve passed through a cloth filter before venting to the atmosphere. The filter was used to catch any lubricant that was carried with the escaping refrigerant vapor. A sample of 75 grams would require approximately 2 hours to vent off the refrigerant component.

The cylinder was then evacuated with a vacuum pump for 1/2 hour to remove any refrigerant that was absorbed into the oil. Weights were recorded at the empty, full, and evacuated stages of the sampling process. These recorded values were used with *ASHRAE Standard 41.4-1984* [58] to calculate the mass fraction of lubricant, with the exception that the sample size was smaller than that stated in the standard. The weights were measured with an electronic scale that has an accuracy of $\pm$ 0.01 g.

CHAPTER 8

DATA ANALYSIS

This chapter presents the governing equations used to calculate the heat transfer performance and the experimental uncertainty. Ten data scans were obtained for each heat flux, and a FORTRAN program was then used to reduce the data. Appendix E contains a copy of the post-processing program. The resulting data from this program were loaded into a spreadsheet, where the values were first inspected for any anomalies. The data were then combined to produce an average value for each parameter at a given heat flux.

DATA REDUCTION

The general procedure for reducing the raw data readings is similar for both condensation and pool boiling, with only minor differences in the governing equations. Both modes of heat transfer incorporate an LMTD method of calculating the shell-side heat transfer coefficient.

Condensation

The shell-side heat transfer coefficient was calculated using the LMTD method. The parameters pertinent to this method are the water inlet and outlet temperatures, which were measured by thermistors. In addition, the test section saturation temperature was also required, which is the measured test section pressure obtained from a curve-fit equation for the temperature-pressure relationship at saturation conditions for either of the two refrigerants. The governing equations for this method during condensation are as follows:

$$q = U_o A_o \, LMTD, \tag{8.1}$$

where the log-mean temperature difference (LMTD) is defined as

$$LMTD = \frac{T_{wo} - T_{wi}}{\ln\left[\frac{T_{sat} - T_{wi}}{T_{sat} - T_{wo}}\right]}. \tag{8.2}$$

The energy transfer rate can be calculated from either the water side or the refrigerant side rate. If the water-side data are used, the energy transfer is calculated by

$$q = \dot{m}_w c_p \Delta T_w \tag{8.3}$$

where ΔT_w is defined as $T_{wo} - T_{wi}$ for condensation. If the refrigerant side is used, then the energy transfer is found from

$$q = \dot{m}_{ref} h_{fg} . \tag{8.4}$$

The separation of the individual thermal resistances from the overall thermal resistance is necessary to calculate the shell-side heat transfer coefficient. The overall heat transfer coefficient (U_o) is given by

$$\frac{1}{U_o} = \frac{A_o}{A_i}\frac{1}{h_i} + \frac{1}{h_o} + A_o R_w \tag{8.5}$$

where

$$R_w = \frac{\ln\left(\frac{D_o}{D_i}\right)}{2\pi k L} . \tag{8.6}$$

Referring to the equations in Chapter 5, the water-side heat transfer coefficient is found through the use of the Sieder-Tate correlation [19].

$$Nu = STC\, Re^{0.8}\, Pr^{0.33} \left(\frac{\mu_h}{\mu_w}\right)^{0.14} = \frac{h_i D_i}{k_w} . \tag{8.7}$$

By rearranging Equation 8.5 and using Equations 8.1, 8.6, and 8.7 to calculate U_o, R_w, and h_i, respectively, the shell-side condensation coefficient can then be found from

$$h_o = \left[\frac{1}{U_o} - \frac{A_o}{A_i}\frac{1}{h_i} - A_o R_w\right]^{-1} . \tag{8.8}$$

The other parameter that is of importance to the post-processing program is the shell-side wall temperature (T_w). This parameter is used to illustrate the effect of the required wall superheat on the heat transfer performance. In condensation, ΔT is equal to $T_{sat} - T_w$. The outer tube wall temperature can be found from

$$T_w = T_b + q\left[\frac{1}{\pi D_i L h_i} + \frac{\ln(D_r / D_i)}{2 \pi k_w L}\right] \tag{8.9}$$

where T_b is the bulk water temperature defined by $T_b = (T_{wi} + T_{wo})/2$ and D_r is the root diameter of the tube. Another equation that can be used to calculate the wall temperature is

$$T_w = \frac{T_b + T_{ref}}{2}. \tag{8.10}$$

The value of T_{ref} is defined as the bulk refrigerant pool temperature and is found by averaging the temperatures from the two thermistors within the test section. Equations 8.1 - 8.10 constitute the majority of calculations required in solving the shell-side heat transfer coefficient in condensation. The data reduction used during pool boiling is found in the following section.

Pool Boiling

The general method for calculating the shell-side heat transfer coefficient in pool boiling is the same as presented above for condensation. The only differences are found in the calculation of the LMTD and ΔT. During pool boiling, the water inlet and outlet temperatures and the tube wall temperature are both above the saturation temperature of the refrigerant pool. The log mean temperature difference is found from

$$LMTD = \frac{T_{wi} - T_{wo}}{\ln\left[\frac{T_{wi} - T_{sat}}{T_{wo} - T_{sat}}\right]} \tag{8.11}$$

and the excess temperature is defined by $\Delta T = Tw - Tsat$.

EXPERIMENTAL UNCERTAINTY

In all experimental investigations, there always exists uncertainties in the measurements. The uncertainties in the shell-side heat transfer coefficients were determined with a propagation-of-error analysis [59]. The general form of the equation used to calculate experimental uncertainty is given by

$$W_r = \left[\left(\frac{\partial R}{\partial x_1} w_1\right)^2 + \left(\frac{\partial R}{\partial x_2} w_2\right)^2 + ... + \left(\frac{\partial R}{\partial x_n} w_n\right)^2\right]^{1/2} \qquad (8.12)$$

where:

R is the result of the calculation,

W_r is the uncertainty of the result R,

$x_1, x_2, ..., x_n$ are the measured independent variables, and

$w_1, w_2, ..., w_n$ are the uncertainties in the measured variables.

The equation for the shell-side heat transfer coefficient, h_o, given in Chapter 8 can be manipulated algebraically to produce the following equation:

$$h_o = \frac{1}{A_o}\left[\frac{1}{\dot{m}_w C_p \ln\left(\frac{T_{sat} - T_{wo}}{T_{sat} - T_{wi}}\right)} - \frac{1}{h_i A_i} - \frac{\ln (D_o/D_i)}{2\pi L k}\right]^{-1} \qquad (8.13)$$

Therefore, the uncertainty in h_o is dependent on six variables: $\dot{m}_w$, C_p, T_{wi}, T_{wo}, T_{sat}, and h_i. The other terms in Equation 8.13 are constants for a given test tube.

Combining Equations 8.12 and 8.13, the uncertainty in the shell-side heat transfer coefficient is defined by

$$\delta h_o = \left[\left(\frac{\partial h_o}{\partial \dot{m}_w}(\delta \dot{m}_w)\right)^2 + \left(\frac{\partial h_o}{\partial h_i}(\delta h_i)\right)^2 + \left(\frac{\partial h_o}{\partial C_p}(\delta C_p)\right)^2 + \right.$$

$$\left.\left(\frac{\partial h_o}{\partial T_{sat}}(\delta T_{sat})\right)^2 + \left(\frac{\partial h_o}{\partial T_{wo}}(\delta T_{wo})\right)^2 + \left(\frac{\partial h_o}{\partial T_{wi}}(\delta T_{wi})\right)^2\right]^{1/2} \qquad (8.14)$$

where $\delta\dot{m}_w$ is the uncertainty of the water mass flow rate, δh_i is the uncertainty of the tube-side heat transfer coefficient, and δC_p is the uncertainty of the water's specific heat, which is calculated with the bulk water temperature, T_b. The remaining three δ terms pertain to uncertainties in temperature measurements, specifically the saturation temperature, water outlet, and water inlet temperatures.

Applying these partial derivatives to Equation 8.13 results in the following equations that calculate each parameters contribution to the uncertainty in the shell-side heat transfer coefficient.

$$\chi = -1\left[\frac{A_o}{\dot{m}_w C_p \ln\left(\frac{T_{sat} - T_{wo}}{T_{sat} - T_{wi}}\right)} - \frac{A_o}{A_i h_i} - \frac{A_o \ln (D_o/D_i)}{2\pi L k}\right]^{-2} \tag{8.15}$$

$$\frac{\partial h_o}{\partial \dot{m}_w} = \chi\left[\frac{-A_o}{\dot{m}_w^2 C_p \ln\left(\frac{T_{sat} - T_{wo}}{T_{sat} - T_{wi}}\right)}\right] \tag{8.16}$$

$$\frac{\partial h_o}{\partial h_i} = \chi\left(\frac{A_o}{h_i^2 A_i}\right) \tag{8.17}$$

$$\frac{\partial h_o}{\partial C_p} = \chi\left[\frac{-A_o}{\dot{m}_w C_p^2 \ln\left(\frac{T_{sat} - T_{wo}}{T_{sat} - T_{wi}}\right)}\right] \tag{8.18}$$

$$\frac{\partial h_o}{\partial T_{sat}} = \chi \frac{Ao}{\dot{m}_w C_p}\left[\frac{-1}{\left(\ln \frac{T_{sat} - T_{wo}}{T_{sat} - T_{wi}}\right)^2}\right]\left(\frac{-1}{T_{sat} - T_{wi}} + \frac{1}{T_{sat} - T_{wo}}\right) \tag{8.19}$$

$$\frac{\partial h_o}{\partial T_{wo}} = \chi \frac{Ao}{\dot{m}_w C_p}\left[\frac{-1}{\left(\ln \frac{T_{sat} - T_{wo}}{T_{sat} - T_{wi}}\right)^2}\right]\left(\frac{-1}{T_{sat} - T_{wo}}\right) \tag{8.20}$$

$$\frac{\partial h_o}{\partial T_{wi}} = \chi \frac{Ao}{\dot{m}_w C_p}\left[\frac{-1}{\left(\ln \frac{T_{sat} - T_{wo}}{T_{sat} - T_{wi}}\right)^2}\right]\left(\frac{1}{T_{sat} - T_{wi}}\right) \tag{8.21}$$

The largest contributor to the uncertainty in h_o comes from the uncertainty in the water mass flow rate. The three temperature uncertainties also make a significant contribution. The other two partial derivatives have a negligible effect on the heat transfer coefficient's uncertainty. It should be noted that the above equations for calculating the uncertainty apply to condensation. To calculate the uncertainty in the boiling coefficient, the temperature differences need to be switched: $T_{wi} - T_{sat}$ and $T_{wo} - T_{sat}$.

The calculations for the shell-side heat transfer coefficient's uncertainties were implemented into the post-processing program found in Appendix E. In addition to reducing the raw data, the program also calculates the corresponding uncertainties. The uncertainties are presented as a percentage of the calculated heat transfer coefficient, and are defined as $\delta h_o/h_o \times 100$. Table 8.1 presents the propagation-of-error uncertainties in the shell-side heat transfer coefficient for condensation of CFC-114 and HFC-236ea. For brevity, only the uncertainties at

the highest and lowest heat fluxes are presented. The uncertainties at the other heat flux points fall within this range.

Table 8.1 shows that the uncertainties in the 26 fpi and 40 fpi tubes are similar. Both tubes had higher heat transfer coefficients than the plain tube, which results in higher uncertainty values. It should be noted that the repeatability analysis conducted for condensation showed that the data for all tubes were repeatable within 2% to 6%.

Table 8.2 summarizes the uncertainty found in pool boiling of the pure refrigerants. The 26 fpi and 40 fpi tubes always produced higher uncertainty values than the plain tube because of the higher heat transfer performance of the finned tubes. The tests conducted with oil concentrations of 1% and 3% showed similar trends in

TABLE 8.1: SHELL-SIDE HEAT TRANSFER COEFFICIENT UNCERTAINTY FOR CONDENSATION OF SATURATED VAPOR

Tube Surface	CFC-114 15 kW/m^2 (percent)	CFC-114 40 kW/m^2 (percent)	HFC-236ea 15 kW/m^2 (percent)	HFC-236ea 40 kW/m^2 (percent)
Plain tube	3.2	2.9	4.3	3.6
26 fpi tube	10.9	5.1	11.7	6.0
40 fpi tube	11.6	5.8	11.4	6.1

the uncertainty. The repeat tests performed during pool boiling showed that the variability in the repeatability analysis was within 3% to 6% of initial test results.

TABLE 8.2: SHELL-SIDE HEAT TRANSFER COEFFICIENT UNCERTAINTY FOR POOL BOILING OF PURE REFRIGERANTS

Tube Surface	CFC-114 15 kW/m^2 (percent)	CFC-114 40 kW/m^2 (percent)	HFC-236ea 15 kW/m^2 (percent)	HFC-236ea 40 kW/m^2 (percent)
Plain tube	5.6	4.8	7.1	5.1
26 fpi tube	6.9	5.7	10.1	6.9
40 fpi tube	6.2	5.4	8.1	6.2

The instrumentation accuracy for the test facility is summarized below. The thermistors and thermo-couples were calibrated with a constant temperature bath in the required testing range. The test section pressure transducer was calibrated with a dead-weight test.

Thermistor temperatures	±0.05°C
Thermocouple temperatures	±0.20°C
Water mass flow meter	±0.20 %
Test-section pressure transducer	±0.76 %

DATA PRESENTATION

This section outlines the formats used in presenting the data to identify trends and evaluate comparisons of the data. During condensation, the research focused on the effects of heat flux and surface enhancement of the two refrigerants on the shell-side heat transfer coefficient. The effects of the heat flux are presented by plotting heat transfer coefficient versus heat flux. A single plot of all three tubes with one refrigerant is used to show the effects of surface enhancement. Also, specific tubes are plotted for both refrigerants to compare the performance of CFC-114 and HFC-236ea.

During pool boiling, the study focused on the effects of heat flux, surface enhancement, and lubricant concentration on the shell-side heat transfer coefficient. The heat flux, surface enhancement, and refrigerant comparison are all plotted in an identical manner to condensation. In addition to these plots, the lubricant effects are illustrated by plotting all three concentration (0, 1, 3%) for a given tube and refrigerant.

The majority of the data are presented by the heat transfer coefficient versus heat flux plot. Other plots include heat transfer coefficient versus temperature difference (LMTD or ΔT). This shows trends for the required wall superheat. Plots of the data for condensation and pool boiling are found in Chapters 8 and 9, respectively.

CHAPTER 9

SOLUBILITY ANALYSIS

As stated previously, this research was concerned with not only pool boiling of pure refrigerant, but also with the effects of refrigerant / lubricant mixtures in a flooded refrigerant evaporator. Compressors used in vapor-compression refrigeration systems require oil for lubrication. The oil used in the compressor is miscible with the refrigerant, which results in a binary mixture. It has been shown that the addition of oil can have significant effects on the pool boiling performance (see Chapter 3). Therefore, it is important to study the influences of known oil concentrations on the heat transfer performance.

The solubility of a refrigerant / lubricant mixture is defined as the relationship among the saturation temperature, saturation pressure, and the lubricant concentration. As oil is introduced into the refrigerant, the saturation temperature increases for a given pressure. Webb [52] notes that as the oil concentration is increased, the bubble point is increased beyond that of pure refrigerant. Since this research incorporates an LMTD approach to calculate the shell-side heat transfer coefficient, it is necessary to account for the solubility effects on T_{sat}.

The two basic techniques for taking pool boiling data with a refrigerant / lubricant mixture are constant pressure and constant temperature. The constant pressure technique can be used by taking data at a constant saturation pressure and using the solubility data to correct for the saturation temperature before calculating the log mean temperature difference.

The investigators selected the constant temperature technique for this study. This was accomplished by calculating the average test section temperature from the two thermistor probes and using that as the saturation temperature. The saturation temperature that was calculated by the data acquisition system from the test section pressure produced values above the pool temperature, which was expected from the solubility analysis. The data acquisition system calculates the saturation temperature from a curve-fit equation for P_{sat} of pure refrigerant. Using this T_{sat} and holding it constant while taking data would produce constant pressure data.

During pool boiling of pure refrigerant, the saturation temperature from the test section pressure was used and allowed to deviate no more than ± 0.1°C from the required T_{sat} of 2°C. As stated above, while testing refrigerant / lubricant mixtures, the average pool temperature was used as T_{sat} and the maximum allowable deviation for this temperature was also ± 0.1°C.

A solubility analysis was conducted for each refrigerant / lubricant mixture that was tested to evaluate the oil effects on the saturation temperature. This involved testing of CFC-114 and HFC-236ea with a miscible oil in

concentrations of 1% and 3%. The oil used with CFC-114 was the mineral oil York "C", which has a viscosity of 315 SUS (68 centistokes at 40°C). The oil used with HFC-236ea was Castrol SW-68 polyol-ester oil, which has a viscosity of 340 SUS at 100°F. The range of the solubility tests was 0°C to 5°C.

SOLUBILITY TEST FACILITY

The test facility used in the solubility analysis was designed for solubility/miscibility testing of refrigerant / lubricant mixtures. Eckels [60] offers a detailed description of the test facility. Each test cell consisted of a double-port, seal-cap type liquid indicator, which is essentially a 31.8 mm pipe cross with sight windows screwed into opposite ports. The side ports allow for complete visibility of the refrigerant / lubricant mixture. A refrigerant charge valve and a pressure transducer are attached to the two remaining ports for charging of refrigerant and monitoring cell pressure. The same pressure transducer was used throughout the testing of each individual refrigerant to eliminate transducer bias in the solubility data.

The test cell was placed in a constant temperature bath to control cell temperature. The bath is capable of operating in a temperature range of -20°C to +50°C. The temperature of the bath was measured with a high precision mercury thermometer calibrated to ±0.05°C.

The testing was conducted in a temperature range of 0°C to 5°C, which satisfied the required pool boiling saturation temperature. The oil concentrations investigated were 0%, 1%, and 3% by mass fraction. Once a steady-state condition existed, the test cell pressure was recorded. The temperature of the bath was also recorded, which is measured by two internal resistance temperature detectors (RTD). Data were recorded in increments of 1°C. The data at 1% oil concentration was repeated for both refrigerants to verify the validity of the results.

SOLUBILITY DATA

Solubility data are presented for CFC-114 and HFC-236ea at lubricant concentrations of 0%, 1%, and 3%. Since the constant temperature method was used during testing of refrigerant / lubricant mixtures, solubility data were not needed to calculate the shell-side heat transfer coefficients. However, the analysis does illustrate how the saturation temperature is affected by the addition of oil and shows the amount that T_{sat} is increased for a given pressure. In this study, the solubility data were used to calculate how much the saturation temperature was increased with the addition of oil. This allowed T_{sat} to be compared to the pool temperature as a check for the presence of noncondensible gases in the system (see Chapter 6).

Figures 9.1 and 9.2 are plots of the solubility data with temperature versus pressure. A pure refrigerant run was needed as a baseline for the 1% and 3% tests. With the pure refrigerant data, an offset can be calculated with respect to the 1% and 3% curves. In general, these plots show that the saturation temperature increases for a specific oil concentration at a given pressure.

Figure 9.1 is the solubility analysis for CFC-114 (also designated R-114). It shows a significant increase in T_{sat} even at the 1% concentration. Because these results were unexpected, the data were repeated four times with two different pressure transducers. An additional oil concentration of 0.5% was also added to determine if the results were valid. Since each test run produced the same results, the analysis is considered to be correct. At an oil concentration of 1%, the saturation temperature of the mixture rises approximately 0.75°C at a constant pressure.

Figure 9.2 is the solubility analysis for HFC-236ea (also designated R-236ea). The 1% oil concentration has negligible effect on the saturation conditions for the HFC-236ea / polyol ester oil mixture. At several locations on the graph, the temperature values for a 1% concentration fall below that of pure HFC-236ea. These errors are within the accuracy of the measurement. The 3% concentration only increases T_{sat} by 0.2°C. Therefore, the addition of a polyol-ester oil with HFC-236ea has a much smaller effect on the saturation temperature than the addition of a mineral oil has on CFC-114.

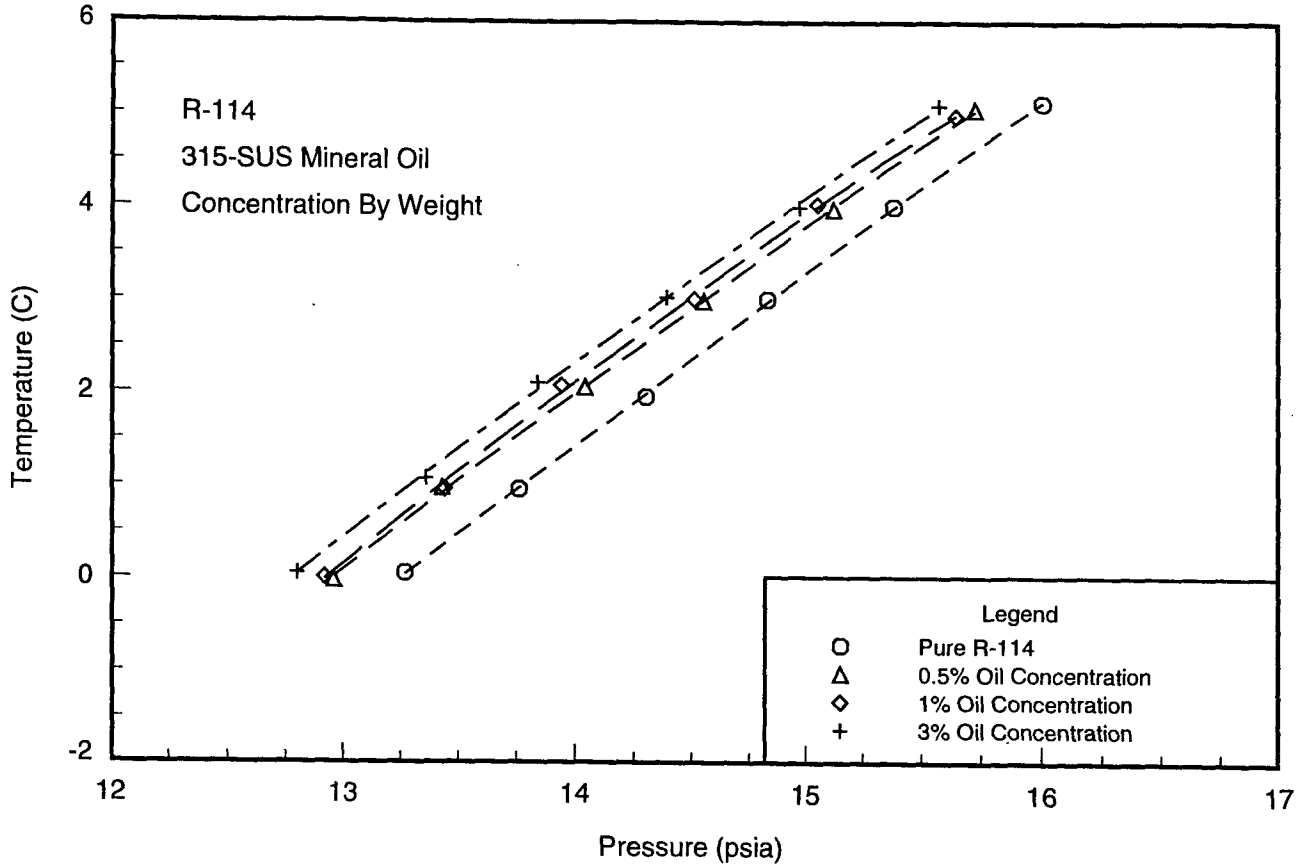

Figure 9.1 Solubility data for CFC-114 and a mineral oil with a viscosity of 315 SUS

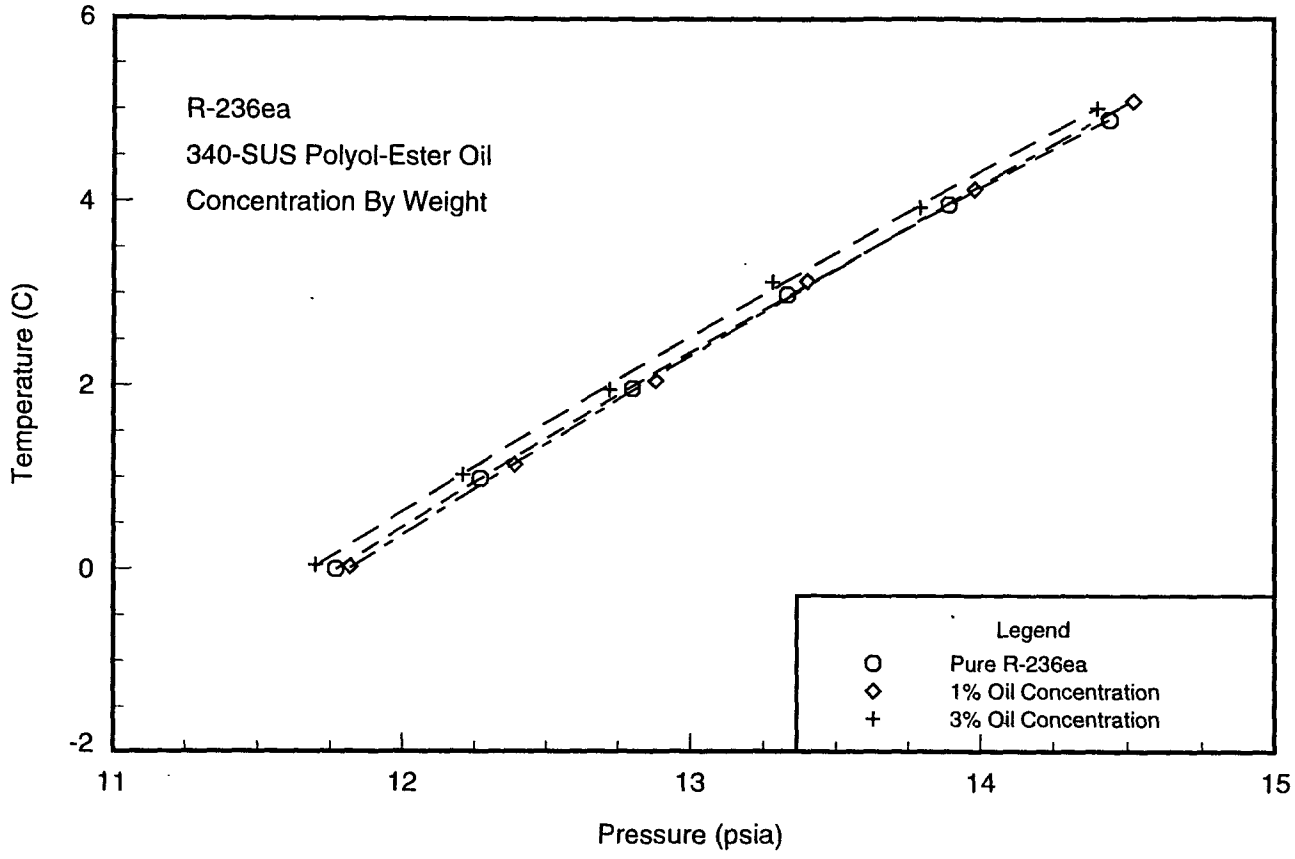

Figure 9.2 Solubility data for HFC-236ea and a polyol-ester oil with a viscosity of 340 SUS

CHAPTER 10

CONDENSATION RESULTS

Heat transfer results are presented for condensation of CFC-114 and HFC-236ea on a plain, 26 fpi, and 40 fpi tube surface. These include data for condensation of both saturated and superheated vapor to investigate the effects on the shell-side heat transfer coefficient. Only saturated vapor results are presented for HFC-236ea. Published correlations are also presented for a comparison with the experimental data from this study.

The refrigerant HFC-236ea is considered to be a potential replacement of CFC-114. For this reason, condensation testing was conducted on both refrigerants, where CFC-114 data represents a baseline for comparison of HFC-236ea. The designer can compare the two refrigerants and assess whether HFC-236ea is a viable replacement. The same holds true for the purpose of testing the plain tube surface. Normally, conventional refrigeration systems do not use the plain tube surface for shell-side condensation. However the plain tube acts as a reference for evaluating the enhancement gained in the integral-fin surface or an enhanced condensation surface.

The tubes tested during condensation all had a nominal outer diameter of 19.1 mm. The exact tube specifications are given in Appendix C. The shell-side heat transfer coefficients that are presented in this chapter are based on the outside surface area of a corresponding smooth tube, with the outer diameter being measured over the fins. Therefore, the calculated heat transfer coefficient (h_o) takes into account the area enhancement and the fin efficiency for the integral-fin tubes tested. The corresponding values for all plotted data points found in this chapter are tabulated in Appendix A.

HEAT TRANSFER RESULTS

Heat transfer coefficients are presented for pure CFC-114 and HFC-236ea condensing on a plain, 26 fpi, and 40 fpi tube surface. During saturated vapor testing, the test section saturation temperature was held constant at 40°C ±0.1°C. The corresponding saturation pressures for CFC-114 and HFC-236ea are 339.41 kPa and 336.50 kPa, respectively. For condensation of superheated vapor, the saturation temperature was also 40°C, but the incoming vapor was 3°C to 5°C higher than T_{sat}.

Saturated Vapor

Figure 10.1 shows the condensation performance for CFC-114 (also designated R-114). As expected, the two finned tubes outperformed the plain tube surface. At the lowest heat flux point, the 26 fpi tube and the 40 fpi tube have approximately the same condensation coefficient. At this same heat flux, the heat transfer coefficient for the plain tube is approximately four times lower than that of the finned tubes. Due to the poor performance of the plain tube, it could only be tested up to 35 kW/m^2. At 40 kW/m^2, the required coolant water temperature was below freezing. As the heat flux was increased, the 40 fpi tube produced slightly higher condensation coefficients than the 26 fpi tube. At the highest heat flux, the 40 fpi tube has a 9% higher heat transfer coefficient than the 26 fpi tube.

The plain tube condensation coefficients show a decrease with increasing heat flux. Generally, as the heat flux is increased, the condensate film becomes thicker on the tube surface. This causes an increase in the resistance to heat transfer. However, the 26 fpi and 40 fpi tubes show an increase in the heat transfer coefficient as heat flux increases. This trend is also seen for condensation of HFC-236ea. As stated in Chapter 2, Huber [18] conducted condensation experiments on four enhanced tube bundles with four refrigerants. These results showed that three of the tube surfaces tested produced increasing condensation coefficients with an increase in heat flux for CFC-11. Two of the tube bundles that exhibited this trend were the 26 fpi and 40 fpi tube surfaces. The fourth tube bundle, which was the Turbo-Cii tube surface, had increasing condensation coefficients from 18 kW/m^2 to 24 kW/m^2. At higher heat fluxes, the heat transfer coefficient decreased.

For condensation of CFC-114, the 40 fpi tube had the highest heat transfer performance, but it was only slightly above the 26 fpi tube. This may be due in part to the shorter fin height of the 40 fpi tube. A shorter fin may have less capillary action, which would allow the condensate to drain easier. Also, the 40 fpi tube used in this study had a slightly larger surface area per unit length than the 26 fpi tube (see Appendix C).

Figure 10.2 shows the heat flux versus the temperature difference, ΔT, for the three tubes tested. Both the 26 fpi tube and the 40 fpi tube produced similar ΔT values at given heat fluxes. The temperature difference for condensation is defined by $T_{sat} - T_w$. As previously mentioned, the wall temperature is calculated, not directly measured. The plain tube surface is also plotted on this figure. The plot shows that for a given heat flux, the required temperature difference for the plain tube is over three times that needed for the finned tubes. A large temperature difference causes an increased heat transfer rate, but a decreased heat transfer coefficient.

Figure 10.3 shows the log mean temperture difference effect on the heat transfer coefficient for CFC-114. For a given LMTD, the average shell-side heat transfer coefficient for the 40 fpi tube is higher than for the 26 fpi tube for condensation of CFC-114, but both produce similar LMTD values. As shown in Figure 10.2, the plain tube required significantly higher temperature differences than the two finned tubes at comparable heat fluxes. Each data point corresponds to a heat flux value from 15 to 40 kW/m^2.

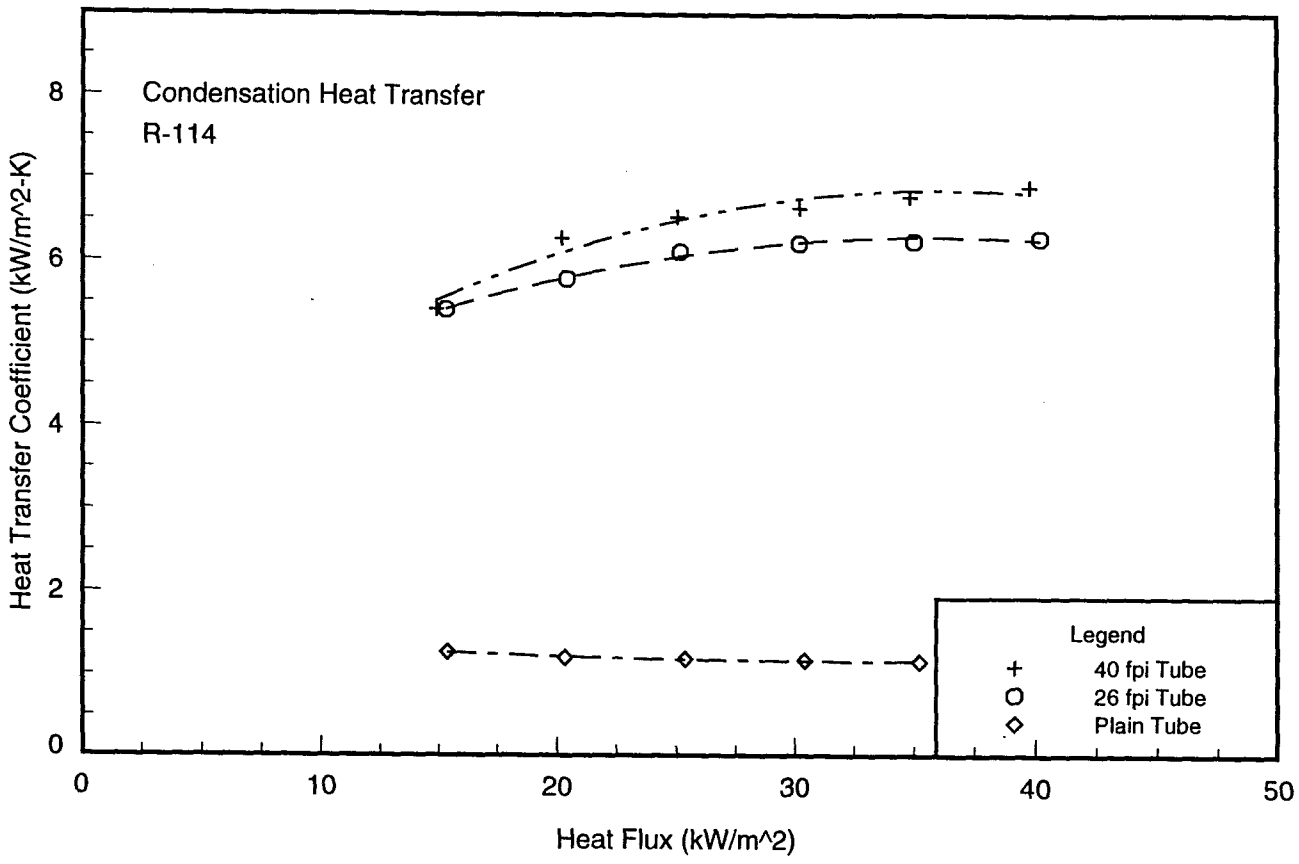

Figure 10.1 Condensation heat transfer coefficient for CFC-114 at $T_{sat} = 40^{o}C$

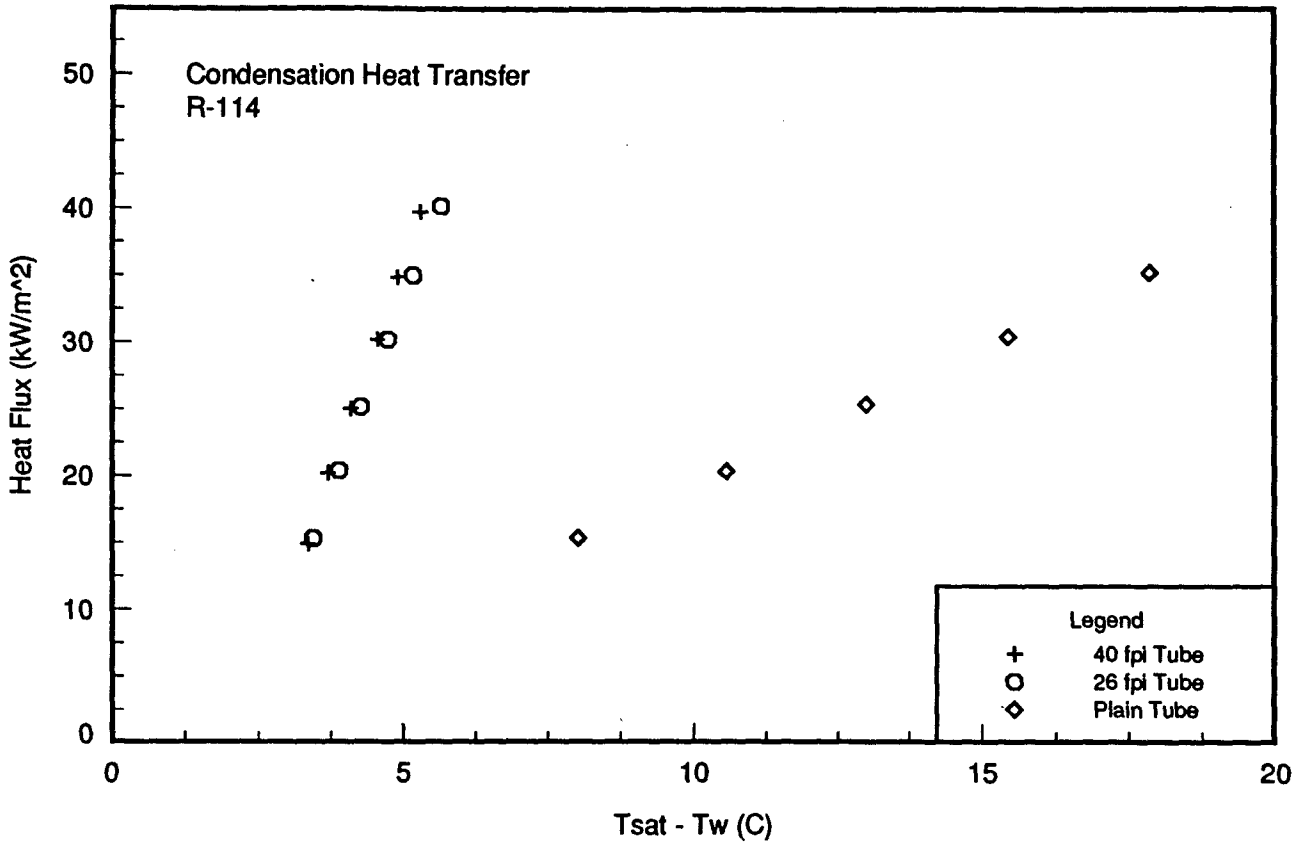

Figure 10.2 Temperature difference effect on heat flux for CFC-114 at $T_{sat} = 40^{o}C$

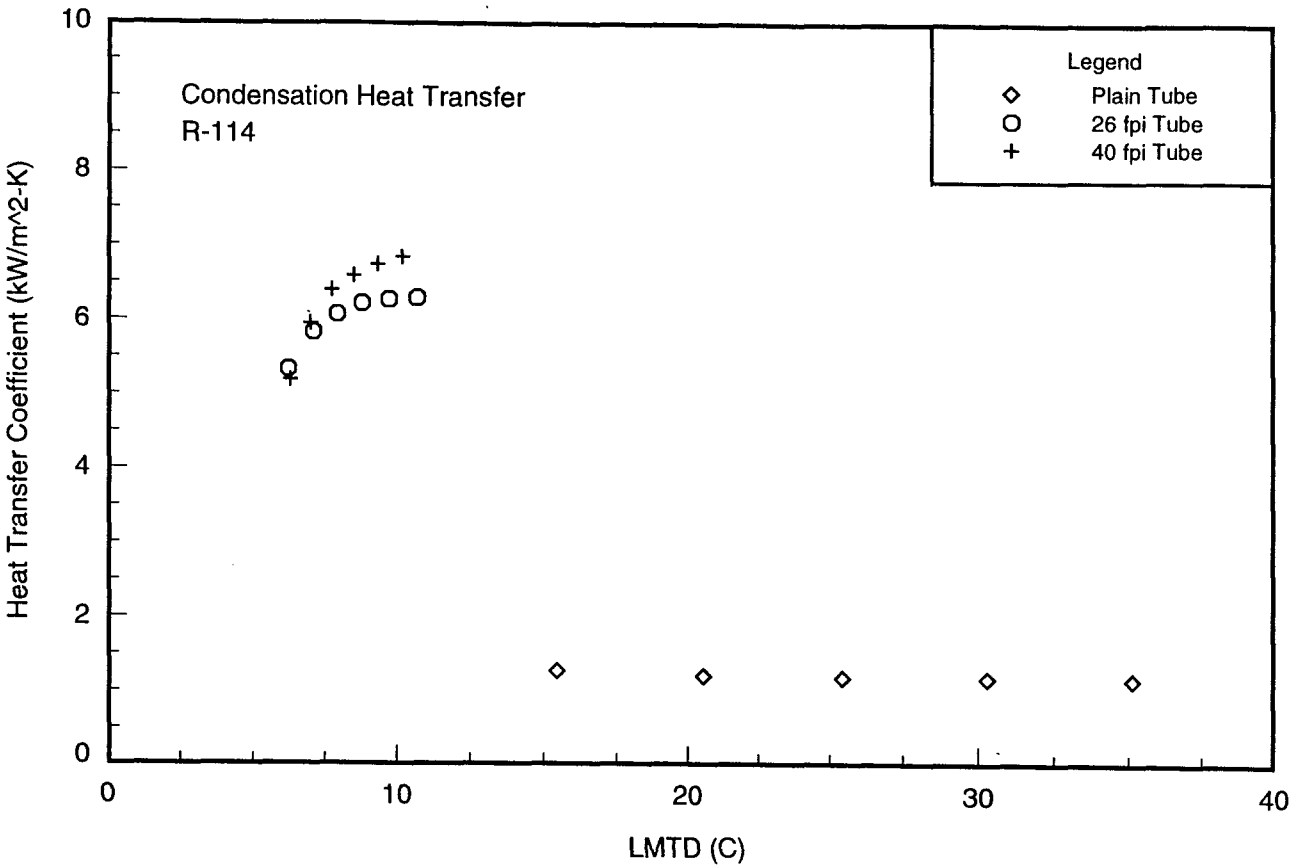

Figure 10.3 LMTD effect on heat transfer coefficient for CFC-114 at T_{sat} = 40°C

Figure 10.4 presents the repeatability analysis for condensation of CFC-114 on the 26 fpi and 40 fpi tubes. The plain tube data was also repeated, but is not included in this plot. The repeat run for the plain tube was within 3% of the original data. The deviation between runs for the 26 fpi tube is less than 2%. The 40 fpi tube shows a deviation of 4% at the lowest heat flux and less than 2% at 40 kW/m^2. Therefore, all three tubes showed excellent repeatability within the tested heat flux range. It should be noted that the deviations found in this repeatability analysis are less than the uncertainties in the calculation of the shell-side heat transfer coefficient, which are presented in Chapter 6.

The condensation coefficient versus the heat flux for HFC-236ea (also designated R-236ea) is shown in Figure 10.5. As was the case with CFC-114, the two finned tubes outperformed the plain tube. But, for HFC-236ea, the 40 fpi tube has higher heat transfer coefficients than the 26 fpi tube only in the low end of the heat flux range. Above 30 kW/m^2, the 26 fpi tube outperformed the 40 fpi tube. At 40 kW/m^2, h_o for the 26 fpi tube is 5% higher than the 40 fpi tube. Since the condensation coefficients are within 5% for both finned tubes, it is evident that they have similar performance in condensation of HFC-236ea, which was also the case with CFC-114 where the deviation was only 9% between the finned tube performances. The condensation of HFC-236ea also showed the same trends that CFC-114 did. Namely, the plain tube condensation coefficients decrease with increasing heat flux, while the finned tubes display an increase in the condensation coefficients.

Figure 10.6 shows the heat transfer coefficient's dependency on the temperature difference, ΔT. The plot shows that for a given ΔT, the two finned tubes have similar heat transfer performance, with both tubes producing approximately the same h_o values. The plot also shows that the plain tube requires a much larger temperature difference to achieve the same heat flux values (data points for each tube correspond to the plots of h_o versus q", with the temperature difference used as the independent variable instead of the heat flux, similar to what is shown in Figure 10.2). Since the saturation temperature is held constant, the larger ΔT values for the plain tube correspond to a much lower shell-side wall temperature (T_w) to achieve condensation than the finned tubes require.

Figure 10.7 shows the repeatability analysis for condensation of HFC-236ea with the two finned tubes. This plot shows that the data are very repeatable for HFC-236ea also. The 26 fpi and 40 fpi tube data were repeatable within 3% and 2%, respectively, of the initial runs. Notice that all condensation results were repeatable within ±3%, while the uncertainty associated with h_o averaged 7%, which shows that the data had good repeatability.

A refrigerant comparison is graphically presented in Figures 10.8 and 10.9 for the two finned tubes. Figure 10.8 shows that the 26 fpi tube produces higher condensation coefficients for HFC-236ea than for CFC-114. The HFC-236ea heat transfer coefficient data also show a greater increase with increasing heat flux than for CFC-114. This may be a reason why the 26 fpi tube showed a greater performance than the 40 fpi tube at higher heat fluxes for HFC-236ea. Figure 10.9 shows that the 40 fpi tube performances for the two refrigerants are almost identical up to a heat flux of 25 kW/m^2. At higher heat fluxes, the HFC-236ea data show slightly higher heat transfer coefficients.

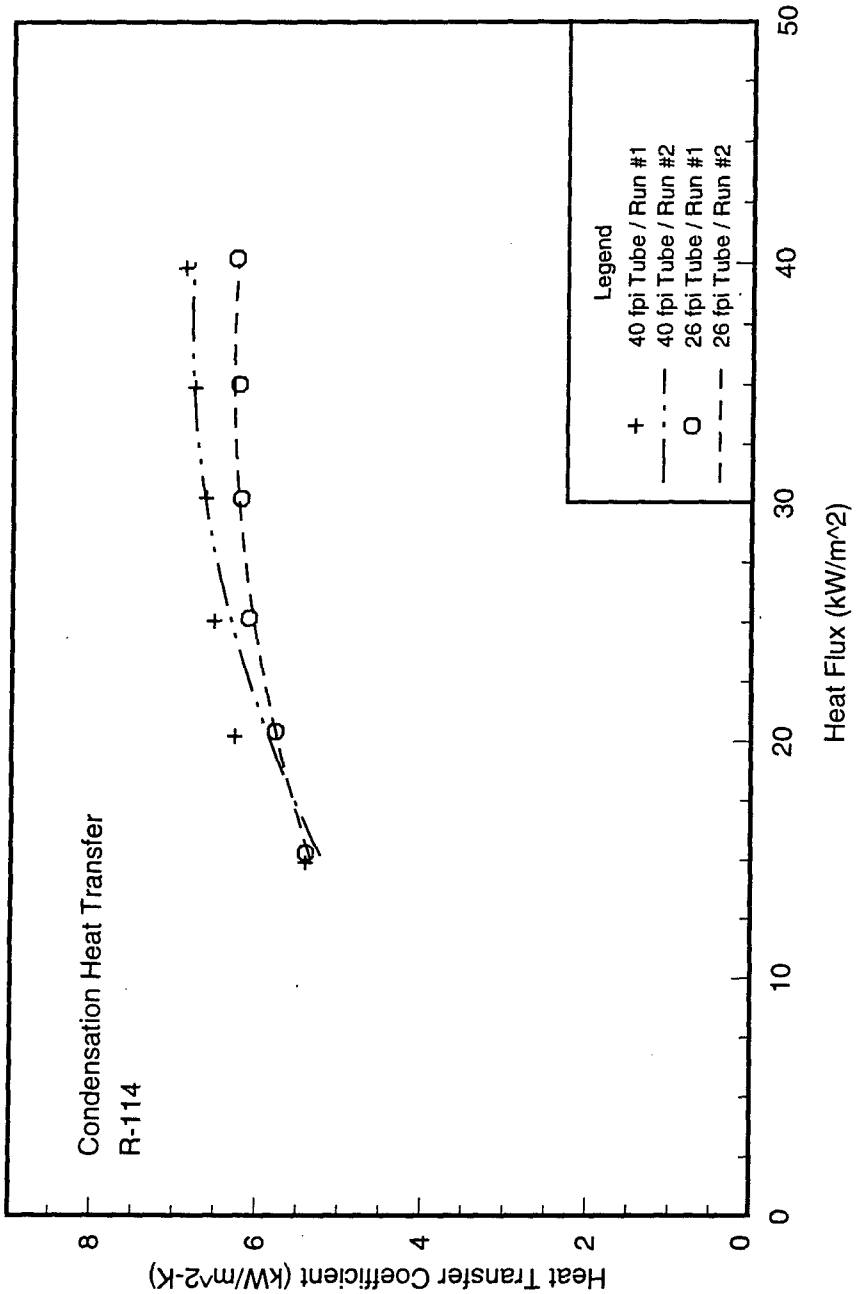

Figure 10.4 Repeatability analysis for CFC-114 at T_{sat} = 40°C

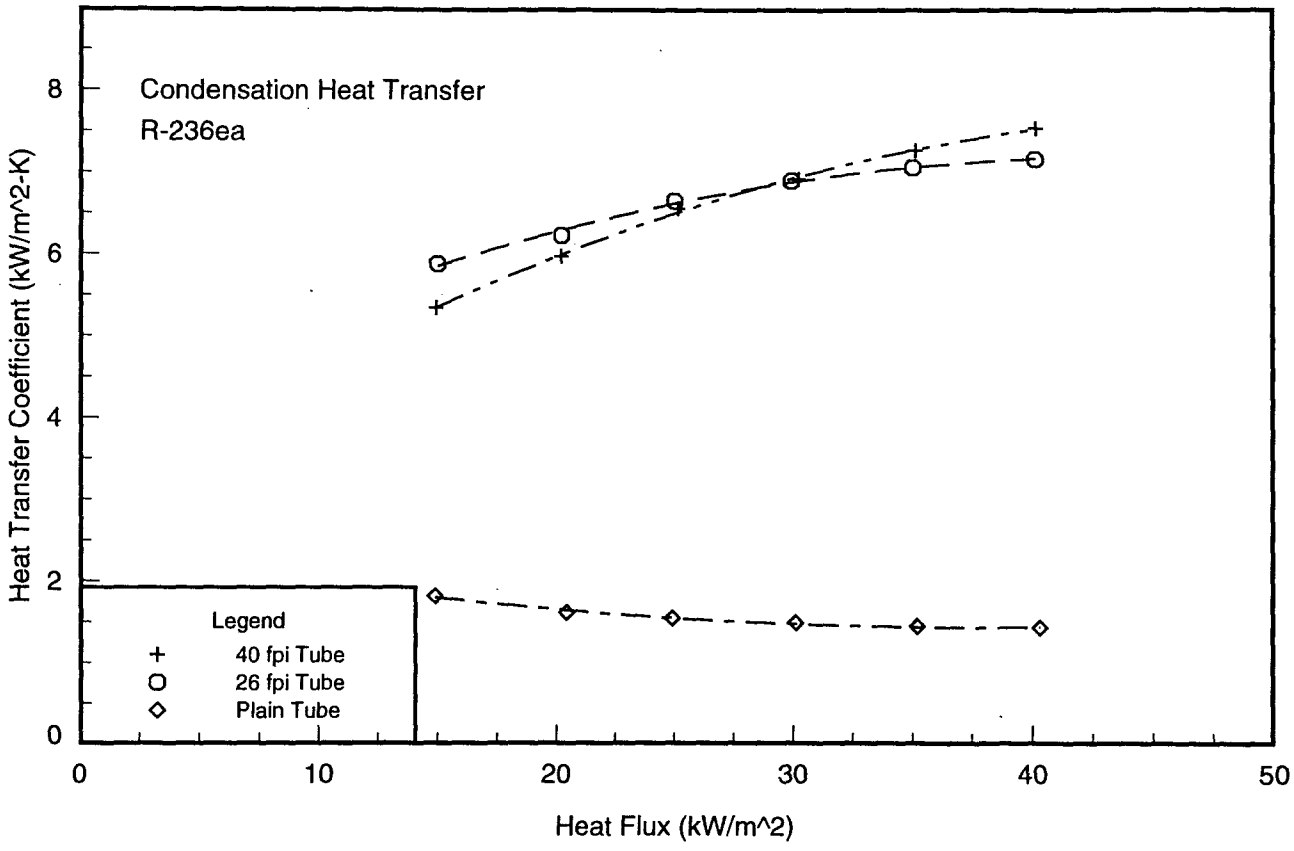

Figure 10.5 Condensation heat transfer coefficient for HFC-236ea at $T_{sat} = 40^{o}C$

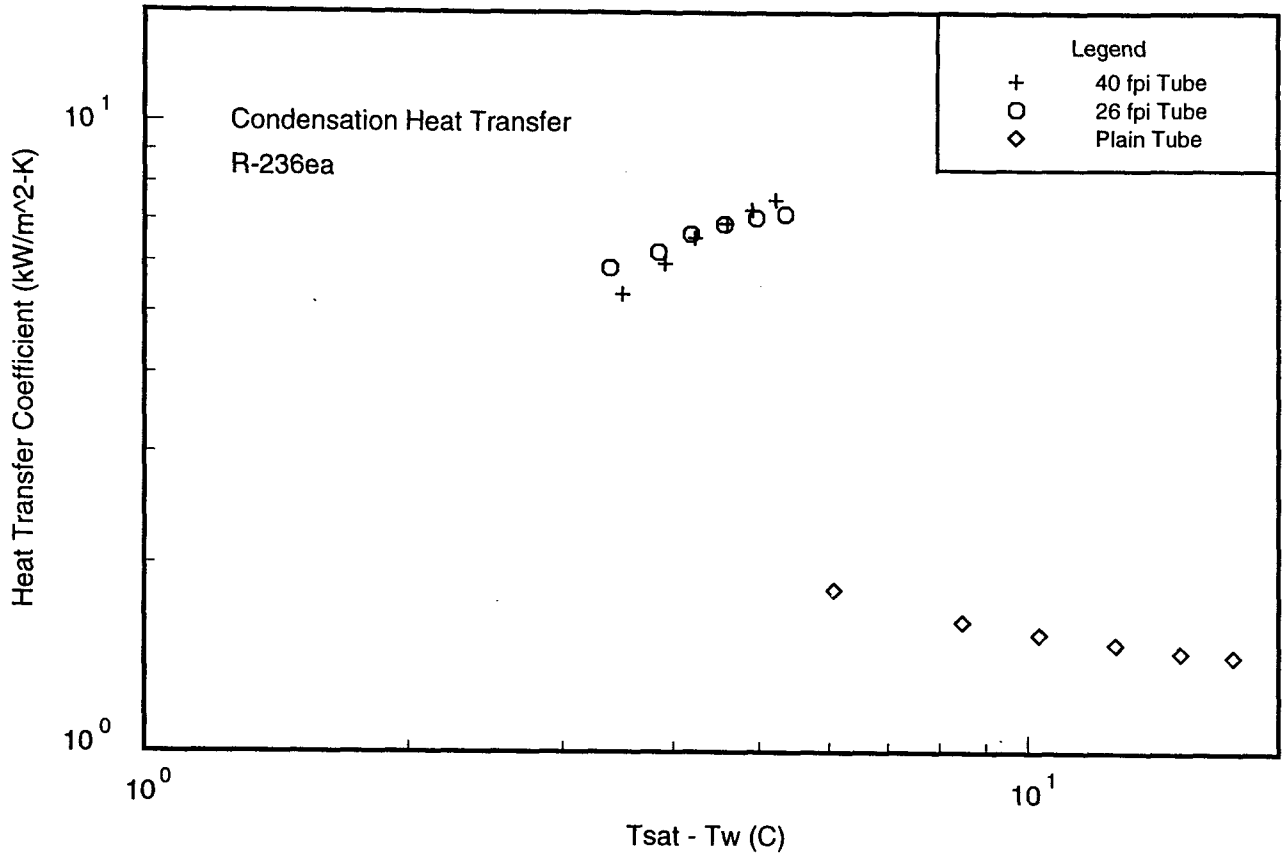

Figure 10.6 Temperature difference effect on heat transfer coefficient for HFC-236ea at T_{sat} = 40°C

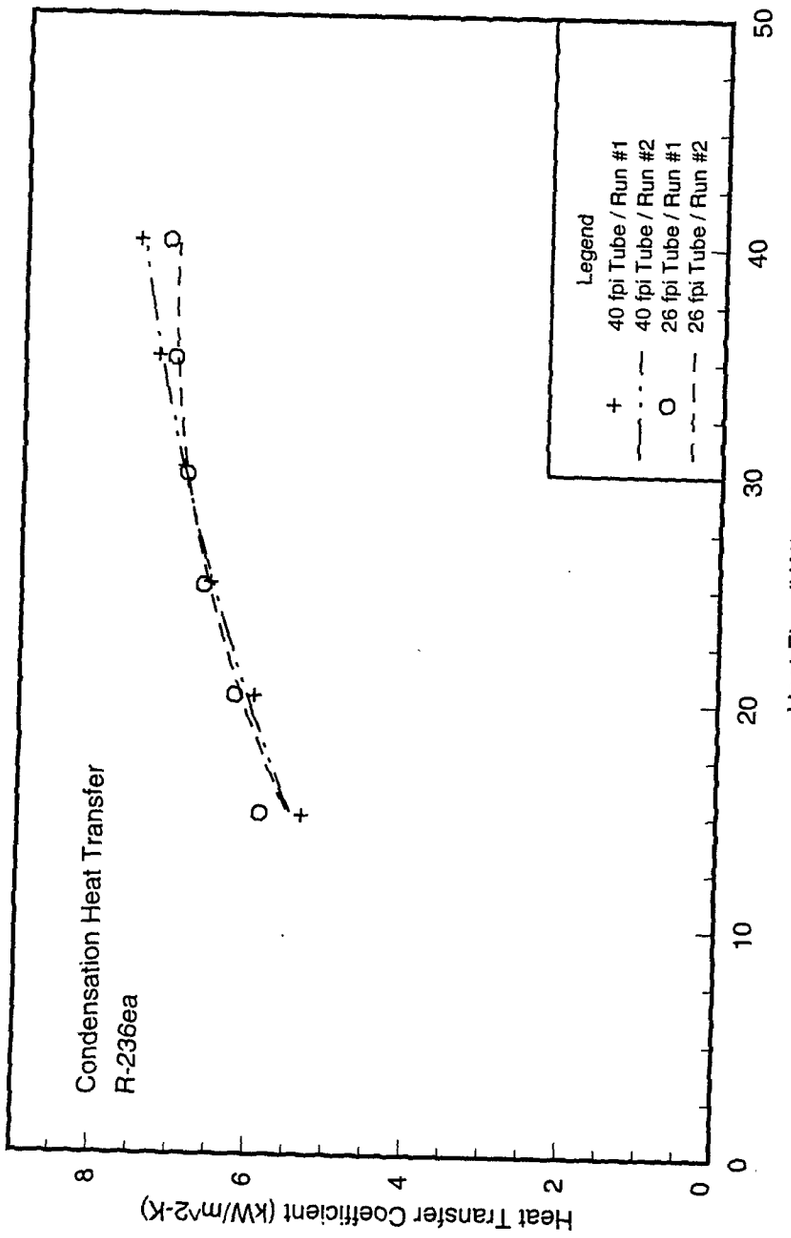

Figure 10.7 Repeatability analysis for HFC-236ea at T_{sat} = 40°C

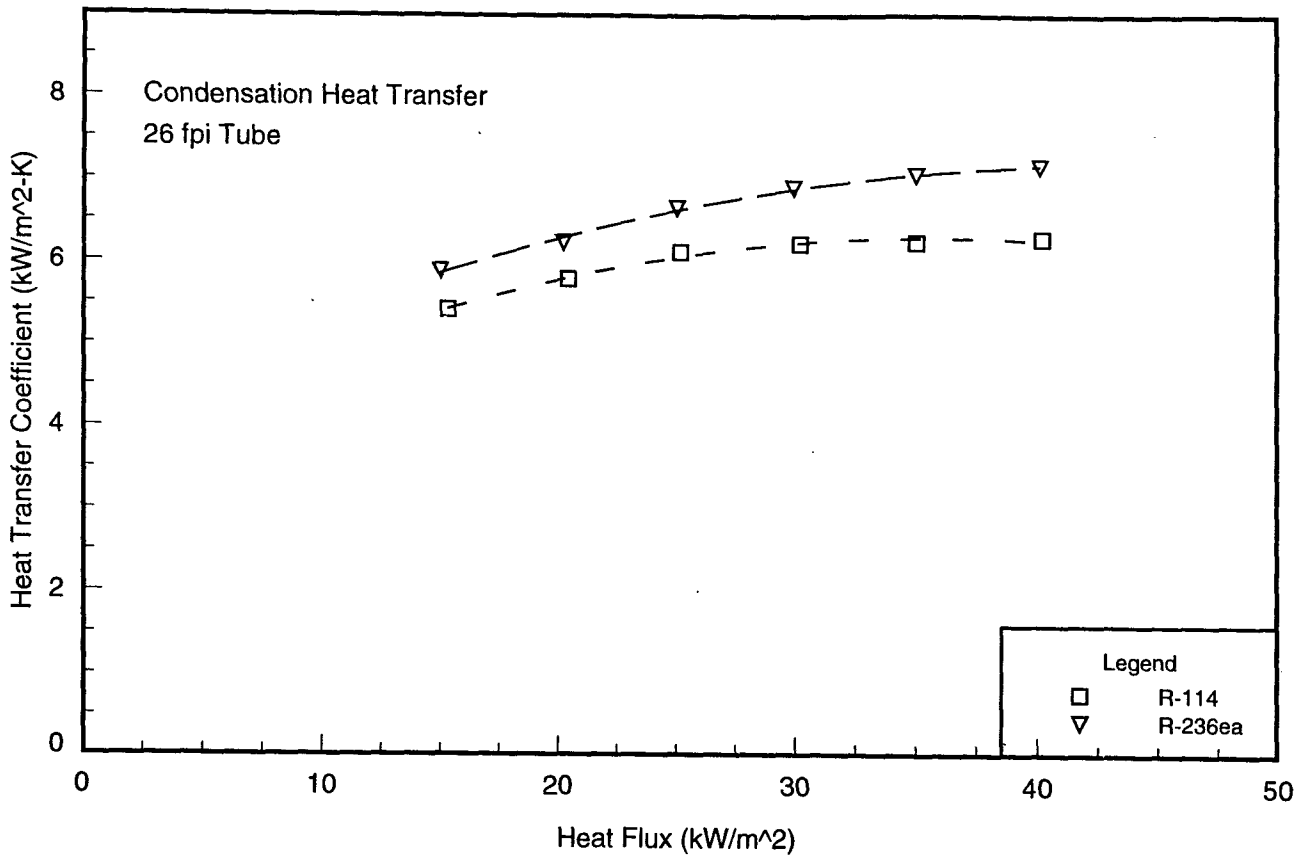

Figure 10.8 Condensation heat transfer coefficient for 26 fpi tube at $T_{sat} = 40^{o}C$

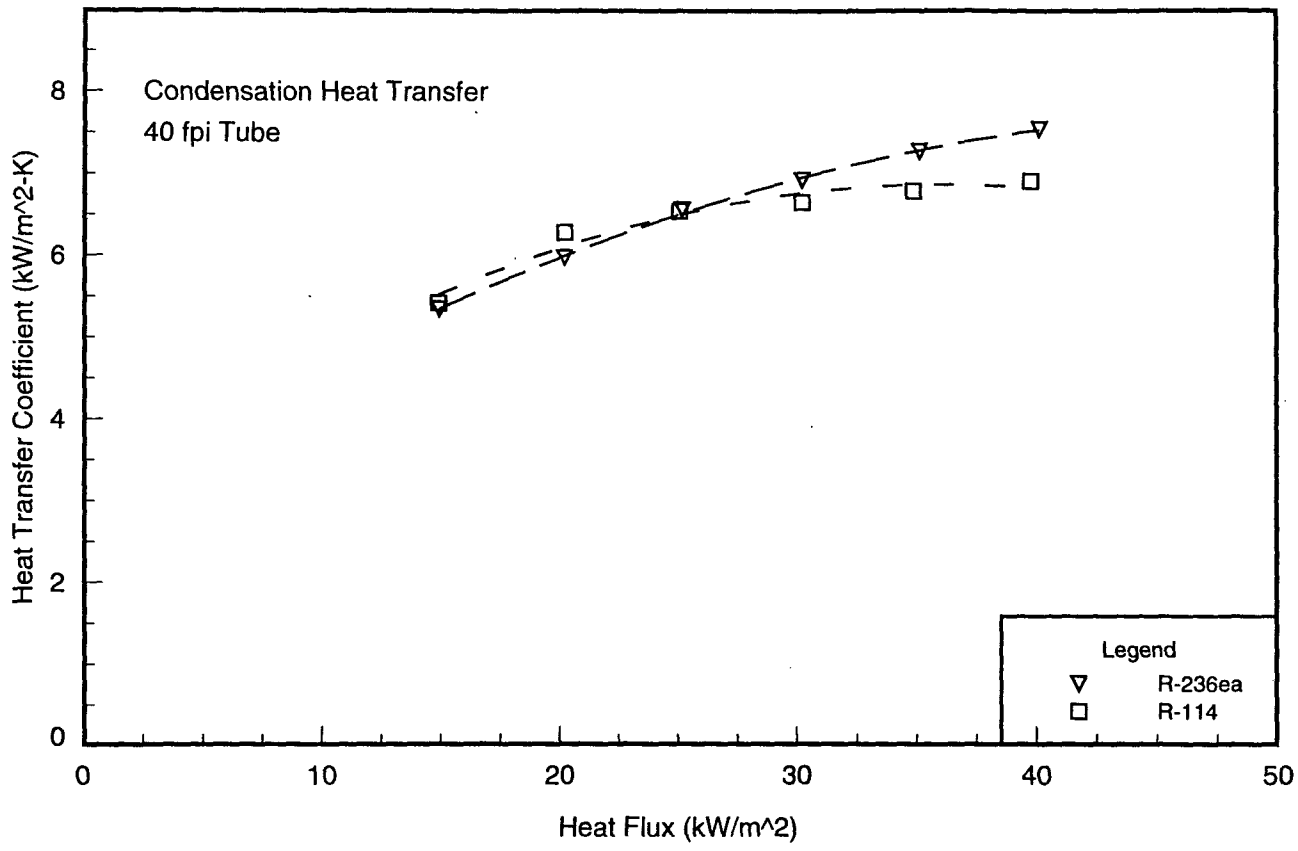

Figure 10.9 Condensation heat transfer coefficient for 40 fpi tube at $T_{sat} = 40^{o}C$

Figure 10.10 presents a comparison of the condensation heat transfer performance for the integral-fin tubes that were tested. This plot shows the condensation coefficients for the two finned tubes with CFC-114 and HFC-236ea. Overall, any combination of the integral-fin tubes and the two refrigerants produce similar heat transfer coefficients.

Superheated Vapor

Condensation data were also taken for superheated vapor of CFC-114 on all three tube surfaces. Certain industrial applications require condensation of superheated vapor, and therefore, it was of interest to examine the effect on the heat transfer performance. If the condensing tube is below the vapor saturation temperature, then the superheated vapor will condense on contact with the surface. McAdams [3] showed that the heat transfer coefficient for condensation of superheated vapor was within a few percent of condensing saturated vapor if the saturation temperature of the vapor was used to calculate the LMTD.

Figure 10.11 shows condensation coefficients for saturated and superheated vapor of CFC-114 on a plain tube surface. The superheated vapor performance falls below that of saturated vapor by approximately 7%. Figure 10.12 displays the 26 fpi tube results, which show a maximum deviation of 5%. The heat transfer coefficients are almost identical for a heat flux of 15 kW/m^2. Figure 10.13 shows the saturated vapor produces slightly higher heat transfer coefficient (above 20 kW/m^2)than the superheated vapor for the 40 fpi tube, where the maximum deviation between the two vapor sources is 3%.

All three tube surfaces showed that the saturated vapor had a higher heat transfer coefficient than the superheated vapor, except for the 40 fpi tube. At a heat flux of 15 kW/m^2, the superheated vapor condensation coefficient was above that for saturated vapor. It is not presently known why the majority of the superheated data fall below the saturated vapor coefficients. It may be caused by the method used to calculate the shell-side heat transfer coefficient, which is the LMTD approach. However, it is evident that condensing superheated vapor has little effect on the heat transfer performance. The deviations stated above for the two finned tubes fall within the uncertainty of the rig.

CORRELATION COMPARISON

The data obtained in this study for condensation of saturated vapor was compared with existing correlations for plain and finned tube surfaces. The plain tube correlation that was used for comparison with the experimental data was Equation 2.1. This is the Nusselt correlation [19] for a plain surface in condensation.

The shell-side heat transfer coefficients were obtained from the Nusselt correlation by substituting the saturation (T_{sat}) and tube wall (T_w) temperatures that were measured during the condensation testing. With these

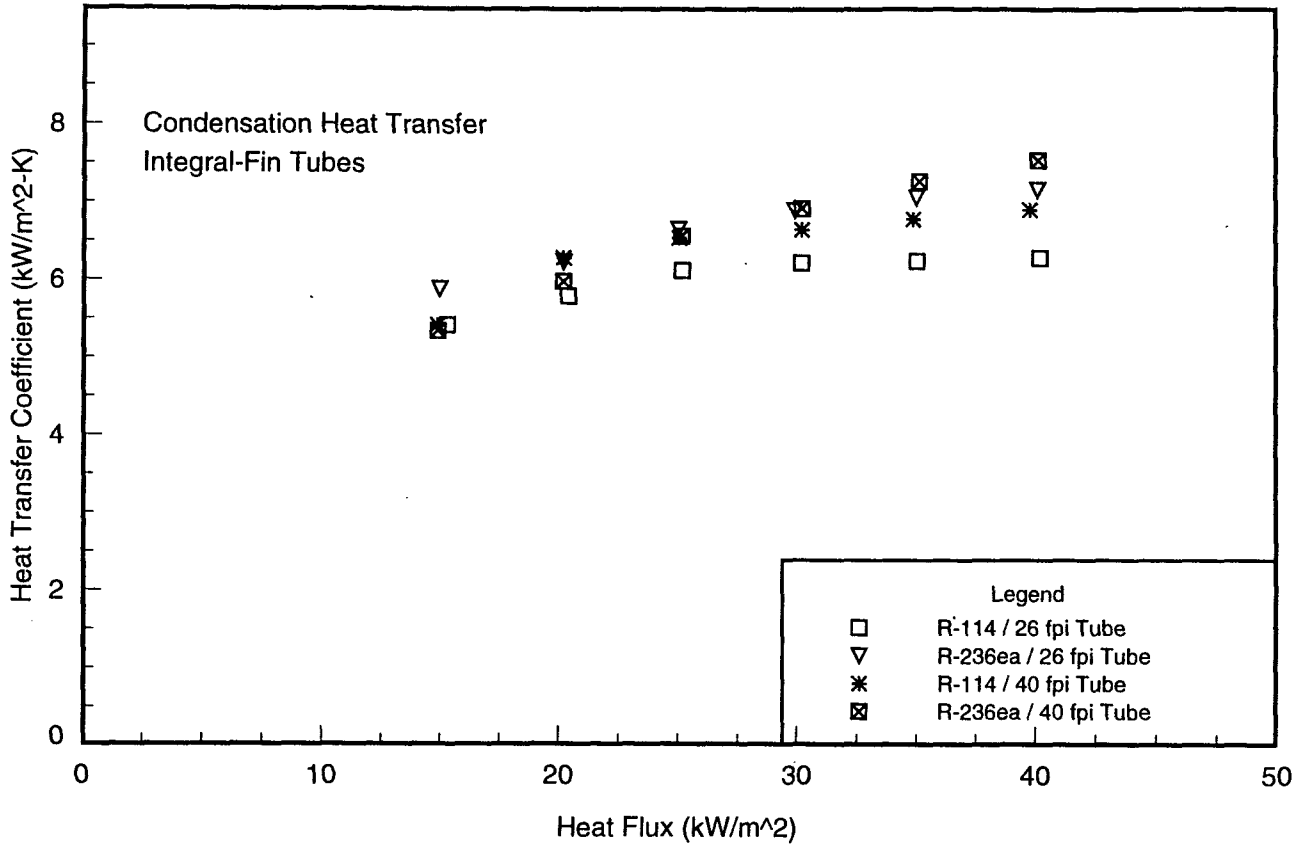

Figure 10.10 Condensation heat transfer performance for integral-fin tubes at $T_{sat} = 40^{o}C$

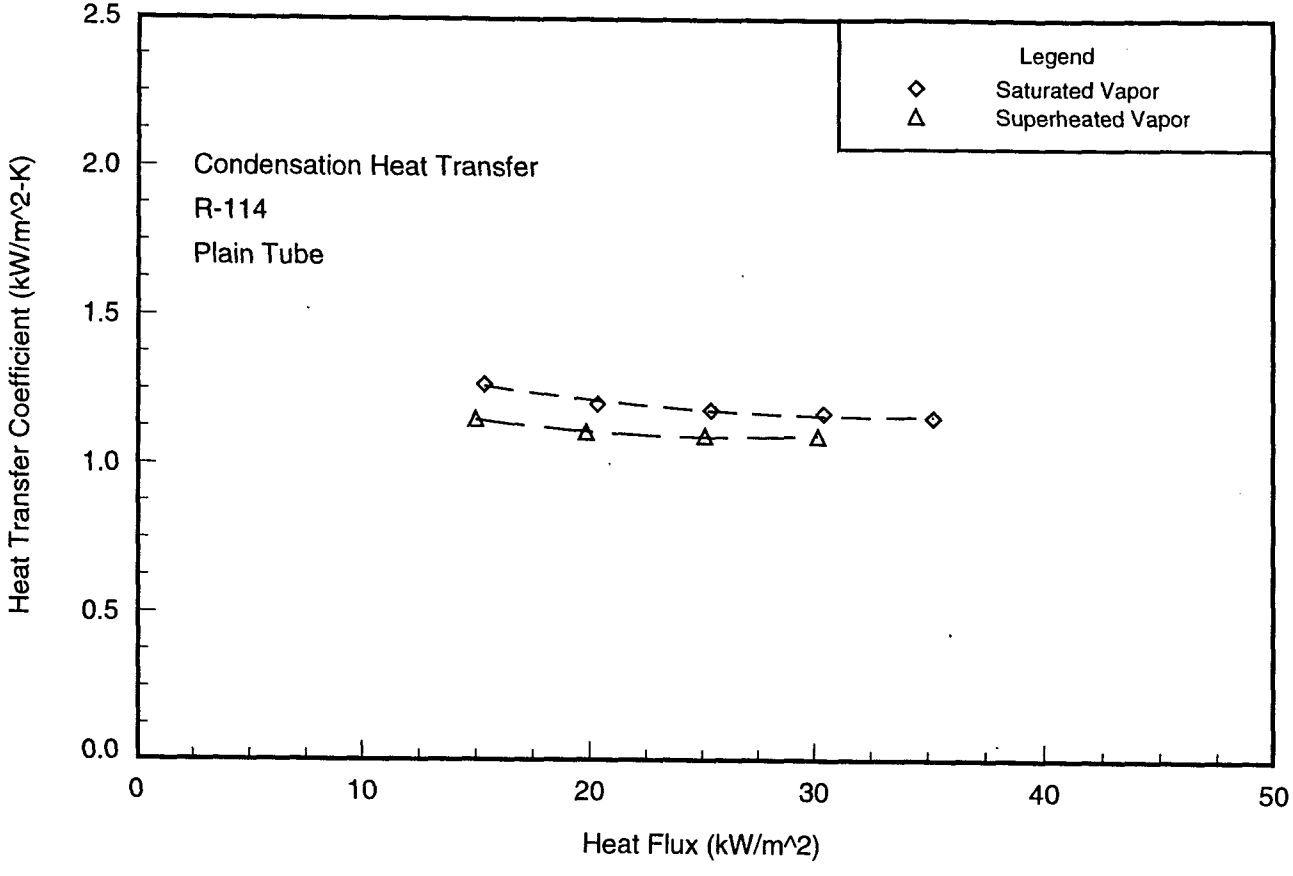

Figure 10.11 CFC-114 superheated vapor effect on heat transfer coefficient for plain tube at $T_{sat} = 40^{o}C$

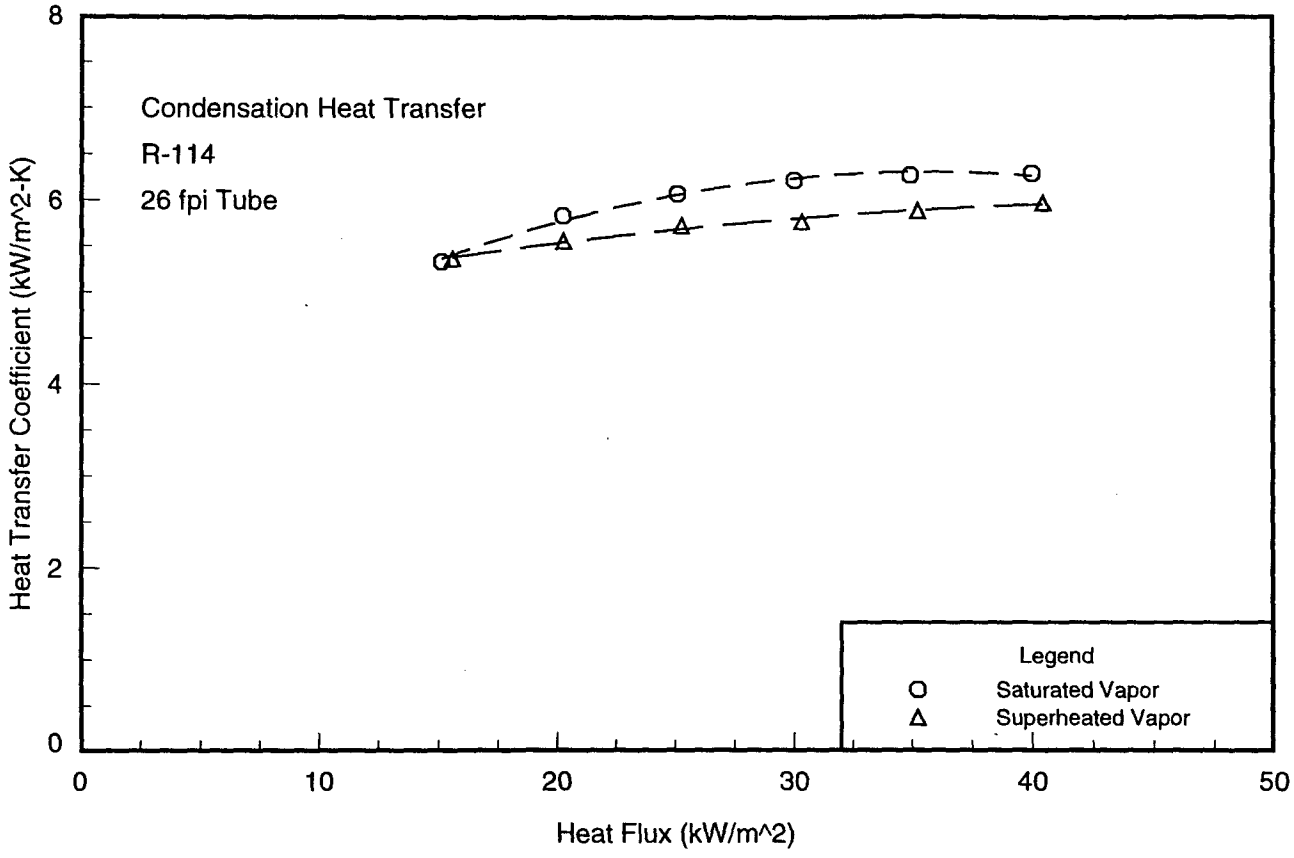

Figure 10.12 CFC-114 superheated vapor effect on heat transfer coefficient for 26 fpi tube at $T_{sat} = 40^{o}C$

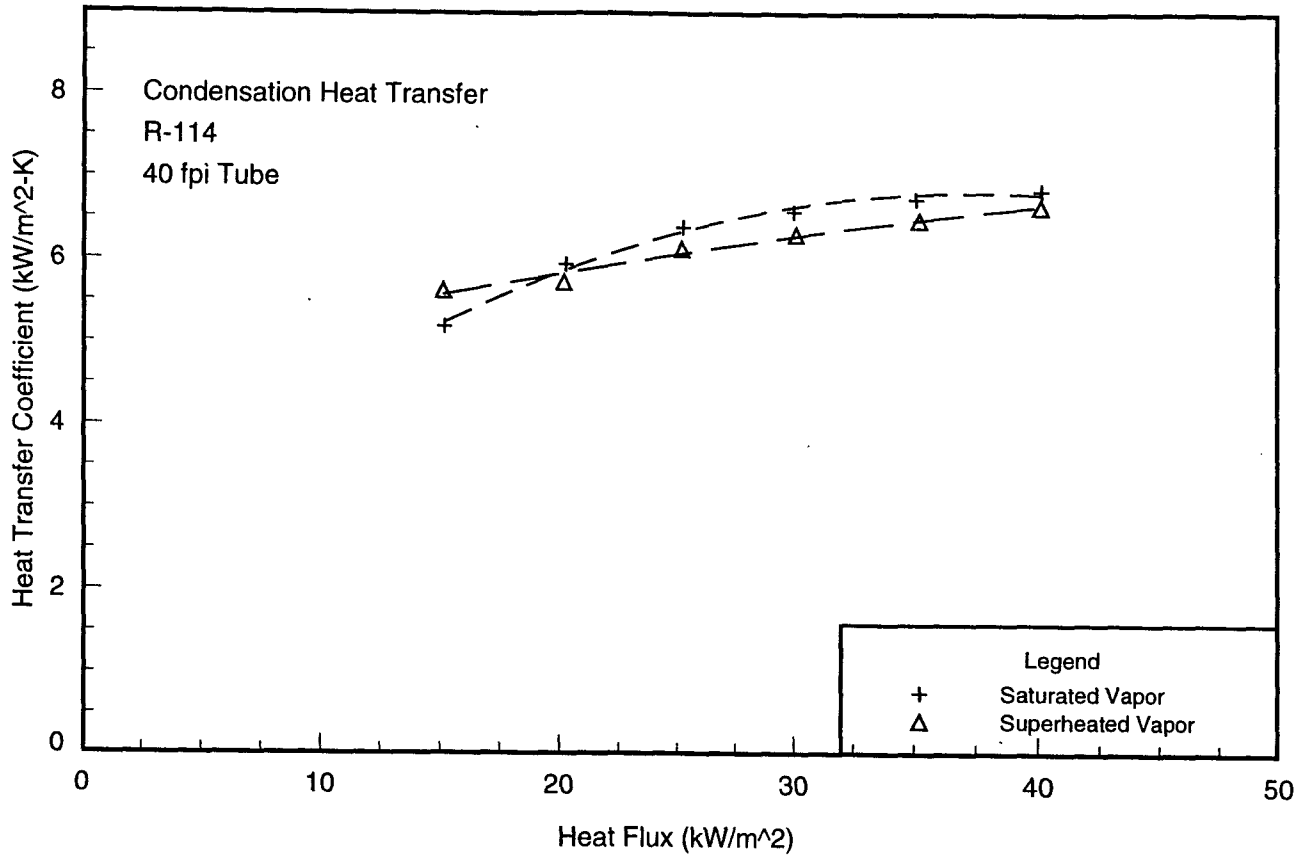

Figure 10.13 CFC-114 superheated vapor effect on heat transfer coefficient for 40 fpi tube at T_{sat} = 40°C

temperatures, a value for h_o was calculated. This heat transfer coefficient was plotted against the measured heat flux value that corresponded to the two temperature measurements.

The integral-fin tube data were compared to the correlation developed by Beatty and Katz [5], which can be seen in Equation 2.3. The method that was used with the Nusselt correlation was also used to obtain shell-side heat transfer coefficients from the Beatty and Katz correlation. This correlation was developed specifically for condensation on fin-tube surfaces with refrigerants. Both correlation comparisons are made on a plot of the shell-side heat transfer coefficient versus the heat flux.

Figure 10.14 shows the plain tube results and the Nusselt correlation results for CFC-114. The Nusselt correlation predicts the data within ±3% for the heat flux range that was tested. In this same figure, the 26 fpi tube results are compared to the Beatty and Katz correlation for CFC-114. Obviously, the correlation predicted that the condensation coefficient would decrease with an increase in heat flux. Even though the experimental value of h_o increases, the correlation still predicts the condensation coefficient to within ±12.5%. The predicted value and the experimental value for h_o are approximately equal at a heat flux of 20 kW/m^2. It is worth noting that Beatty and Katz found their experimental data to be within ±10% of the values predicted by the correlation.

The Beatty and Katz model was also compared with the 40 fpi tube results for CFC-114 as shown in Figure 10.15. The correlation did not predict the condensation coefficients for the 40 fpi tube as well as the 26 fpi tube. At 15 kW/m^2 and 40 kW/m^2, the deviation between the predicted and experimental values are 14.2% and 18.0%, respectively. This deviation becomes less than 1% at a heat flux of 20 kW/m^2, where the data intersect.

Rudy and Webb [31] showed that their theoretical model produced the best predicted values for fin densities greater than 1200 fpm and that the Beatty and Katz model is better suited for fin densities less than 1200 fpm. Their comparisons showed that the Beatty and Katz model always underpredicted their data by a range of 5% to 70%. The 5% prediction occurred at a fin density of 748 fpm (fins per meter). As the fin density increased, the error in the model also increased. The Beatty and Katz correlation was originally developed for fin densities of 600 to 900 fpm. The 26 fpi and 40 fpi tubes are equivalent to 1024 and 1575 fpm, respectively. Therefore, it follows that the 40 fpi tube results would have a larger deviation from the predicted values of Beatty and Katz than the 26 fpi tube would.

Figure 10.16 shows the Nusselt correlation results along with the plain tube data for HFC-236ea. The correlation does not predict the experimental condensation coefficients as well as with CFC-114, but the deviation is still within 10%. Figure 10.16 also contains the 26 fpi tube comparison for HFC-236ea. The Beatty and Katz correlation overpredicts the data at 15 kW/m^2 by 12.7% and underpredicts the data at 40 kW/m^2 by 15.6%. The deviation between predicted and experimental values is smallest at approximately 25 kW/m^2.

The 40 fpi tube comparison is plotted in Figure 10.17. As was the case with CFC-114, the predicted values for the 40 fpi tube have a larger deviation from the experimental values than the 26 fpi tube shows. At 15 kW/m^2, the correlation overpredicts the data by 21.3% and at 40 kW/m^2, the correlation underpredicts the data by 18.2%.

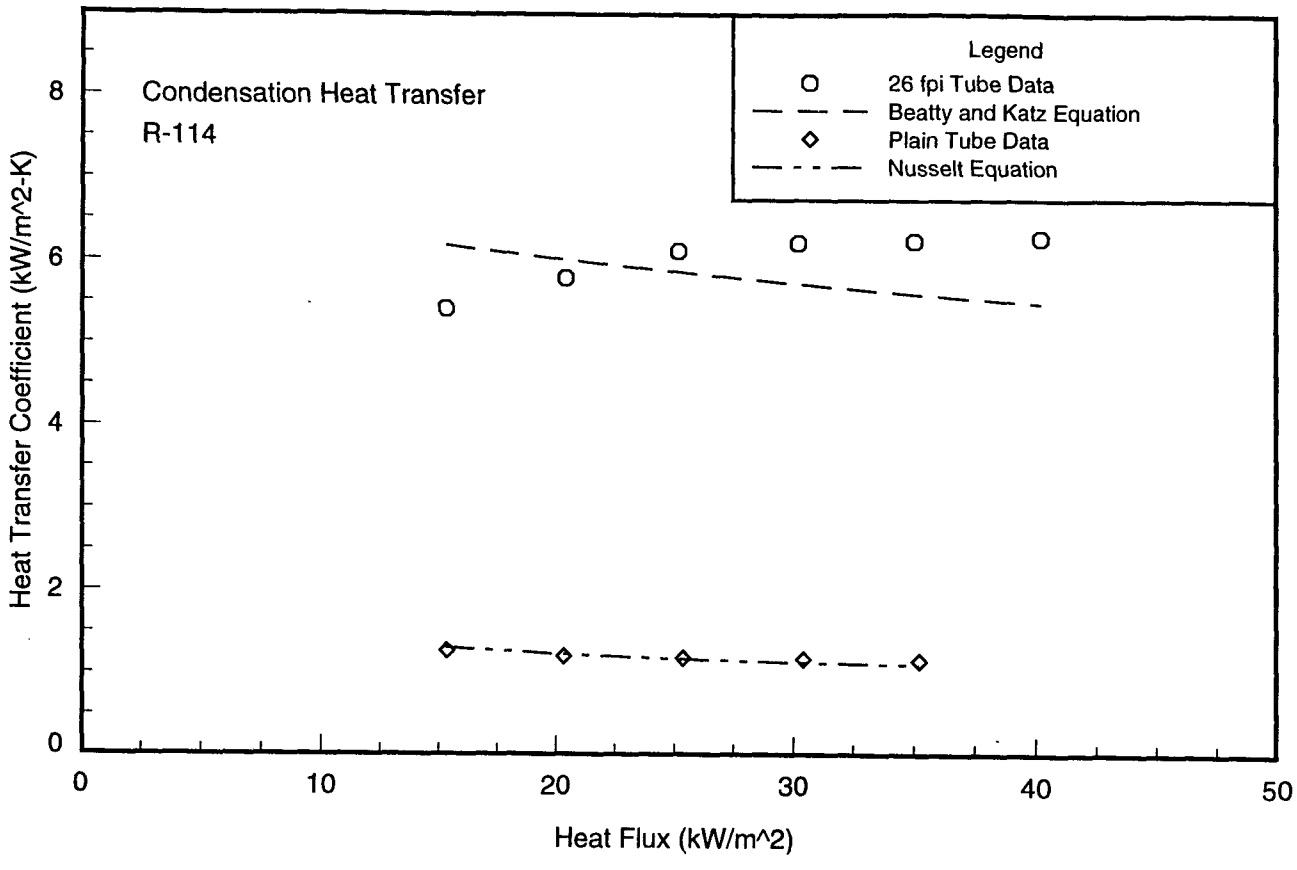

Figure 10.14 Comparison of measured and predicted heat transfer of CFC-114 for 26 fpi tube and plain tube

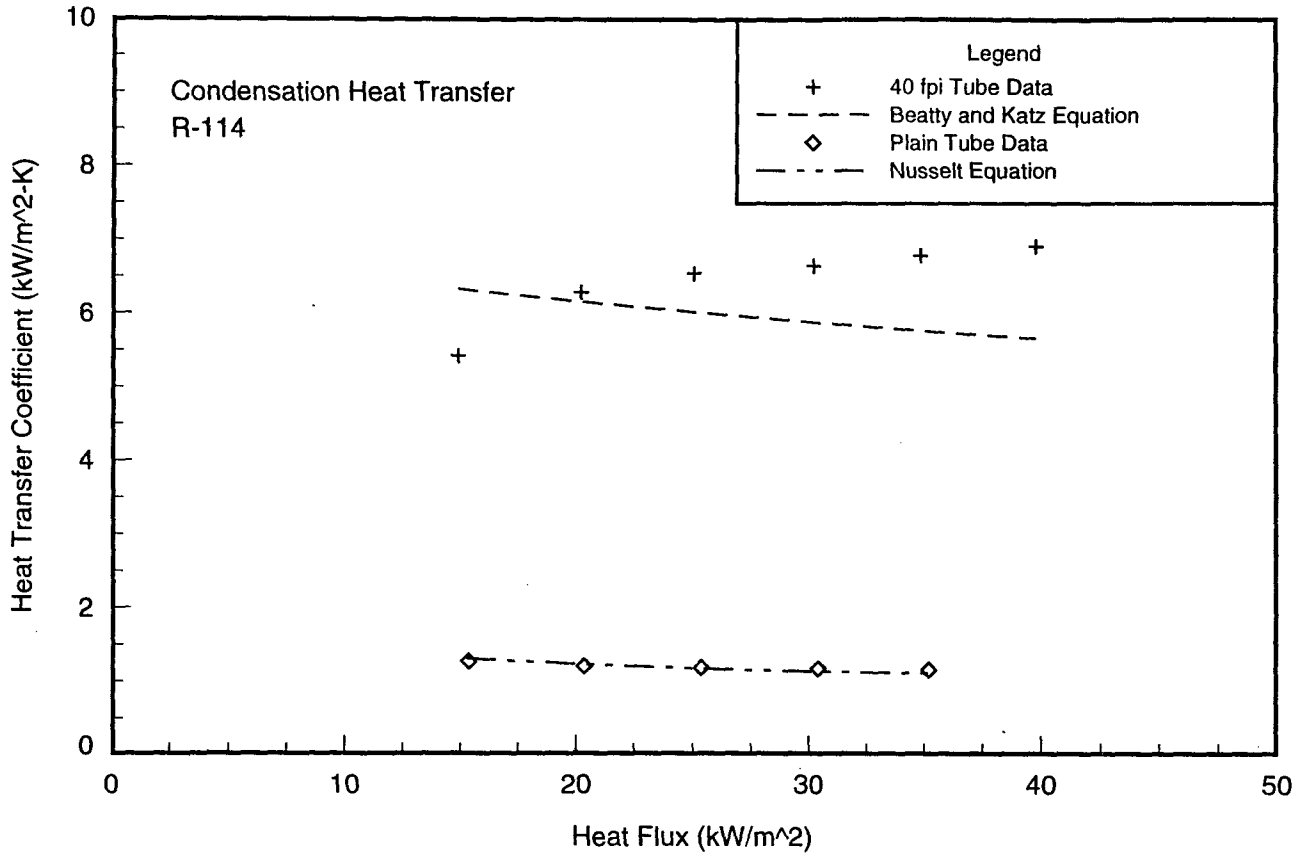

Figure 10.15 Comparison of measured and predicted heat transfer of CFC-114 for 40 fpi tube and plain tube

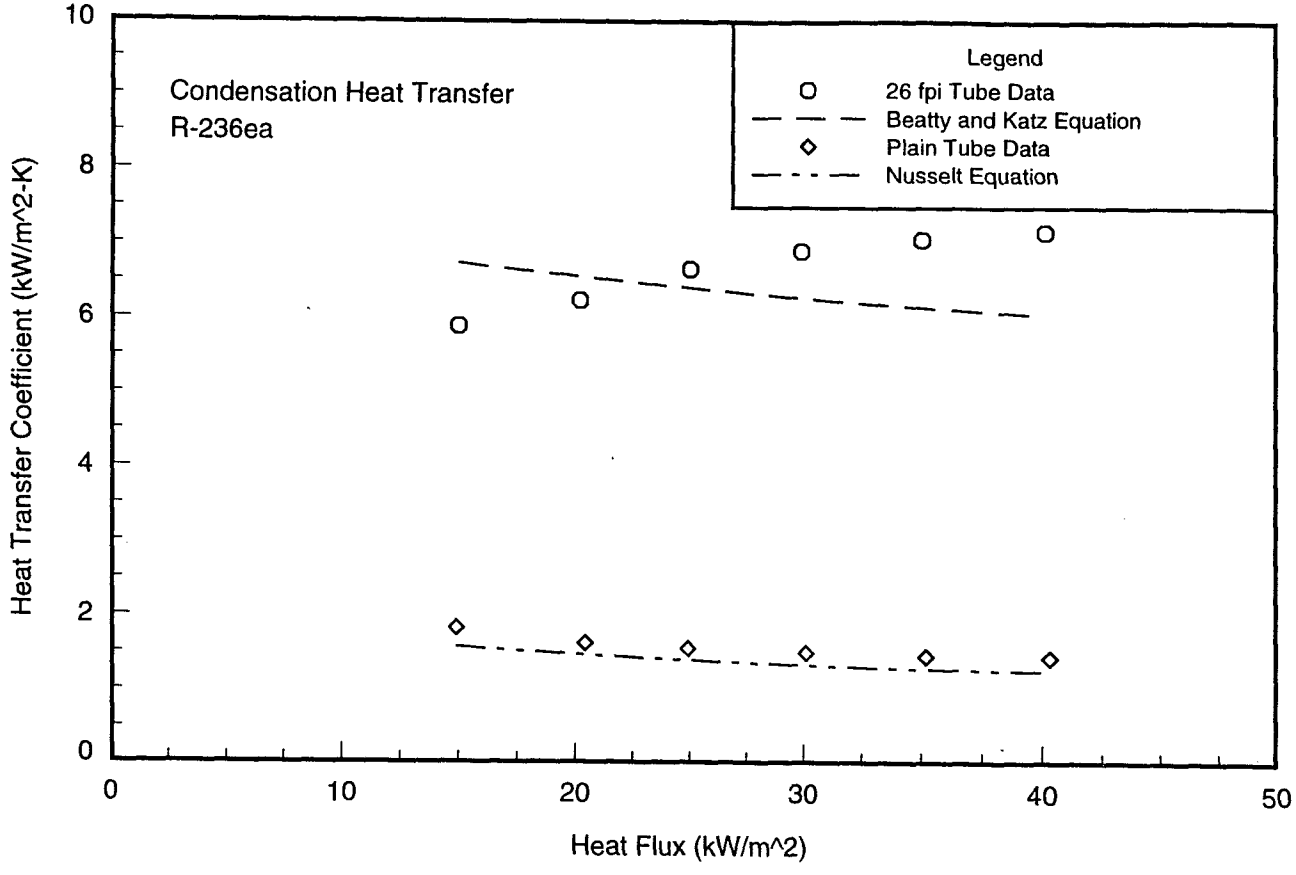

Figure 10.16 Comparison of measured and predicted heat transfer of HFC-236ea for 26 fpi tube and plain tube

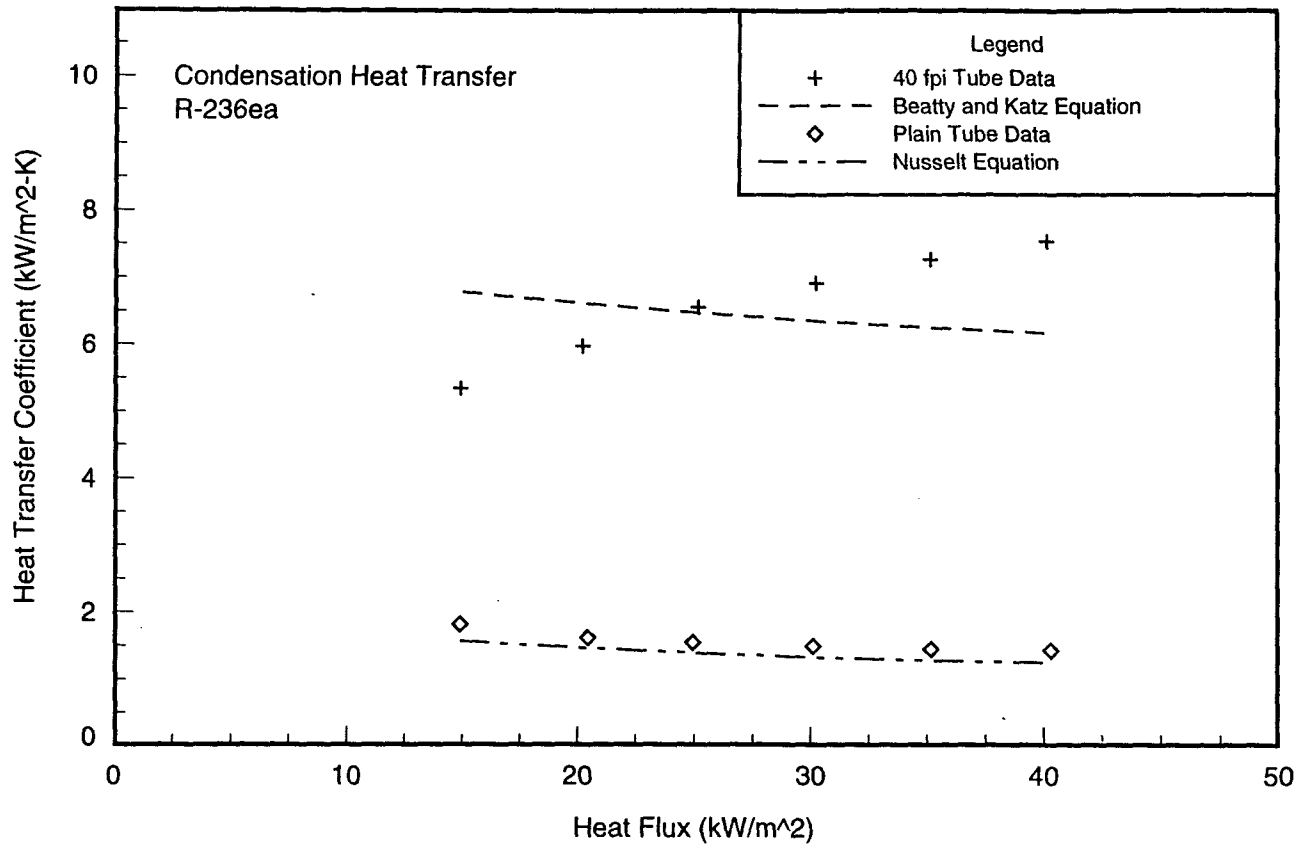

Figure 10.17 Comparison of measured and predicted heat transfer of HFC-236ea for 40 fpi tube and plain tube

SUMMARY

Shell-side heat transfer coefficients were presented for CFC-114 and HFC-236ea during condensation of saturated and superheated vapor. Data were taken at a saturation temperature of 40°C over a heat flux range of 15 kW/m^2 to 40 kW/m^2. A summary of the general conclusions from this section are given below.

1. The condensation heat transfer coefficients for the integral-fin tubes were four to six times those produced with the plain tube for both refrigerants.
2. The heat transfer performance for the integral-fin tubes with CFC-114 and HFC-236ea were similar. The maximum deviation in heat transfer coefficients between the two tubes was 9%. In general, all combinations of the finned tubes and refrigerants produced similar shell-side heat transfer coefficients in the heat flux range that was tested.
3. Condensing superheated vapor was found to have little effect on the shell-side heat transfer coefficient with respect to saturated vapor results.
4. The Nusselt correlation was able to accurately predict the plain tube results for both refrigerants. The Beatty and Katz correlation was able to predict the 26 fpi tube results within ±15% and the 40 fpi tube results within ±21%.

CHAPTER 11

POOL BOILING RESULTS

This chapter presents the results obtained in pool boiling tests of CFC-114 and HFC-236ea. The tubes of interest for pool boiling were the plain, 26 fpi, and 40 fpi tube surfaces. In addition, results are presented for refrigerant / lubricant mixtures tested in the pool boiling environment with oil concentrations of 1% and 3%. Comparisons are made for tube surfaces, refrigerants, and oil concentrations. A comparison is also made between the plain tube results of this chapter and correlations for nucleate pool boiling from Chapter 3.

As was the case in condensation testing, CFC-114 and the plain tube surface were incorporated into the testing matrix for pool boiling to act as a baseline for comparison. The pure refrigerant tests have this same role for investigating the heat transfer effects of a refrigerant / lubricant mixture. The pure refrigerant data presented in this chapter acted as a reference by which specific oil concentrations could be evaluated.

All of the data were taken at a saturation temperature of 2°C and with a decreasing heat flux to avoid any hysteresis effects. Pool boiling tests had the same heat flux range as condensation: 15 kW/m^2 to 40 kW/m^2. The refrigerant / lubricant mixtures that were tested used a 315-SUS mineral oil and a 340 SUS polyol-ester oil for CFC-114 and HFC-236ea, respectively. Approximately 20% of the data runs were repeated to verify the validity of the results and the rig's repeatability. A plot of the repeatability has been included in this chapter.

The tubes tested during pool boiling had a nominal outer diameter of 19.1 mm. The exact dimensions of each tube can be found in Appendix C. The shell-side heat transfer coefficients presented in this chapter are based on the outside area of a corresponding smooth tube. Therefore, the calculated h_o includes the area enhancement, fin efficiency, and surface enhancement. The tabulated pool boiling data are presented in Appendix B.

HEAT TRANSFER RESULTS

Heat transfer coefficients for CFC-114 and HFC-236ea are presented for pool boiling of pure refrigerant as well as refrigerant / lubricant mixtures. The pure refrigerant testing used the plain, 26 fpi, and 40 fpi tubes. The saturation temperature was held constant at 2°C ±0.1°C. The testing of refrigerant / lubricant mixtures only used the finned tube surfaces. The saturation temperature was also held constant during these tests, but due to solubility effects, T_{sat} was calculated from the average pool temperature.

Pure Refrigerant

Figure 11.1 shows the pool boiling performance for CFC-114 (also designated R-114) with the three tubes of interest. As expected, the integral-fin tubes had higher boiling coefficients than the plain tube. The test of the 26 fpi tube resulted in boiling coefficients approximately 12% higher than the 40 fpi tube and 30% higher than the plain tube.

Figure 11.2 presents the ΔT effect on the shell-side heat transfer coefficient for CFC-114. In the pool boiling environment, ΔT is defined as $T_w - T_{sat}$. Each data point that is plotted represents a heat flux value, with the lowest ΔT value corresponding to 15 kW/m^2. The plot shows that the two integral-fin tubes produce larger boiling coefficients than the plain tube, while also experiencing smaller temperature differences at a given heat flux. Figure 11.3 presents the LMTD effect on the heat flux. This plot shows that the integral-fin tubes require a smaller LMTD to achieve the same heat fluxes as the plain tube.

The pool boiling performance for HFC-236ea (also designated R-236ea) is illustrated in Figure 11.4. The integral-fin tubes again produced higher heat transfer coefficients than the plain tube in the heat flux range tested. The 26 fpi tube had the highest performance for HFC-236ea, followed by the 40 fpi tube, and then the plain tube. It appears that a greater heat transfer performance is gained in pool boiling of low-pressure refrigerants with the 26 fpi tube than for the 40 fpi tube. It should be noted that the deviation between the 26 fpi and 40 fpi tubes begins to decrease with an increase in heat flux. Therefore, at a heat flux greater than 40 kW/m^2, the boiling coefficients for the two tubes may converge and cross. At 25 kW/m^2, the 26 fpi tube boiling coefficients are approximately 18% and 41% higher than those for the 40 fpi and plain tubes, respectively.

Figure 11.5 shows the effect of the required wall temperature (T_w) on the shell-side heat transfer coefficient. This plot shows similar trends to Figure 11.2 in that the finned tubes show a greater heat transfer performance than the plain tube tested, while also requiring a smaller ΔT to acquire the same heat flux. Since the saturation temperature is held constant, a smaller ΔT corresponds to a lower wall temperature.

As previously stated, a repeatability analysis was conducted on 20% of the data runs for pool boiling. Figure 11.6 illustrates the data repeatability for CFC-114 during pool boiling. For brevity, only one repeat run is presented. The 40 fpi tube data were repeated for CFC-114. The second data run fell within ±3% of the initial data run. A finned tube was used to illustrate the repeatability since these tubes have a higher uncertainty than the plain tube.

In addition to the tube comparison presented for CFC-114 and HFC-236ea, a refrigerant comparison was also conducted. Figure 11.7 is a plot of the heat transfer coefficient of CFC-114 and HFC-236ea for the 26 fpi and plain tubes. Both tubes show that HFC-236ea has a higher heat transfer performance than CFC-114 in nucleate boiling, but the refrigerant data tend to converge for both tubes as the heat flux is increased. It appears that CFC-114 and HFC-236ea may have similar heat transfer performance at heat fluxes greater than 40 kW/m^2. At 15

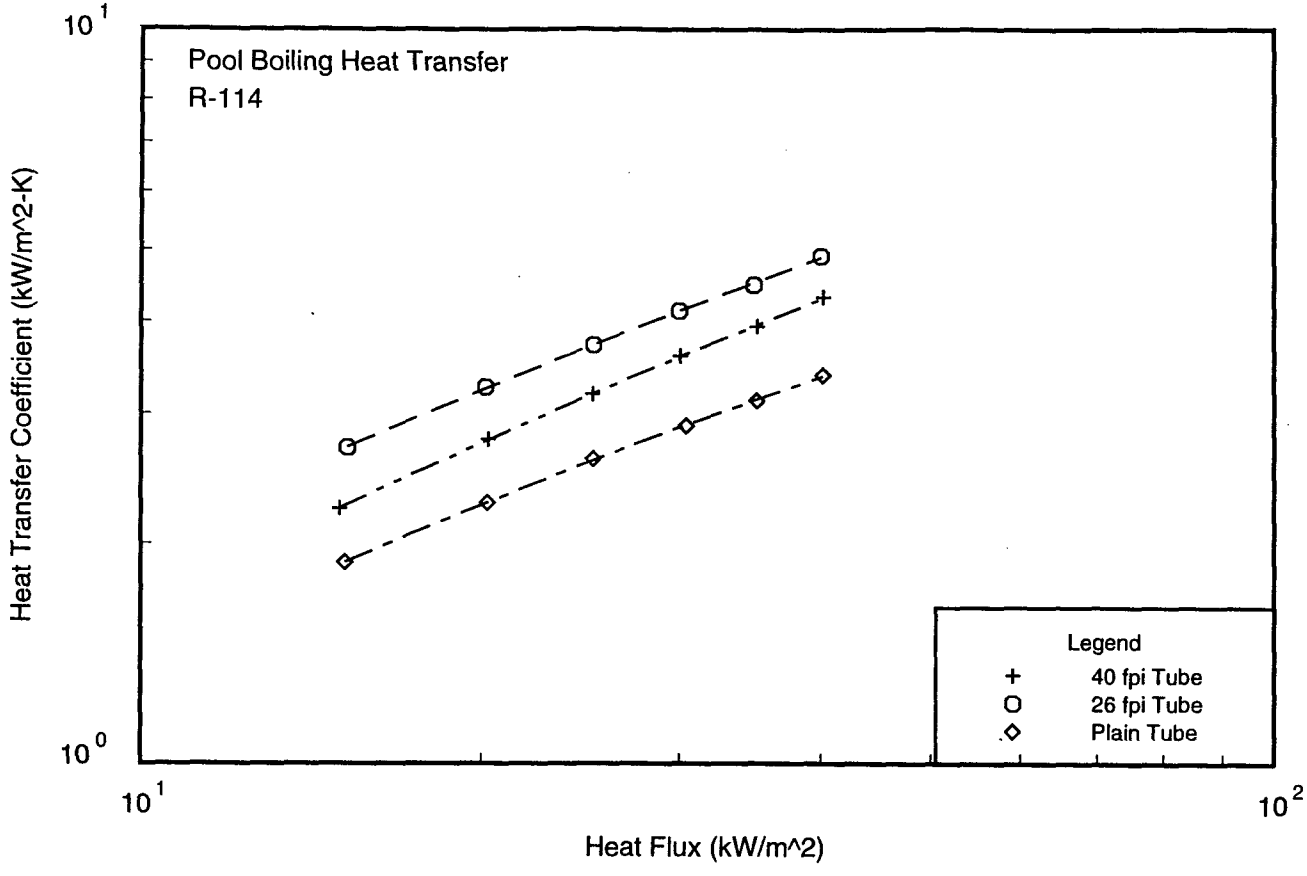

Figure 11.1 Pool boiling heat transfer coefficient for CFC-114 at T_{sat} = 2°C

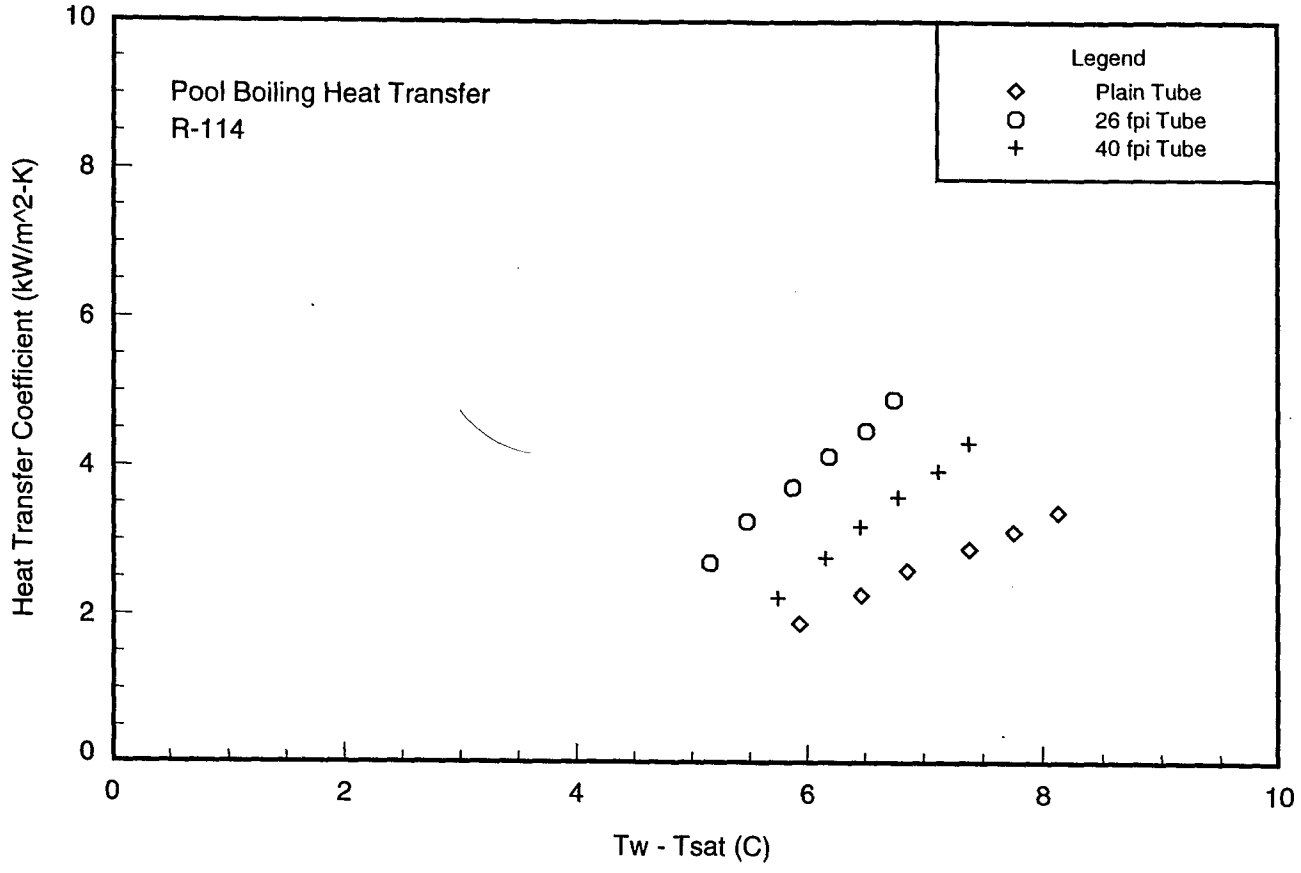

Figure 11.2 Temperature difference effect on heat transfer coefficient for CFC-114 at T_{sat} = 2°C

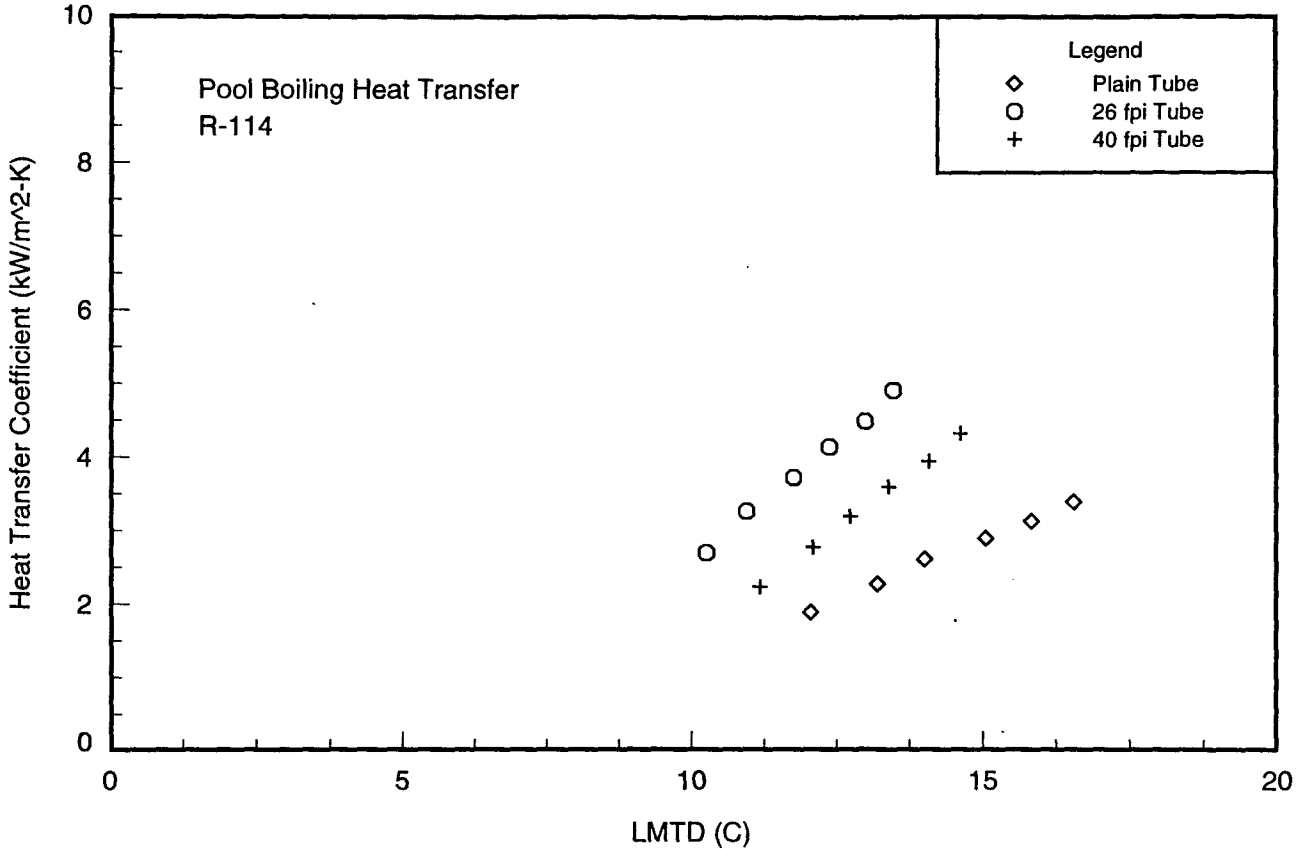

Figure 11.3 LMTD effect on heat flux for CFC-114 at $T_{sat} = 2^{o}C$

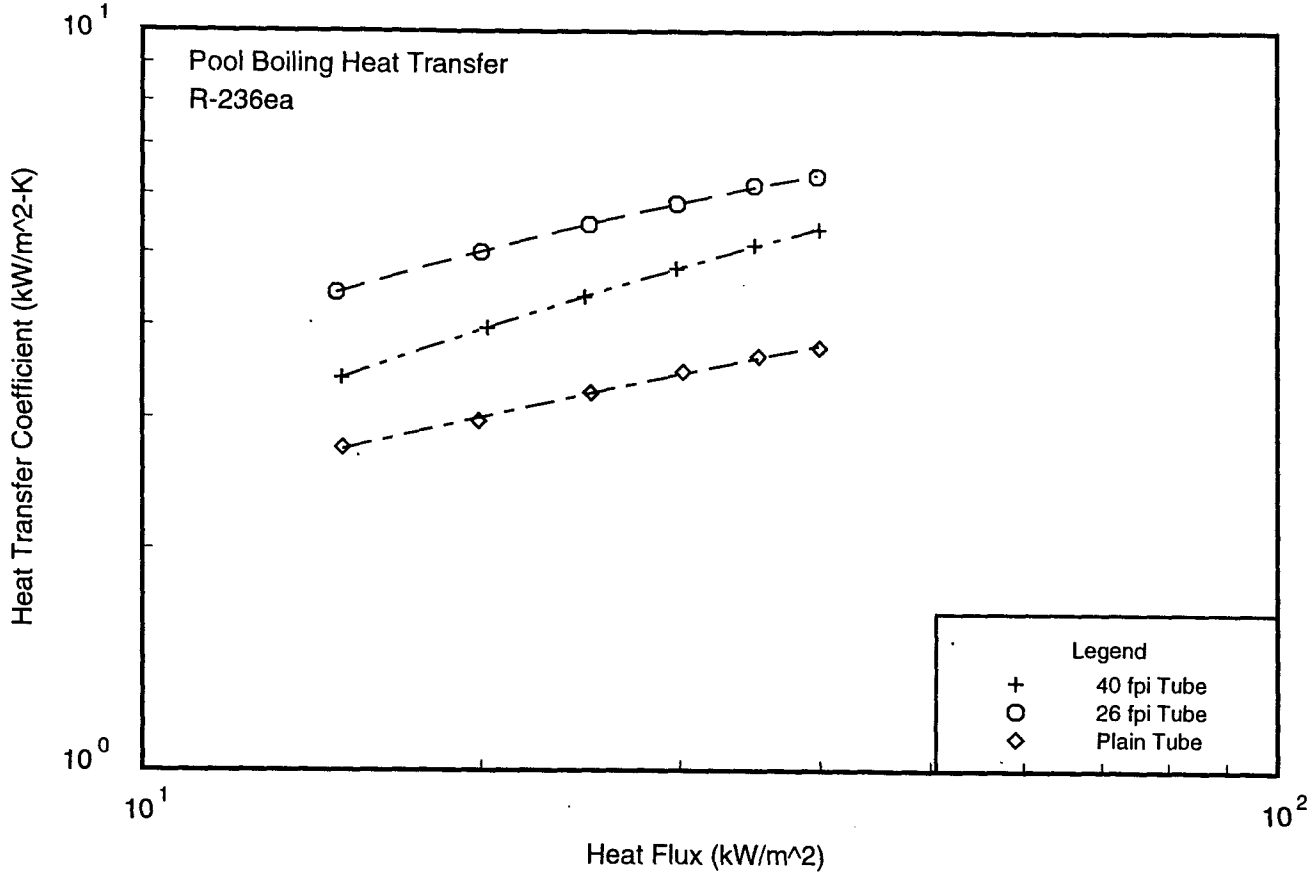

Figure 11.4 Pool boiling heat transfer coefficient for HFC-236ea at T_{sat} = 2°C

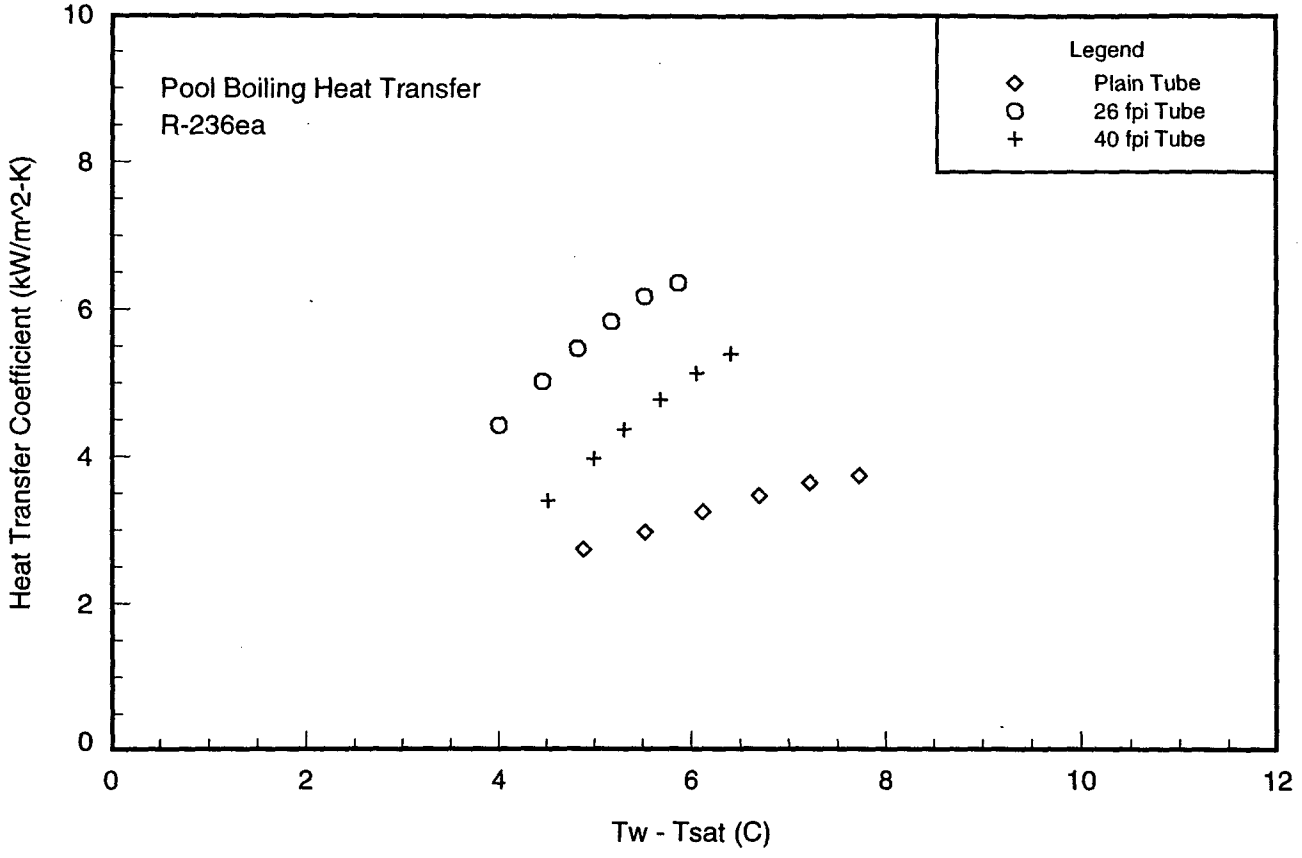

Figure 11.5 Temperature difference effect on heat transfer coefficient for HFC-236ea at $T_{sat} = 2^{o}C$

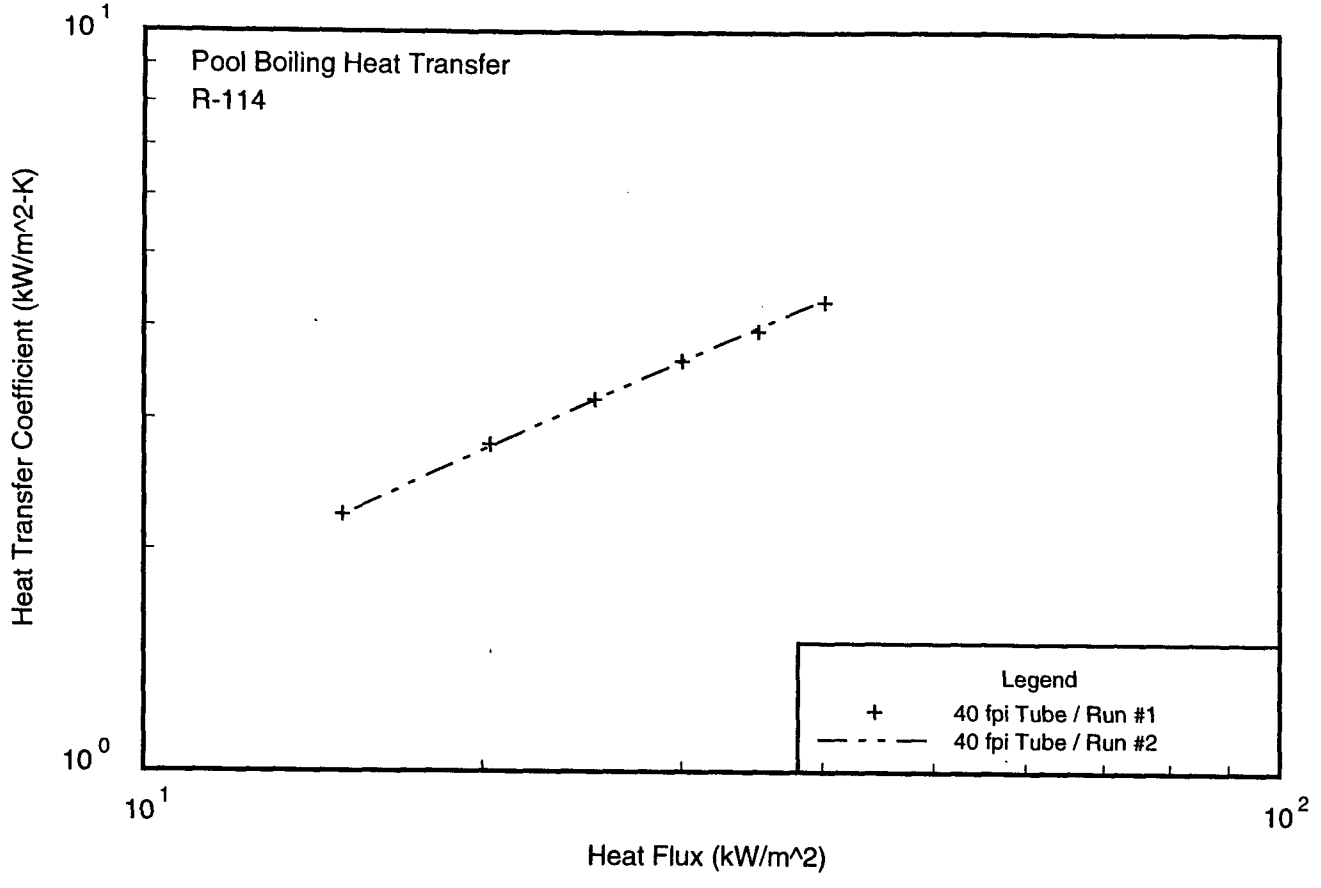

Figure 11.6 Repeatability analysis for CFC-114 at T_{sat} = 2°C

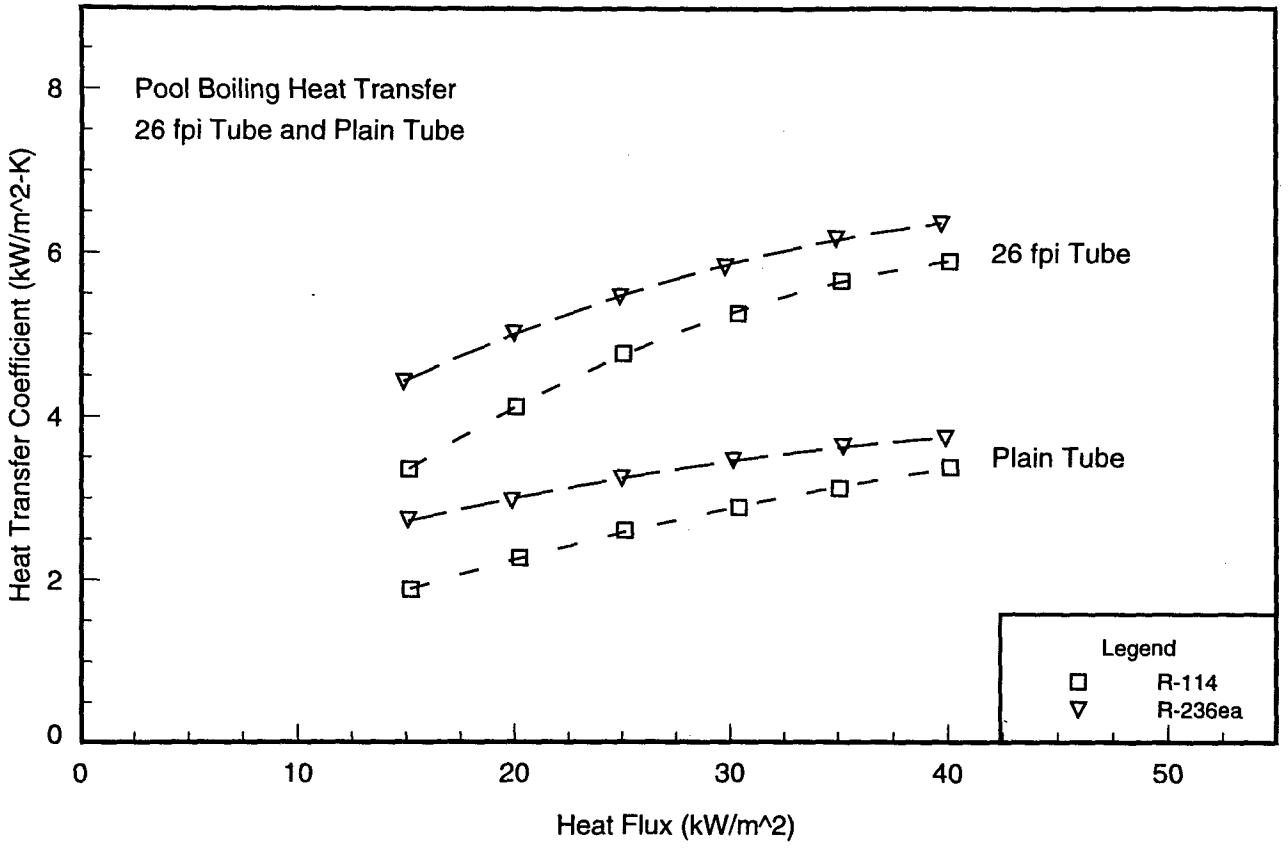

Figure 11.7 Refrigerant comparison for 26 fpi tube and plain tube at $T_{sat} = 2^{o}C$

kW/m^2, the boiling coefficient for HFC-236ea is approximately 39% higher than CFC-114 for both tube surfaces. At 40 kW/m^2, this deviation is decreased to 23%.

Figure 11.8 is also a refrigerant comparison plot, but presents the 40 fpi tube results. This tube shows a similar trend to the tubes presented in Figure 11.7, namely, that HFC-236ea outperforms CFC-114 in the heat flux range tested. The boiling coefficient of HFC-236ea for the 40 fpi tube at the lowest heat flux is 34% higher than that of CFC-114. But, at 40 kW/m^2, the deviation again decreases to 20%. Therefore, all three tubes that were tested showed a higher heat transfer performance with HFC-236ea than with CFC-114 during nucleate boiling of pure refrigerant.

Refrigerant / Lubricant Mixtures

Figure 11.9 shows the results for pool boiling of an CFC-114 / oil mixture with the 26-fpi tube. The 1% and 3% oil concentrations produced a significant enhancement in the shell-side heat transfer coefficient. This is consistent with studies documented in Chapter 3 that show oil concentrations of 3% or less can enhance nucleate boiling heat transfer. On average, the 1% oil concentration improved the heat transfer performance by 27% with respect to the pure refrigerant. In the low heat flux range, the 3% mixture produces similar boiling coefficients to the 1% oil concentration. At 35 kW/m^2, the 3% oil concentration shows only a minor improvement to the 1% concentration data. A foam layer was visible at both oil concentrations. In the higher heat flux range, the foam layer was very close to the top of the tube. It is evident that the foaming phenomenon was a factor in the increased heat transfer performance.

The 40 fpi tube results, shown in Figure 11.10, illustrate similar trends to the 26 fpi tube. The average oil enhancement of the boiling coefficient was 28% for a 1% oil concentration. At the low heat fluxes, there is little difference in the performance between the 1% and 3% concentrations, but at 35 kW/m^2 the heat transfer coefficient at 3% is significantly higher than that of the 1% and pure refrigerant. At this heat flux, it was observed that the top of the tube was immersed in the foam layer, which accounts for the increase. It appears that significant improvement can be obtained in the heat transfer performance of CFC-114 with small concentrations of the 68-centistoke mineral oil. Obviously, the turbulent mixing present in the foam layer enhances the heat transfer performance for this particular refrigerant / lubricant mixture. As shown in Chapter 3, the heat transfer coefficient for each refrigerant / lubricant mixture has a unique reaction to the addition of oil. It is very dependent upon the type of refrigerant and the type of lubricant used. Some mixtures show an improvement in the heat transfer performance over the pure refrigerant results, while other mixtures have a decrease in performance. In general, if the oil does improve the heat transfer performance, the maximum enhancement is usually found at an oil concentration of 3% [48, 50, 54, 55].

Pool boiling results for the refrigerant / lubricant mixture of HFC-236ea and 340-SUS polyol-ester oil are presented in Figures 11.11 and 11.12. Figure 11.11 shows the 26 fpi tube performance with the addition of oil. The 1% and 3% oil concentrations decreased the heat transfer coefficient by 6% and 17%, respectively, from the

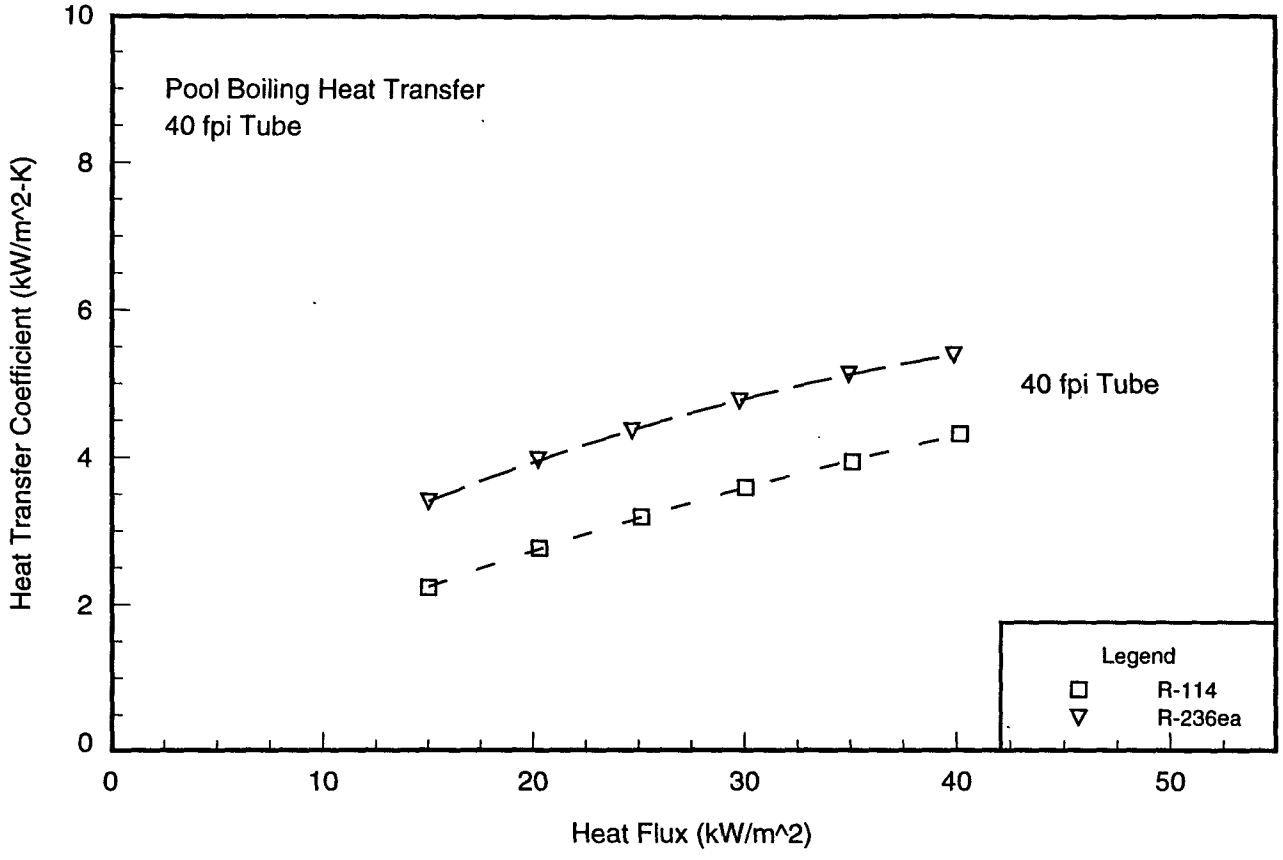

Figure 11.8 Refrigerant comparison for 40 fpi tube at $T_{sat} = 2^{o}C$

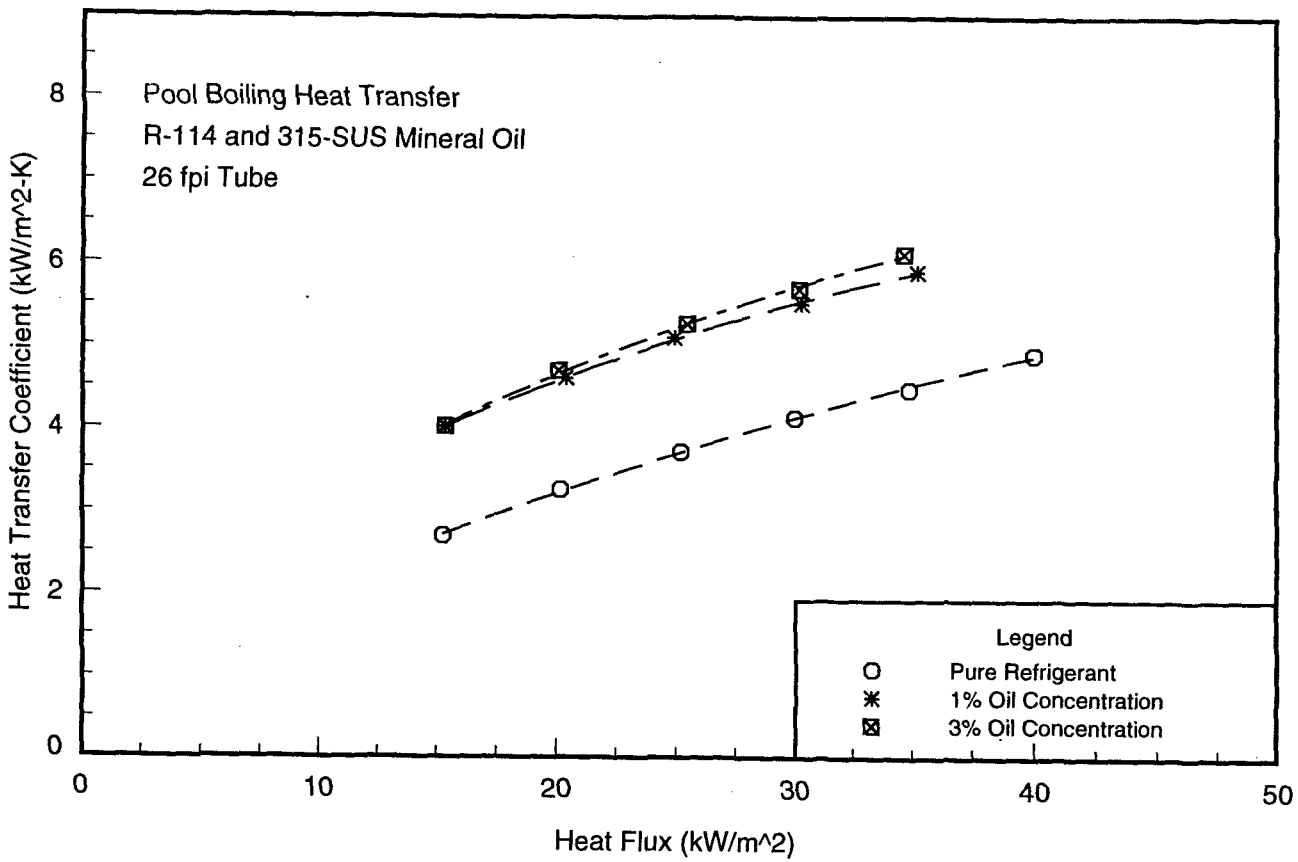

Figure 11.9 Lubricant effects on heat transfer for CFC-114 and 26 fpi tube at T_{sat} = 2°C

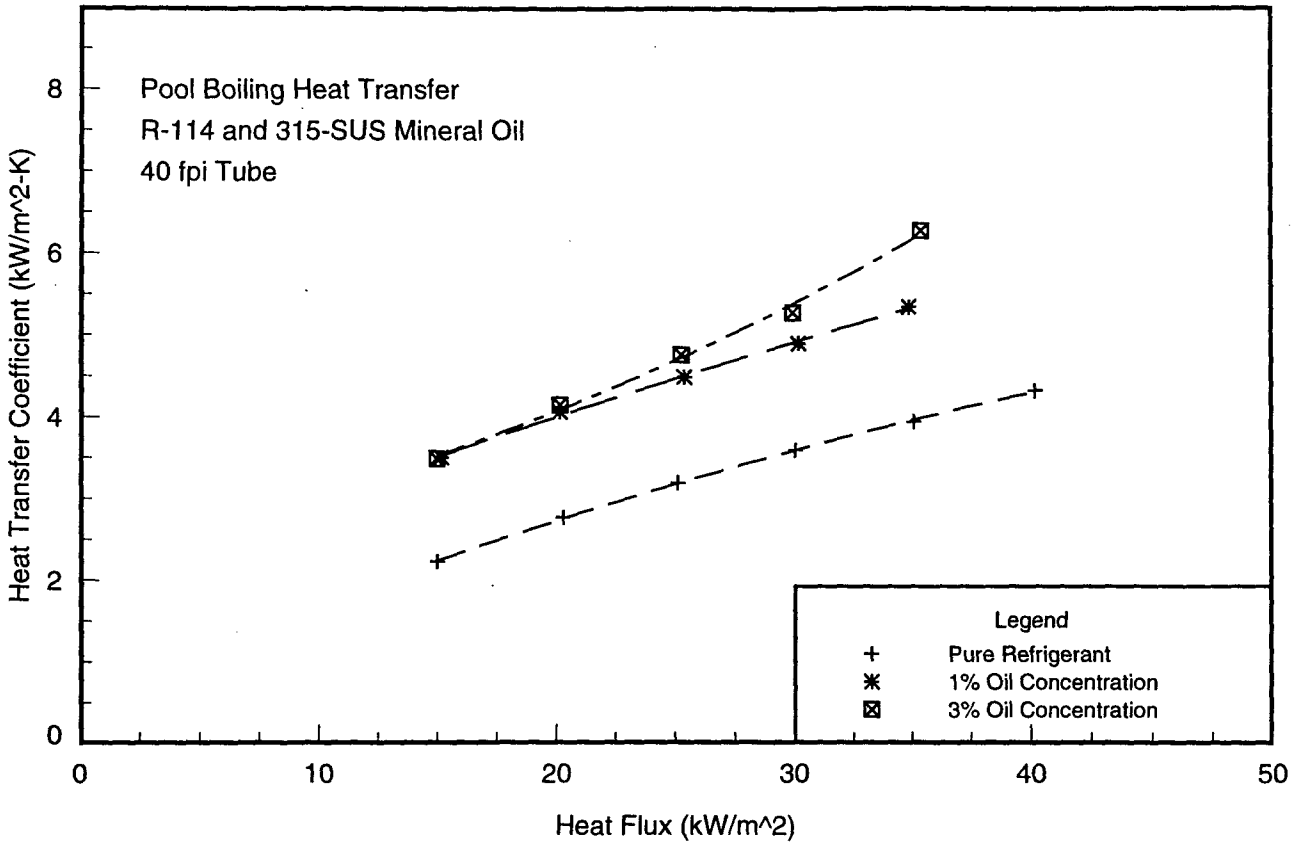

Figure 11.10 Lubricant effects on heat transfer for CFC-114 and 40 fpi tube at $T_{sat} = 2^{o}C$

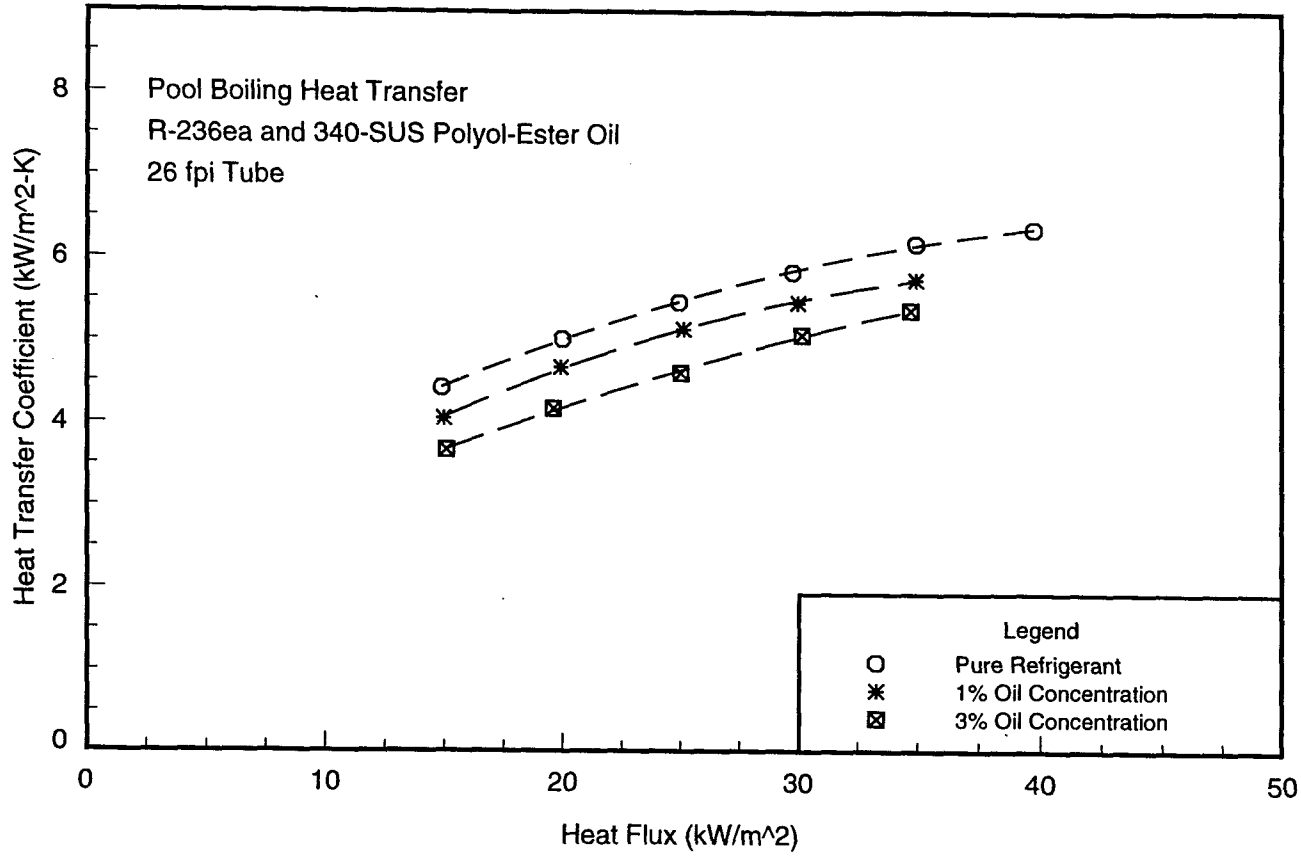

Figure 11.11 Lubricant effects on heat transfer for HFC-236ea and 26 fpi tube at $T_{sat} = 2^{o}C$

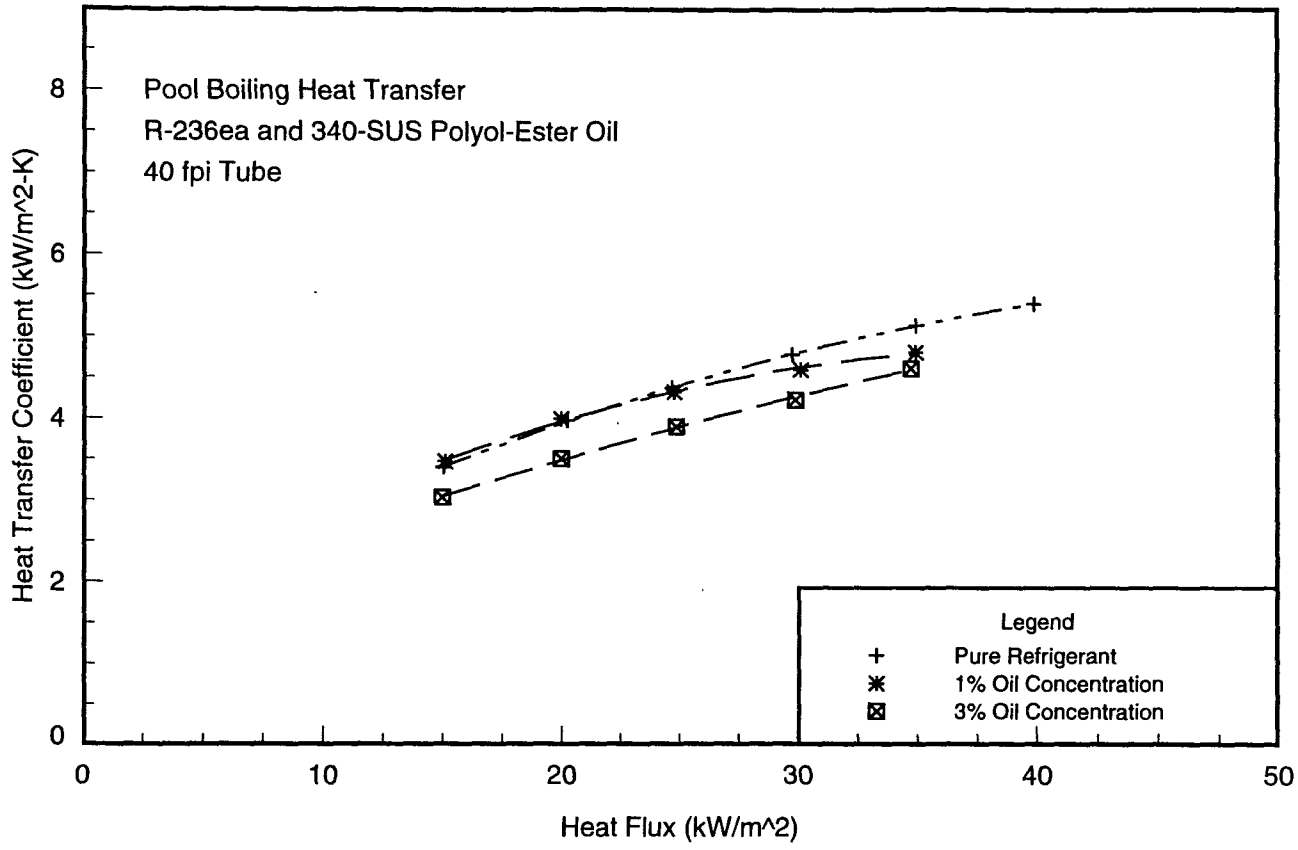

Figure 11.12 Lubricant effects on heat transfer for HFC-236ea and 40 fpi tube at T_{sat} = 2°C

pure refrigerant results. Figure 11.12 contains the 40 fpi tube data for the refrigerant / lubricant mixture. There was little effect in the performance of this tube with a 1% oil concentration at a heat flux of 15 kW/m^2 to 25 kW/m^2. At higher heat fluxes, the performance of the 1% mixture is only slightly degraded. When the concentration was increased to 3%, the boiling coefficients decreased 10% from the pure refrigerant results.

Figures 11.13 and 11.14 show the refrigerant / lubricant mixture results as a performance comparison between the two refrigerants. Figure 11.13 presents the 1% and 3% oil concentrations for the 26 fpi tube with both CFC-114 and HFC-236ea. The 26 fpi tube produced similar results for both refrigerants at an oil concentration of 1%. But, at a 3% oil concentration, the CFC-114 had a higher performance than HFC-236ea throughout the heat flux range tested. The boiling coefficient for CFC-114 at 35 kW/m^2 was 12% higher than that of HFC-236ea.

The results for the 40 fpi tube, which are presented in Figure 11.14, show trends that are similar to the results for the 26 fpi tube. At an oil concentration of 1%, there is no significant difference in the performance between CFC-114 and HFC-236ea at heat fluxes from 15 to 25 kW/m^2. In the higher heat flux range, CFC-114 produced slightly larger boiling coefficients than HFC-236ea. When the oil concentration was increased to 3%, the 40 fpi tube followed the same trend as the 26 fpi tube. Throughout the heat flux range, the boiling coefficients for CFC-114 were consistently above those of HFC-236ea. At heat fluxes of 15 kW/m^2 and 35 kW/m^2, CFC-114 showed an increase in the boiling coefficient over HFC-236ea of 13% and 27%, respectively. Therefore, for both finned tubes, CFC-114 produced significantly higher boiling coefficients than HFC-236ea at a 3% oil concentration.

CORRELATION COMPARISON

The correlations that were investigated for pool boiling are applicable for any refrigerant and saturation temperature. However, these generic correlations can only predict heat transfer coefficients for the plain tube surface. No correlation exists for pool boiling on finned or enhanced surfaces. Therefore, the comparison is only made between the correlations and the plain tube results for CFC-114 and HFC-236ea.

There were three correlations used for comparison. The two refrigerant correlations were the Rohsenow [40] correlation (Equation 3.1) and the Stephan-Abdelsalam [42] correlation (Equation 3.8). These correlations predict a heat transfer coefficient with knowledge of the heat flux, temperature, and fluid properties. The third correlation used was a general fluids correlation developed by Cooper [43] and shown in Equation 3.12. Cooper's equation also requires values for the heat flux and saturation temperature but does not incorporate any thermodynamic or transport properties. The three components are the heat flux, a pressure ratio (P/P_c), and the molecular weight of the fluid.

Figure 11.15 shows the plain tube results for CFC-114 along with the three boiling correlations. The Rohsenow and Stephan-Abdelsalam equations underpredict the plain tube data by a factor of 5, but both equations agree within ±3%. The Cooper correlation shows the best agreement. It underpredicts the data by an average of

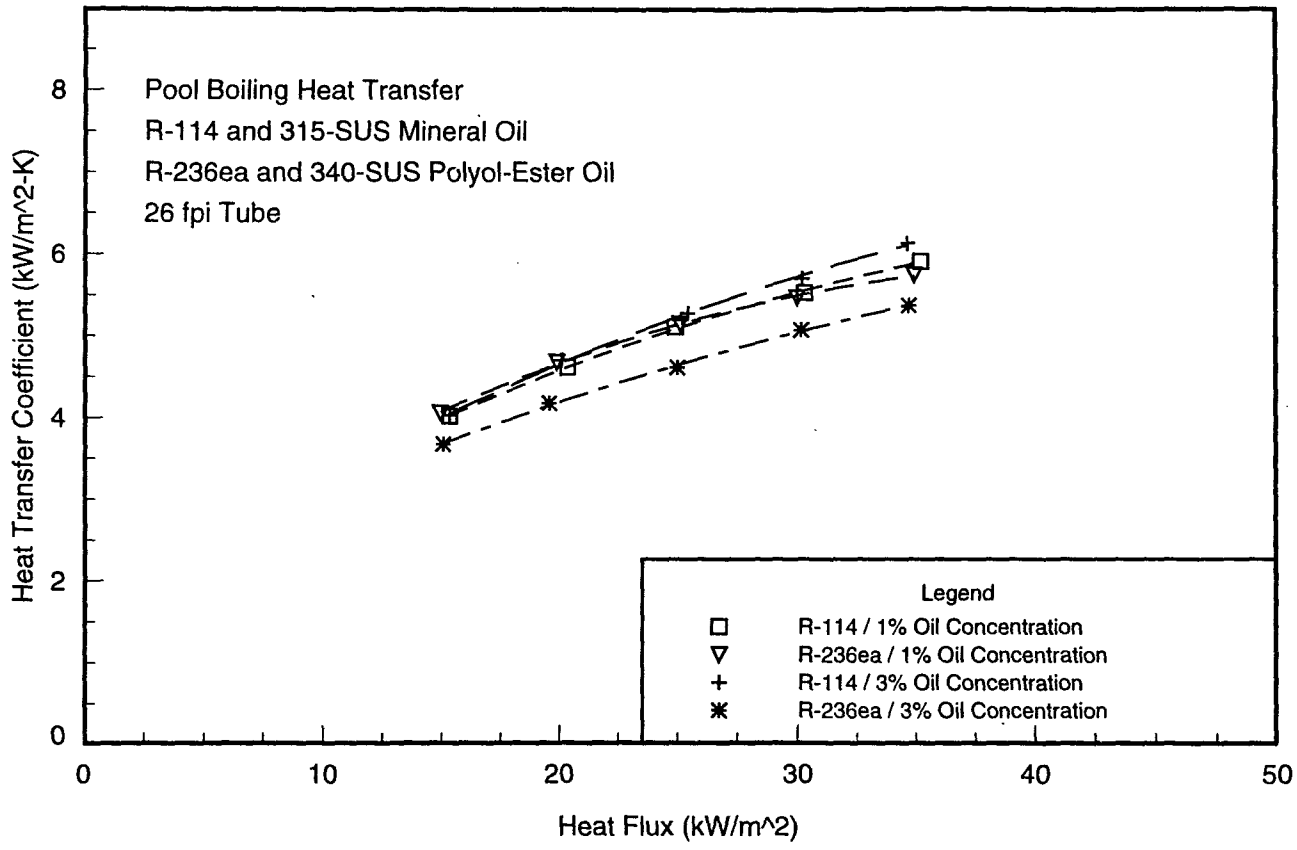

Figure 11.13 Refrigerant comparison of lubricant effects on heat transfer for 26 fpi tube at T_{sat} = 2°C

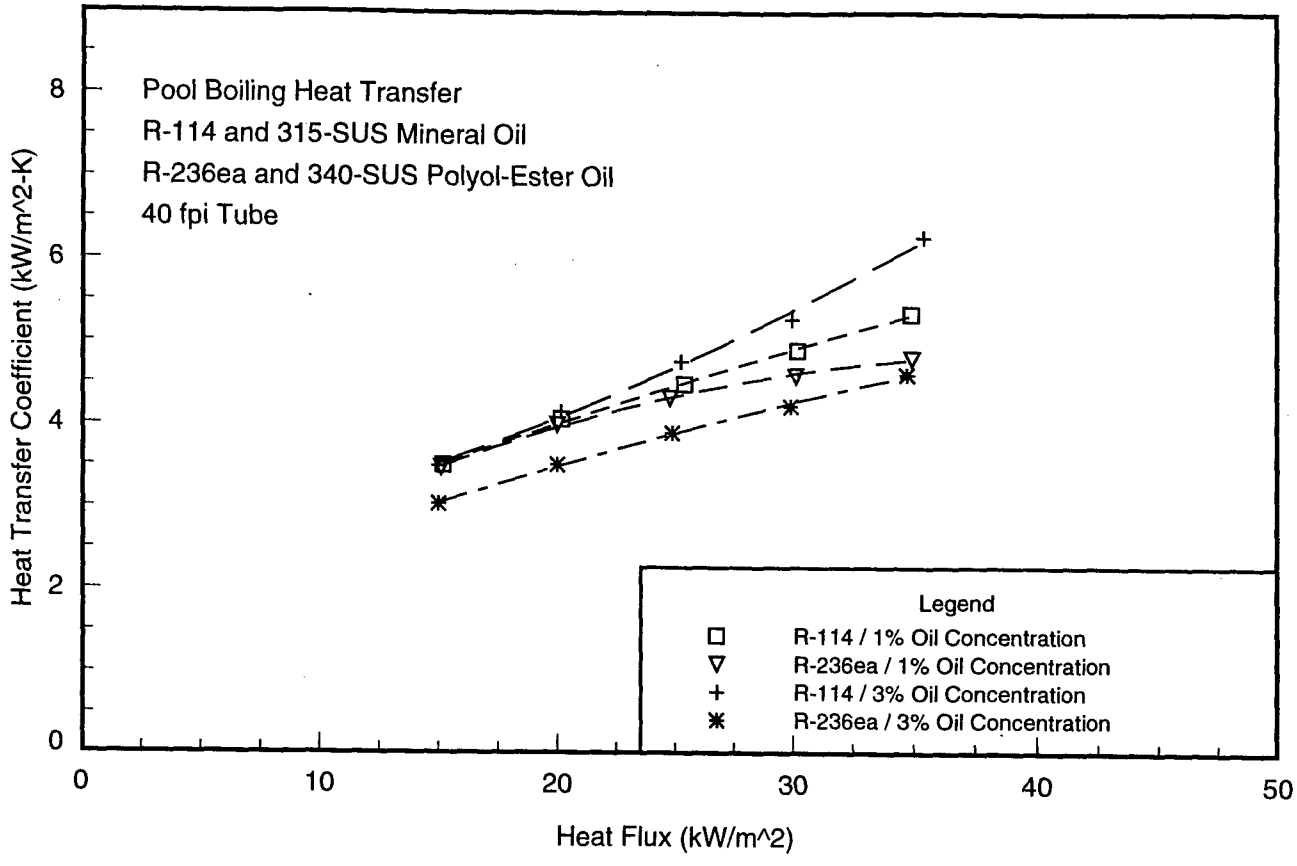

Figure 11.14 Refrigerant comparison of lubricant effects on heat transfer for 40 fpi tube at $T_{sat} = 2^{o}C$

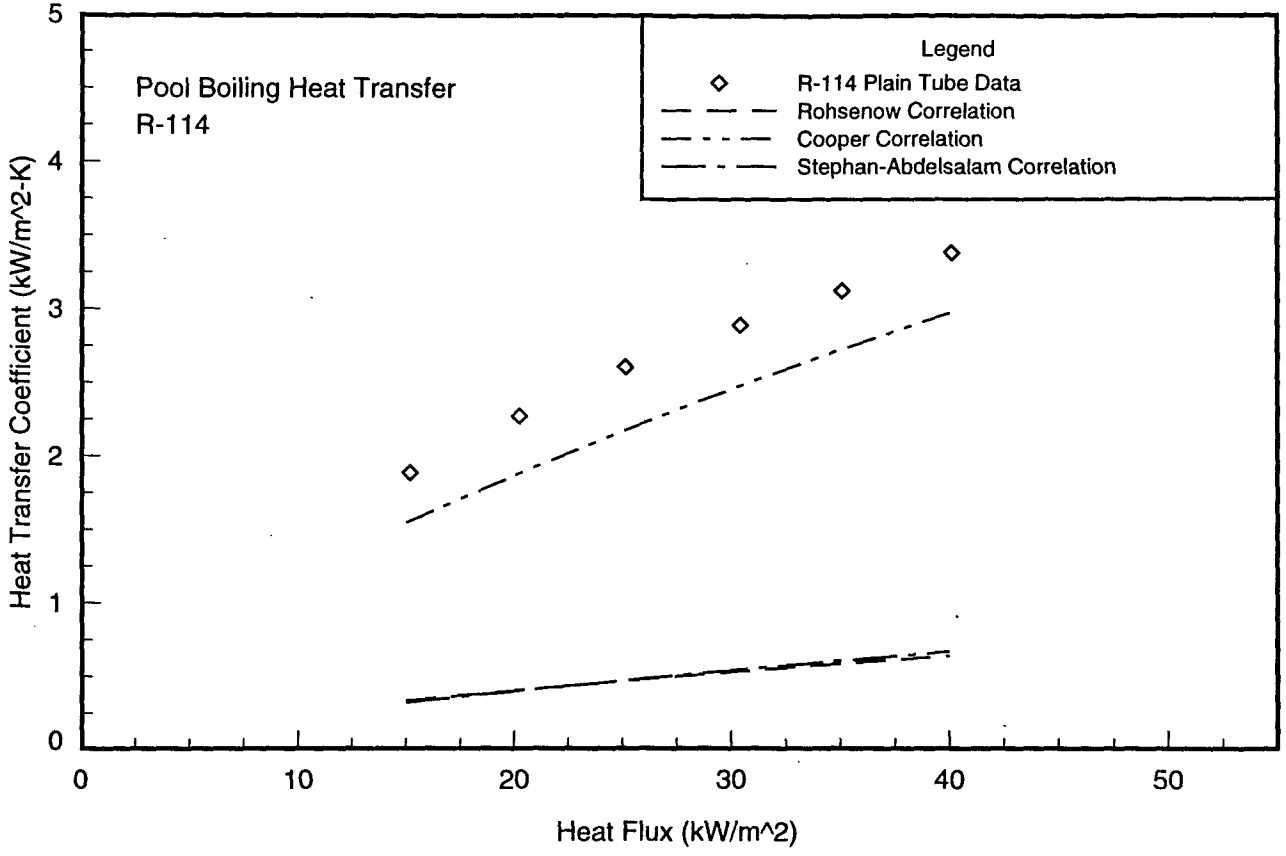

Figure 11.15 Comparison of measured and predicted heat transfer of CFC-114 and plain tube

16%. It is not presently understood why the two refrigerant correlations underpredict the data so greatly, other than the fact that they were designed for use with any refrigerant and a large range of saturation temperatures. It is also noted that the proportionality constant, C_{sf}, used in the Rohsenow equation was for CFC-11.

The correlation comparison for HFC-236ea is shown in Figure 11.16. The three correlations show the same trends as they did with CFC-114. The two refrigerant correlations underpredict the data by factors of 7 and 10, while the Cooper correlation underpredicts the data by an average of 33%.

SUMMARY

Shell-side heat transfer coefficients were presented for pool boiling of pure CFC-114 and HFC-236ea. Data were taken at a saturation temperature of 2°C over a heat flux range of 15 kW/m^2 to 40 kW/m^2. In addition, results were presented for pool boiling of refrigerant / lubricant mixtures at oil concentrations of 1% and 3%. General boiling correlations were also compared with the plain tube results. A summary of the overall conclusions from the pool boiling segment of this research are given below.

1. The pool boiling results for the pure refrigerants show that the tube performance for CFC-114 and HFC-236ea fall in the following order from high to low: 26 fpi, 40 fpi, and plain. The integral-fin tubes produced consistently higher heat transfer coefficients than the plain tube for both refrigerants.
2. HFC-236ea produced higher boiling coefficients than CFC-114 for all three tubes tested. The maximum increase with HFC-236ea was 39% for the 26 fpi tube and 34% for the 40 fpi tube.
3. Boiling of the CFC-114 / oil mixture produced enhancement in the heat transfer coefficients, with the maximum enhancement at an oil concentration of 3% for both of the integral-fin tubes.
4. Pool boiling of HFC-236ea with the polyol-ester oil produced consistent decreases in the heat transfer performance. As the oil concentration was increased from 0% to 3%, the heat transfer coefficients for the 26 fpi tube showed a steady decrease at each heat flux point. At an oil concentration of 1%, the 40 fpi tube showed negligible oil effects in the low heat flux range, but the 3% concentration produced degraded heat transfer performance at all heat fluxes.
5. The 26 fpi tube produced the highest heat transfer coefficients for both refrigerants, but also showed the largest decrease in performance with the addition of oil.
6. Even though the pure HFC-236ea results are higher than those for pure CFC-114, the oil effects on CFC-114 cause the boiling coefficients to be higher than the HFC-236ea results for the 26 fpi tube. In addition, the boiling coefficients for both refrigerants are within 12% for the this tube at an oil concentration of 3%. Therefore, the addition of oil decreased the deviation in the heat transfer coefficients between the two refrigerants.
7. It is evident that the oil enhancement gained from the turbulent mixing within the foaming layer is dependent upon the type of oil. The mineral oil used with CFC-114 showed a general improvement in the

heat transfer performance, while the polyol-ester oil consistently degraded the performance of HFC-236ea.

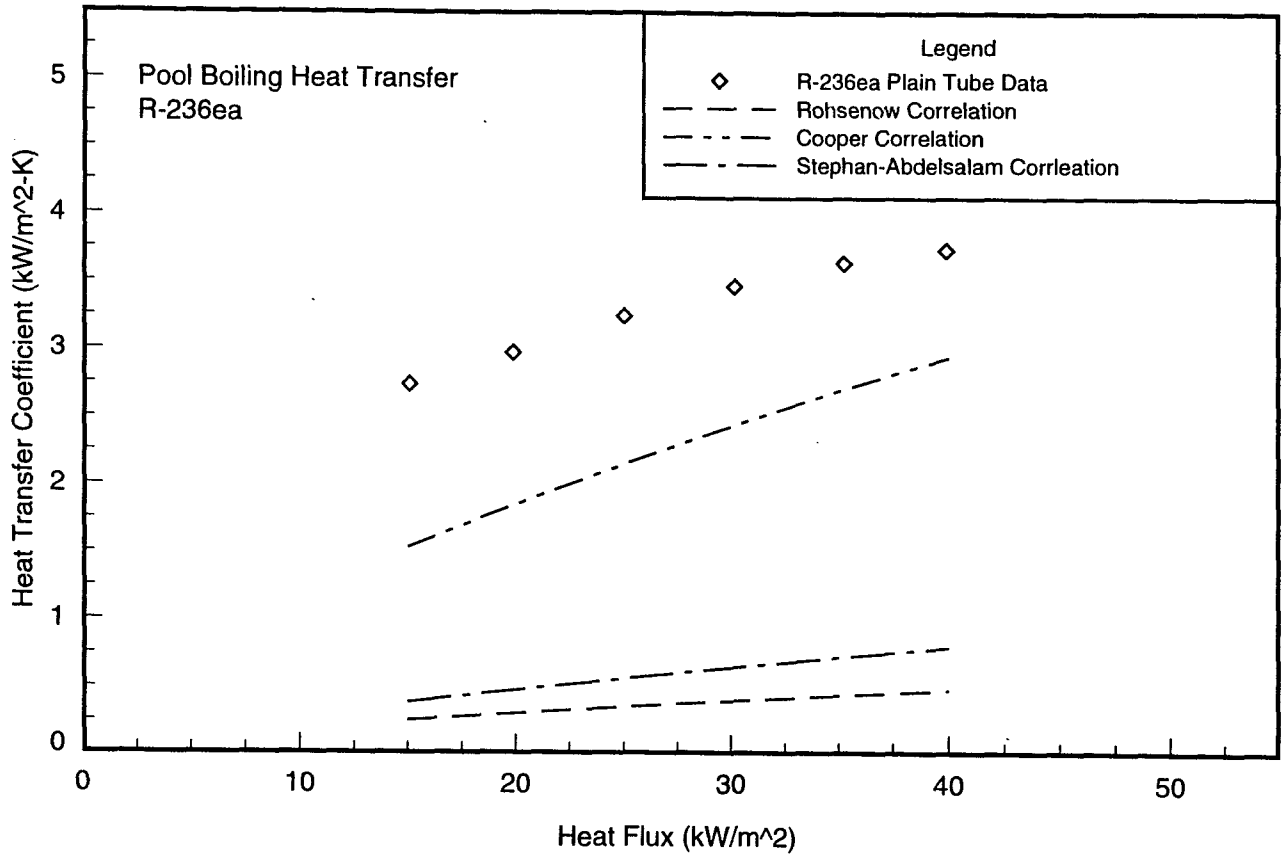

Figure 11.16 Comparison of measured and predicted heat transfer of HFC-236ea and plain tube

BIBLIOGRAPHY

1. Brna, T. Environmental Protection Agency, Personal communication, 1993.

2. Webb, R.L., and C.G. Murawski. "Row effect for CFC-11 condensation on enhanced tubes." *ASME Journal of Heat Transfer*, Vol. 112, pp. 768-776, August 1990.

3. McAdams, W.H. Heat Transmission. 3rd ed. McGraw-Hill Book Co., Inc., New York, 1954.

4. Goto, M., H. Hotta, and S. Tezuka. "Film condensation of refrigerant vapours on a horizontal tube." *Journal of Refrigeration*, Vol. 3, pp. 101-109, 1980.

5. Beatty, K.O., and K.L. Katz. "Condensation of vapors on outside of finned tubes." *Chemical Engineering Progress*, Vol. 44, No. 1, pp. 55-70, January 1948.

6. Karkhu, V.A., and V.P. Borovkov. "Film condensation of vapor at finely-finned horizontal tubes." *Heat Transfer-Soviet Research*, Vol. 3, No. 2, pp. 183-191, 1971.

7. Carnavos, T.C. "An experimental study: condensing CFC-11 on augmented tubes." *ASME Paper No. 80-HT-54*, 1980.

8. Rudy, T.M. "A theoretical and experimental study of condensation on single, integral-fin tubes." Ph.D. Dissertation, Pennsylvania State University, University Park, PA, 1982.

9. Honda, H., S. Nozu, and K. Mitsumori. "Augmentation of condensation on horizontal finned tubes by attaching a porous drainage plate." *Proc. ASME-JSME Thermal Engineering Joint Conference*, T. Mori and W.J. Tang, eds., Vol. 3, pp. 289-296, Honolulu, 1983.

10. Yau, K.K., J.R. Cooper, and J.W. Rose. "Effects of drainage strips and fin spacing on heat transfer and condensate retention for horizontal finned and plain condenser tubes." *Fundamentals of Phase Change: Boiling and Condensation*, C.T. Avedisian and T.M. Rudy (Eds.), ASME, pp. 151-156, 1984.

11. Kabov, O.A. "Film condensation of immobile vapor on a horizontal finned cylinder." *Heat Transfer - Soviet Research*, Vol. 16, No. 6, pp. 76-83, 1984.

12. Sukhatme, S.P., B.S. Jagadish, and P. Prabhakaran. "Film condensation of CFC-11 vapour on single horizontal enhanced condenser tubes." *ASME Journal of Heat Transfer*, Vol. 112, pp. 229-234, 1990.

13. Marto, P.J., D. Zebrowski, A.S. Wanniarachchi, and J.W. Rose. "Film condensation of CFC-113 on horizontal finned tubes." *Fundamentals of Phase Change: Boiling and Condensation*, Proc. 1988 National Heat Transfer Conference., H.R. Jacobs, ed., ASME, Vol. 2, pp. 583-592, 1988.

14. Masuda, H., and J.W. Rose. "An experimental study of condensation of Refrigerant 113 on low integral-fin tubes." *Proceedings of the International Symposium on Heat Transfer*, Vol.2, Paper 32, Beijing, PRC, 1985.

15. Yau, K.K., J.R. Cooper, and J.W. Rose. "Horizontal plain and low-finned condenser tubes-effect of fin spacing and drainage strips on heat transfer and condensate retention." *ASME Journal of Heat Transfer*, Vol. 108, pp. 946-950, 1986.

16. Huber, J.B., L.E. Rewerts, and M.B. Pate. "Shell-side condensation heat transfer of HFC-134a-part 1: finned-tube performance." Paper presented at the ASHRAE Summer Conference, Orlando, Florida, June 1994.

17. Huber, J.B., L.E. Rewerts, and M.B. Pate. "Shell-side condensation heat transfer of HFC-134a-part 2: enhanced-tube performance." Paper presented at the ASHRAE Summer Conference, Orlando, Florida, June 1994.

18. Huber, J.B. "Experimental determination of shell-side condenser bundle heat transfer design factors for refrigerants HCFC-123 and HFC-134a." Ph.D. Dissertation, Iowa State University, 1994.

19. Incropera, F.P., and D.P. De Witt. Fundamentals of Heat and Mass Transfer (Third Edition), New York: Wiley, 1990.

20. Webb, R.L., "Shell-side condensation in refrigerant condensers," *ASHRAE Transactions*, Vol. 90, No. 1, pp. 5-25, 1984.

21. Marto, P.J., "An evaluation of film condensation on horizontal integral-fin tubes." *ASME Journal of Heat Transfer*, Vol. 110, pp. 1287-1305, 1988.

22. Gregorig, R. "Film condensation on finely rippled surfaces with consideration of surface tension." Z. Angew. Math. Phys., Vol. 5, pp. 36-49, 1954.

23. Karkhu, V.A., and V.P. Borovkov. "Film condensation of vapor at finely-finned horizontal tubes." *Heat Transfer-Soviet Research*, Vol. 3, No. 2, pp. 183-191, March-April 1971.

24. Rudy, T.M., and R.L. Webb. "Condensate retention of horizontal integral-finned tubing." *Advances in Enhanced Heat Transfer*, HTD-Vol. 18, pp. 35-41, 20th National Heat Transfer Conference, Milwaukee, Wisconsin, August 1981.

25. Webb, R.L., T.M. Rudy, and M.A. Kedzierski. "Prediction of the condensation coefficient on horizontal integral-fin tubes." *ASME Journal of Heat Transfer*, Vol. 107, pp. 369-376, 1985.

26. Honda, H., and S. Nozu. "A prediction for heat transfer during film condensation on horizontal low integral-fin tubes." *Fundamentals of Phase Change: Boiling and Condensation*, ASME HTD-Vol. 38, pp. 107-114, C.T. Avedisian and T.M. Rudy (eds), 1984.

27. Adamek, T., and R.L. Webb. "Extended prediction theory for film condensation on finned surfaces including heat transfer within the channel." *Int. Journal Heat and Mass Transfer*, Vol. 31, pp. 167-181, 1988.

28. Katz, D.L., R.E. Hope, and S.C. Dasko. "Liquid retention on finned tubes." Department of Engineering Research, University of Michigan, Ann Arbor, MI, Project No. M592, 1946.

29. Masuda, H., and J.W. Rose. "Static configuration of liquid films on horizontal tubes with low radial fins: implications for condensation heat transfer." *Proc. Roy. Soc. London*, A410, pp. 125-139, 1987.

30. Marto, P.J., A.S. Wanniarachchi, O. Cakan, and J.W. Rose "Enhancement of steam condensation on a horizontal finned tube by using drainage strips." *Proc. 2nd U.K. National Heat Transfer Conference*, Glasgow, Scotland, 1988.

31. Rudy, T.M., and R.L. Webb. "Theoretical model for condensation on horizontal, integral-fin tubes." *AIChE Symposium Series*, Heat Transfer, Vol. 79, No. 225, pp. 11-18, 1983.

32. Rudy, T.M., and R.L. Webb. "An analytical model to predict condensation retention on horizontal integral-finned tubes." *ASME Journal of Heat Transfer*, Vol. 107, pp. 361-368, 1985.

33. Webb, R.L. "The evolution of enhanced surface geometries for nucleate boiling." *Heat Transfer Engineering*, Vol. 2, No. 3-4, pp.46-69, 1981.

34. Yilmaz, S., and J.W. Westwater. "Effect of commercial enhanced surfaces on the boiling heat transfer curve." *20th National Heat Transfer Conference*, Milwaukee, AIChE Paper, August 2-5, 1981.

35. Nakayama, W., T. Daikoku, and T. Nakajima. "Effects of pore diameters and system pressure on saturated pool nucleate boiling heat transfer from porous surfaces." *ASME Journal of Heat Transfer*, Vol. 104, pp. 286-291, 1982.

36. Gorenflo, D., and W. Fath. "Heat transfer on the outside of finned tubes at high saturation pressures." *Proceedings of the 17th International Congress on Refrigeration*, Vol. B, pp. 329-335, 1987.

37. Ayub, Z.H., and A.E. Bergles. "Pool boiling from gewa surfaces in water and R-113." *Warme-und Stoffubertragung*, Vol. 21, pp. 209-219, 1987.

38. Webb, R.L., and C. Pais. "Pool boiling data for five refrigerants on three tube geometries." *ASHRAE Transactions*, Vol. 97, pp. 72-78, 1991.

39. Webb, R.L., and C. Pais. "Nucleate pool boiling data for five refrigerants on plain, integral-fin and enhanced tube geometries." *Int. Journal of Heat and Mass Transfer*, Vol. 35, No. 8, pp. 1893-1904, 1992.

40. Rohsenow, W.M. "A method of correlating heat transfer for surface boiling of liquids." *ASME Transactions*, Vol. 74, pp. 969-983, 1952.

41. Mikic, B.B., and W.M. Rohsenow. "A new correlation of pool-boiling data including the effect of heating surface characteristics." *Journal of Heat Transfer*, Transactions of the ASME, pp. 245-250, May 1969.

42. Stephan, K., and M. Abdelsalam. "Heat-transfer correlations for natural convection boiling." *Int. Journal of Heat and Mass Transfer*, Vol. 23, pp. 73-87, 1980.

43. Cooper, M.G. "Saturation nucleate, pool boiling - a simple correlation." *Int. Chem. Engineering Symposium*, Ser. 86, pp. 785-792, 1984.

44. Chen, J.C. "A correlation for boiling heat transfer to saturated fluids in convective flow." ASME Paper 63-HT-34, presented at the 6th National Heat Transfer Conference, Boston, 1963.

45. Webb, R.L., K.D. Choi, and T.R. Apparao. "A theoretical model to predict the heat duty and pressure drop in flooded refrigerant evaporators." *ASHRAE Transactions*, Vol. 95, Part 1, pp. 326-338, 1989.

46. Stephan, K. "Influence of oil on heat transfer of boiling of Freon 12 and Freon 22." *XI International Congress of Refrigeration*, I.I.R. Bulletin No. 3, 1963.

47. Dougherty, R.L., and H.J. Sauer Jr. "Nucleate pool boiling of refrigerant-oil mixtures from tubes." *ASHRAE Transactions*, Vol. 80, pp. 175-186, 1975.

48. Sauer, H.J., R.K. Gibson, and S. Chongrungreong. "Influence of oil on the nucleate boiling performance of refrigerant." Paper presented at the 6th International Heat Transfer Conference, Toronto, Ontario, 1978.

49. Chongrungreong, S., and H.J. Sauer, Jr. "Nucleate boiling performance of refrigerants and refrigerant-oil mixtures." *ASME Journal of Heat Transfer*, Vol. 102, pp. 701-705, 1980.

50. Stephan, K., and J. Mitrovic. "Heat transfer in natural convective boiling of refrigerant-oil mixtures." *7th International Heat Transfer Conference*, Munich, pp. 73-87, 1982.

51. Wanniarachchi, A.S., P.J. Marto, and J.T. Reilly. "The effect of oil contamination on the nucleate pool-boiling performance of CFC-114 from a porous-coated surface." *ASHRAE Transactions,* Vol. 92, pp. 1021-1039, 1986.

52. Webb, R.L., and W.F. McQuade. "Pool boiling of CFC-11 and HCFC-123 oil-refrigerant mixtures on plain and enhanced tube geometries." *ASHRAE Transactions*, Vol. 99, No. 1, pp. 1225-1236, 1993.

53. Jensen, M.K., and D.L. Jackman. "Prediction of nucleate pool boiling heat transfer coefficients of refrigerant-oil mixtures." *ASME Journal of Heat Transfer*, Vol. 106, pp.184-190, 1984.

54. Sauer, H.J., G.W. Davidson, and S. Chongrungreong. "Nucleate boiling of refrigerant-oil mixtures from finned tubing." Paper presented at the Joint ASME/AIChE National Heat Transfer Conference, Orlando, Florida, July, 1980.

55. Arai, N., R. Fukushima, A. Arai, T. Nakajuma, K. Fujie, and Y. Nakayama. "Heat transfer tubes enhancing boiling and condensation in the heat exchanger of a refrigerating machine." *ASHRAE Transactions*, Vol. 83, pp. 58-70, 1977.

56. Glamm, P. Trane Co., Personal communication, 1993.

57. Thors, P. Wolverine Tube Co., Personal communication, 1992.

58. ASHRAE. ANSI/ASHRAE Standard 41.4-1984, Standard method for measurements of proportion of oil in liquid refrigerant. Atlanta: American Society of Heating, Refrigerating and Air-Conditioning Engineers, Inc. 1984.

59. Beckwith, T.G., N.L. Buck, and R.D. Marangoni. Mechanical Measurements, Reading, Massachusetts: Addison-Wesley Publishing Co., 1982.

60. Eckels, S.J. "Heat transfer and pressure drop during condensation and evaporation of HFC-134a/oil mixtures in smooth and micro-fin tubes." Ph.D. Dissertation, Iowa State University, 1993.

61. ASHRAE. 1993 ASHRAE Handbook Fundamentals, SI Edition, Atlanta, GA: ASHRAE Inc., 1993.

62. Gallagher, J., M. Huber, G. Morrison, and M. McLinden, NIST Thermodynamic Properties of Refrigerants and Refrigerant Mixtures Database (REFPROP), Version 4.0, NIST, U.S. Department of Commerce, 1993.

APPENDIX A

TABULATED DATA FOR CONDENSATION

The experimental data obtained in the condensation tests are presented in this appendix. Data that were plotted in Chapter 8 include the shell-side heat transfer coefficient, the heat flux, LMTD, and ΔT. Tables A.1 - A.6 contain data values for condensation of pure CFC-114 and HFC-236ea at a saturation temperature of $40^{o}C$. The condensation results include data for the plain, 26 fpi, and 40 fpi tube surfaces. For brevity, the condensation data of superheated CFC-114 vapor are not tabulated. The condensation results are discussed in Chapter 8.

All of the values presented in Tables A.1 - A.6 have been calculated from equations given in Chapter 6. The shell-side heat transfer coefficients were based on an outside surface area calculated from the outside diameter over the tube enhancement (i.e., the corresponding outside area of a smooth tube).

TABLE A.1: CONDENSATION OF PURE CFC-114 ON A PLAIN TUBE
WITH A SATURATION TEMPERATURE OF 40°C

h_o (W/m^2K)	Heat Flux (W/m^2)	Energy Transfer (Watts)	LMTD (^oC)	ΔT (^oC)	h_i (W/m^2K)	Reynolds Number	U_o (W/m^2K)
1.27E+03	1.54E+04	7.71E+02	1.55E+01	8.02E+00	4791.531	7.41E+03	9.74E+02
1.20E+03	2.03E+04	1.02E+03	2.06E+01	1.06E+01	5725.808	8.78E+03	9.70E+02
1.18E+03	2.54E+04	1.27E+03	2.54E+01	1.30E+01	6449.573	9.65E+03	9.77E+02
1.17E+03	3.04E+04	1.53E+03	3.03E+01	1.54E+01	7000.626	1.01E+04	9.83E+02
1.16E+03	3.52E+04	1.77E+03	3.51E+01	1.78E+01	7469.779	1.03E+04	9.82E+02

TABLE A.2: CONDENSATION OF PURE HFC-236EA ON A PLAIN TUBE
WITH A SATURATION TEMPERATURE OF 40°C

h_o (W/m^2K)	Heat Flux (W/m^2)	Energy Transfer (Watts)	LMTD (^oC)	ΔT (^oC)	h_i (W/m^2K)	Reynolds Number	U_o (W/m^2K)
1.82E+03	1.49E+04	7.48E+02	1.14E+01	6.07E+00	4.98E+03	8.10E+03	1.28E+03
1.62E+03	2.04E+04	1.03E+03	1.62E+01	8.46E+00	6.01E+03	9.77E+03	1.24E+03
1.54E+03	2.49E+04	1.25E+03	1.99E+01	1.03E+01	6.92E+03	1.12E+04	1.23E+03
1.49E+03	3.01E+04	1.51E+03	2.43E+01	1.25E+01	7.54E+03	1.19E+04	1.21E+03
1.45E+03	3.52E+04	1.76E+03	2.87E+01	1.47E+01	8.08E+03	1.23E+04	1.20E+03
1.43E+03	4.03E+04	2.02E+03	3.30E+01	1.68E+01	8.52E+03	1.25E+04	1.20E+03

TABLE A.3: CONDENSATION OF PURE CFC-114 ON A 26 FPI TUBE
WITH A SATURATION TEMPERATURE OF 40°C

h_o (W/m^2K)	Heat Flux (W/m^2)	Energy Transfer (Watts)	LMTD (^oC)	ΔT (^oC)	h_i (W/m^2K)	Reynolds Number	U_o (W/m^2K)
5.41E+03	1.53E+04	7.68E+02	6.26E+00	3.44E+00	6.01E+03	1.10E+04	2.45E+03
5.79E+03	2.04E+04	1.02E+03	7.16E+00	3.89E+00	7.58E+03	1.45E+04	2.85E+03
6.11E+03	2.52E+04	1.26E+03	7.95E+00	4.27E+00	8.90E+03	1.77E+04	3.17E+03
6.22E+03	3.02E+04	1.51E+03	8.89E+00	4.74E+00	1.02E+04	2.07E+04	3.40E+03
6.24E+03	3.50E+04	1.76E+03	9.77E+00	5.17E+00	1.14E+04	2.38E+04	3.58E+03
6.28E+03	4.02E+04	2.02E+03	1.07E+01	5.65E+00	1.26E+04	2.67E+04	3.74E+03

TABLE A.4: CONDENSATION OF PURE HFC-236EA ON A 26 FPI TUBE WITH A SATURATION TEMPERATURE OF 40°C

h_o (W/m^2K)	Heat Flux (W/m^2)	Energy Transfer (Watts)	LMTD (^oC)	ΔT (^oC)	h_i (W/m^2K)	Reynolds Number	U_o (W/m^2K)
5.88E+03	1.50E+04	7.52E+02	5.93E+00	3.39E+00	5.98E+03	1.09E+04	2.53E+03
6.23E+03	2.02E+04	1.01E+03	6.86E+00	3.85E+00	7.56E+03	1.45E+04	2.95E+03
6.65E+03	2.50E+04	1.25E+03	7.53E+00	4.18E+00	8.99E+03	1.80E+04	3.32E+03
6.90E+03	2.99E+04	1.50E+03	8.31E+00	4.56E+00	1.02E+04	2.10E+04	3.60E+03
7.06E+03	3.50E+04	1.76E+03	9.10E+00	4.95E+00	1.15E+04	2.41E+04	3.85E+03
7.16E+03	4.01E+04	2.01E+03	9.88E+00	5.34E+00	1.28E+04	2.74E+04	4.06E+03

TABLE A.5: CONDENSATION OF PURE CFC-114 ON A 40 FPI TUBE WITH A SATURATION TEMPERATURE OF 40°C

h_o (W/m^2K)	Heat Flux (W/m^2)	Energy Transfer (Watts)	LMTD (^oC)	ΔT (^oC)	h_i (W/m^2K)	Reynolds Number	U_o (W/m^2K)
5.41E+03	1.49E+04	7.47E+02	6.06E+00	3.36E+00	5.62E+03	1.01E+04	2.48E+03
6.28E+03	2.02E+04	1.01E+03	6.80E+00	3.71E+00	7.05E+03	1.33E+04	3.00E+03
6.54E+03	2.50E+04	1.26E+03	7.59E+00	4.10E+00	8.35E+03	1.64E+04	3.33E+03
6.64E+03	3.02E+04	1.52E+03	8.52E+00	4.56E+00	9.58E+03	1.92E+04	3.58E+03
6.78E+03	3.49E+04	1.75E+03	9.24E+00	4.91E+00	1.07E+04	2.21E+04	3.81E+03
6.90E+03	3.98E+04	2.00E+03	1.00E+01	5.29E+00	1.19E+04	2.48E+04	4.01E+03

TABLE A.6: CONDENSATION OF PURE HFC-236EA ON A 40 FPI TUBE WITH A SATURATION TEMPERATURE OF 40°C

h_o (W/m^2K)	Heat Flux (W/m^2)	Energy Transfer (Watts)	LMTD (^oC)	ΔT (^oC)	h_i (W/m^2K)	Reynolds Number	U_o (W/m^2K)
5.34E+03	1.49E+04	7.49E+02	6.13E+00	3.50E+00	5.58E+03	1.00E+04	2.46E+03
5.97E+03	2.02E+04	1.01E+03	6.95E+00	3.91E+00	7.08E+03	1.34E+04	2.93E+03
6.56E+03	2.52E+04	1.26E+03	7.60E+00	4.22E+00	8.39E+03	1.65E+04	3.34E+03
6.92E+03	3.02E+04	1.52E+03	8.33E+00	4.59E+00	9.60E+03	1.94E+04	3.66E+03
7.27E+03	3.51E+04	1.76E+03	8.97E+00	4.90E+00	1.07E+04	2.21E+04	3.95E+03
7.54E+03	4.01E+04	2.01E+03	9.60E+00	5.21E+00	1.19E+04	2.49E+04	4.22E+03

APPENDIX B

TABULATED DATA FOR POOL BOILING

The experimental data obtained in the pool boiling tests are presented in this appendix. Data that were plotted in Chapter 9 include the shell-side heat transfer coefficient, the heat flux, LMTD, and ΔT. The pool boiling results of pure CFC-114 and HFC-236ea for the plain, 26 fpi, and 40 fpi tubes are presented in Tables B.1 - B.6. Results from pool boiling of refrigerant / lubricant mixtures with the 26 fpi and 40 fpi tubes are shown in Tables B.7 - B.14. Pool boiling tests of pure refrigerant as well as refrigerant / lubricant mixtures were conducted at a saturation temperature of $2^{o}C$. The pool boiling results are discussed in Chapter 9.

All of the values presented in Tables B.1 - B.14 have been calculated from equations given in Chapter 6. The shell-side heat transfer coefficients for pool boiling were based on an outside surface area calculated from the outside diameter over the tube enhancement (i.e., the corresponding outside area of a smooth tube).

TABLE B.1: POOL BOILING OF PURE CFC-114 ON A PLAIN TUBE
WITH A SATURATION TEMPERATURE OF 2°C

h_o (W/m^2K)	Heat Flux (W/m^2)	Energy Transfer (Watts)	LMTD (^oC)	ΔT (^oC)	h_i (W/m^2K)	Reynolds Number	U_o (W/m^2K)
3.38E+03	4.01E+04	2.01E+03	1.66E+01	8.12E+00	9.16E+03	1.70E+04	2.37E+03
3.12E+03	3.51E+04	1.76E+03	1.58E+01	7.75E+00	8.16E+03	1.46E+04	2.17E+03
2.89E+03	3.04E+04	1.52E+03	1.50E+01	7.38E+00	7.19E+03	1.24E+04	1.98E+03
2.60E+03	2.51E+04	1.26E+03	1.40E+01	6.86E+00	6.17E+03	1.01E+04	1.76E+03
2.27E+03	2.02E+04	1.02E+03	1.32E+01	6.46E+00	5.06E+03	7.80E+03	1.50E+03
1.88E+03	1.52E+04	7.62E+02	1.20E+01	5.93E+00	4.07E+03	5.87E+03	1.23E+03

TABLE B.2: POOL BOILING OF PURE HFC-236EA ON A PLAIN TUBE
WITH A SATURATION TEMPERATURE OF 2°C

h_o (W/m^2K)	Heat Flux (W/m^2)	Energy Transfer (Watts)	LMTD (^oC)	ΔT (^oC)	h_i (W/m^2K)	Reynolds Number	U_o (W/m^2K)
3.73E+03	3.99E+04	2.00E+03	1.54E+01	7.72E+00	9.06E+03	1.66E+04	2.53E+03
3.64E+03	3.52E+04	1.77E+03	1.44E+01	7.21E+00	8.04E+03	1.41E+04	2.40E+03
3.46E+03	3.01E+04	1.51E+03	1.34E+01	6.69E+00	6.99E+03	1.17E+04	2.21E+03
3.24E+03	2.50E+04	1.25E+03	1.22E+01	6.12E+00	5.99E+03	9.52E+03	2.01E+03
2.97E+03	1.99E+04	9.97E+02	1.10E+01	5.52E+00	4.97E+03	7.45E+03	1.77E+03
2.73E+03	1.51E+04	7.56E+02	9.73E+00	4.88E+00	3.86E+03	5.34E+03	1.52E+03

TABLE B.3: POOL BOILING OF PURE CFC-114 ON A 26 FPI TUBE
WITH A SATURATION TEMPERATURE OF 2°C

h_o (W/m^2K)	Heat Flux (W/m^2)	Energy Transfer (Watts)	LMTD (^oC)	ΔT (^oC)	h_i (W/m^2K)	Reynolds Number	U_o (W/m^2K)
4.90E+03	4.00E+04	2.00E+03	1.35E+01	6.74E+00	1.02E+04	1.93E+04	2.97E+03
4.48E+03	3.48E+04	1.75E+03	1.30E+01	6.51E+00	9.06E+03	1.65E+04	2.68E+03
4.13E+03	3.00E+04	1.50E+03	1.24E+01	6.18E+00	7.91E+03	1.38E+04	2.42E+03
3.72E+03	2.52E+04	1.26E+03	1.18E+01	5.87E+00	6.80E+03	1.14E+04	2.14E+03
3.26E+03	2.02E+04	1.01E+03	1.09E+01	5.47E+00	5.71E+03	9.06E+03	1.84E+03
2.70E+03	1.53E+04	7.65E+02	1.02E+01	5.15E+00	4.47E+03	6.61E+03	1.49E+03

TABLE B.4: POOL BOILING OF PURE HFC-236EA ON A 26 FPI TUBE
WITH A SATURATION TEMPERATURE OF 2°C

h_o (W/m^2K)	Heat Flux (W/m^2)	Energy Transfer (Watts)	LMTD (^oC)	ΔT (^oC)	h_i (W/m^2K)	Reynolds Number	U_o (W/m^2K)
6.35E+03	3.97E+04	1.99E+03	1.17E+01	5.86E+00	9.90E+03	1.82E+04	3.40E+03
6.18E+03	3.49E+04	1.75E+03	1.10E+01	5.51E+00	8.85E+03	1.57E+04	3.18E+03
5.83E+03	2.98E+04	1.49E+03	1.03E+01	5.17E+00	7.73E+03	1.31E+04	2.89E+03
5.47E+03	2.49E+04	1.25E+03	9.60E+00	4.82E+00	6.66E+03	1.08E+04	2.59E+03
5.02E+03	2.00E+04	1.00E+03	8.87E+00	4.45E+00	5.49E+03	8.43E+03	2.25E+03
4.42E+03	1.49E+04	7.45E+02	7.96E+00	4.00E+00	4.34E+03	6.21E+03	1.87E+03

TABLE B.5: POOL BOILING OF PURE CFC-114 ON A 40 FPI TUBE
WITH A SATURATION TEMPERATURE OF 2°C

h_o (W/m^2K)	Heat Flux (W/m^2)	Energy Transfer (Watts)	LMTD (^oC)	ΔT (^oC)	h_i (W/m^2K)	Reynolds Number	U_o (W/m^2K)
4.31E+03	4.02E+04	2.01E+03	1.46E+01	7.38E+00	9.58E+03	1.80E+04	2.77E+03
3.94E+03	3.51E+04	1.76E+03	1.41E+01	7.12E+00	8.58E+03	1.56E+04	2.52E+03
3.59E+03	3.00E+04	1.51E+03	1.34E+01	6.78E+00	7.55E+03	1.32E+04	2.27E+03
3.19E+03	2.51E+04	1.26E+03	1.27E+01	6.46E+00	6.50E+03	1.09E+04	1.99E+03
2.77E+03	2.03E+04	1.02E+03	1.21E+01	6.16E+00	5.35E+03	8.45E+03	1.69E+03
2.23E+03	1.50E+04	7.53E+02	1.12E+01	5.74E+00	4.23E+03	6.24E+03	1.36E+03

TABLE B.6: POOL BOILING OF PURE HFC-236EA ON A 40 FPI TUBE
WITH A SATURATION TEMPERATURE OF 2°C

h_o (W/m^2K)	Heat Flux (W/m^2)	Energy Transfer (Watts)	LMTD (^oC)	ΔT (^oC)	h_i (W/m^2K)	Reynolds Number	U_o (W/m^2K)
5.39E+03	3.99E+04	2.00E+03	1.28E+01	6.40E+00	9.36E+03	1.71E+04	3.15E+03
5.13E+03	3.49E+04	1.75E+03	1.21E+01	6.05E+00	8.35E+03	1.48E+04	2.92E+03
4.77E+03	2.97E+04	1.49E+03	1.13E+01	5.67E+00	7.35E+03	1.25E+04	2.65E+03
4.37E+03	2.47E+04	1.24E+03	1.06E+01	5.30E+00	6.27E+03	1.01E+04	2.36E+03
3.97E+03	2.02E+04	1.01E+03	9.94E+00	4.99E+00	5.21E+03	7.98E+03	2.05E+03
3.40E+03	1.50E+04	7.53E+02	8.98E+00	4.51E+00	4.09E+03	5.84E+03	1.69E+03

TABLE B.7: POOL BOILING OF CFC-114 ON A 26 FPI TUBE WITH A SATURATION TEMPERATURE OF 2°C AND AN OIL CONCENTRATION OF 1%

h_o (W/m^2K)	Heat Flux (W/m^2)	Energy Transfer (Watts)	LMTD (^oC)	ΔT (^oC)	h_i (W/m^2K)	Reynolds Number	U_o (W/m^2K)
5.91E+03	3.52E+04	1.77E+03	1.14E+01	5.69E+00	8.82E+03	1.57E+04	3.10E+03
5.52E+03	3.03E+04	1.52E+03	1.08E+01	5.40E+00	7.75E+03	1.33E+04	2.81E+03
5.10E+03	2.49E+04	1.25E+03	9.93E+00	4.98E+00	6.65E+03	1.08E+04	2.51E+03
4.61E+03	2.04E+04	1.02E+03	9.36E+00	4.70E+00	5.55E+03	8.59E+03	2.18E+03
4.02E+03	1.54E+04	7.70E+02	8.55E+00	4.29E+00	4.37E+03	6.31E+03	1.80E+03

TABLE B.8: POOL BOILING OF HFC-236EA ON A 26 FPI TUBE WITH A SATURATION TEMPERATURE OF 2°C AND AN OIL CONCENTRATION OF 1%

h_o (W/m^2K)	Heat Flux (W/m^2)	Energy Transfer (Watts)	LMTD (^oC)	ΔT (^oC)	h_i (W/m^2K)	Reynolds Number	U_o (W/m^2K)
5.74E+03	3.49E+04	1.75E+03	1.14E+01	5.72E+00	8.87E+03	1.58E+04	3.06E+03
5.46E+03	3.00E+04	1.50E+03	1.07E+01	5.37E+00	7.76E+03	1.33E+04	2.80E+03
5.14E+03	2.51E+04	1.26E+03	9.94E+00	4.99E+00	6.70E+03	1.09E+04	2.52E+03
4.67E+03	1.99E+04	9.98E+02	9.11E+00	4.57E+00	5.53E+03	8.52E+03	2.19E+03
4.05E+03	1.50E+04	7.51E+02	8.32E+00	4.18E+00	4.35E+03	6.25E+03	1.80E+03

TABLE B.9: POOL BOILING OF CFC-114 ON A 40 FPI TUBE WITH A SATURATION TEMPERATURE OF 2°C AND AN OIL CONCENTRATION OF 1%

h_o (W/m^2K)	Heat Flux (W/m^2)	Energy Transfer (Watts)	LMTD (^oC)	ΔT (^oC)	h_i (W/m^2K)	Reynolds Number	U_o (W/m^2K)
5.34E+03	3.49E+04	1.75E+03	1.18E+01	5.81E+00	8.34E+03	1.47E+04	2.99E+03
4.89E+03	3.02E+04	1.51E+03	1.14E+01	5.66E+00	7.30E+03	1.24E+04	2.68E+03
4.48E+03	2.54E+04	1.27E+03	1.07E+01	5.33E+00	6.30E+03	1.02E+04	2.39E+03
4.06E+03	2.01E+04	1.01E+03	9.76E+00	4.87E+00	5.24E+03	8.02E+03	2.08E+03
3.50E+03	1.52E+04	7.61E+02	8.97E+00	4.48E+00	4.07E+03	5.79E+03	1.71E+03

TABLE B.10: POOL BOILING OF HFC-236EA ON A 40 FPI TUBE WITH A SATURATION TEMPERATURE OF 2°C AND AN OIL CONCENTRATION OF 1%

h_o (W/m^2K)	Heat Flux (W/m^2)	Energy Transfer (Watts)	LMTD (^oC)	ΔT (^oC)	h_i (W/m^2K)	Reynolds Number	U_o (W/m^2K)
4.80E+03	3.49E+04	1.75E+03	1.25E+01	6.26E+00	8.42E+03	1.50E+04	2.82E+03
4.59E+03	3.01E+04	1.51E+03	1.17E+01	5.87E+00	7.34E+03	1.25E+04	2.59E+03
4.32E+03	2.48E+04	1.24E+03	1.06E+01	5.34E+00	6.30E+03	1.02E+04	2.35E+03
3.99E+03	2.00E+04	1.00E+03	9.80E+00	4.92E+00	5.20E+03	7.94E+03	2.06E+03
3.47E+03	1.51E+04	7.57E+02	8.94E+00	4.49E+00	4.10E+03	5.84E+03	1.71E+03

TABLE B.11: POOL BOILING OF CFC-114 ON A 26 FPI TUBE WITH A SATURATION TEMPERATURE OF 2°C AND AN OIL CONCENTRATION OF 3%

h_o (W/m^2K)	Heat Flux (W/m^2)	Energy Transfer (Watts)	LMTD (^oC)	ΔT (^oC)	h_i (W/m^2K)	Reynolds Number	U_o (W/m^2K)
6.13E+03	3.46E+04	1.74E+03	1.10E+01	5.50E+00	8.81E+03	1.56E+04	3.15E+03
5.70E+03	3.02E+04	1.51E+03	1.06E+01	5.30E+00	7.74E+03	1.32E+04	2.86E+03
5.27E+03	2.54E+04	1.28E+03	9.97E+00	5.00E+00	6.67E+03	1.09E+04	2.55E+03
4.70E+03	2.01E+04	1.01E+03	9.18E+00	4.61E+00	5.52E+03	8.53E+03	2.19E+03
4.02E+03	1.54E+04	7.70E+02	8.55E+00	4.30E+00	4.36E+03	6.30E+03	1.80E+03

TABLE B.12: POOL BOILING OF HFC-236EA ON A 26 FPI TUBE WITH A SATURATION TEMPERATURE OF 2°C AND AN OIL CONCENTRATION OF 3%

h_o (W/m^2K)	Heat Flux (W/m^2)	Energy Transfer (Watts)	LMTD (^oC)	ΔT (^oC)	h_i (W/m^2K)	Reynolds Number	U_o (W/m^2K)
5.37E+03	3.47E+04	1.74E+03	1.17E+01	5.88E+00	8.92E+03	1.60E+04	2.96E+03
5.07E+03	3.01E+04	1.51E+03	1.11E+01	5.59E+00	7.84E+03	1.35E+04	2.70E+03
4.61E+03	2.50E+04	1.25E+03	1.05E+01	5.24E+00	6.70E+03	1.10E+04	2.39E+03
4.17E+03	1.96E+04	9.82E+02	9.43E+00	4.73E+00	5.56E+03	8.63E+03	2.08E+03
3.67E+03	1.51E+04	7.56E+02	8.72E+00	4.38E+00	4.39E+03	6.37E+03	1.73E+03

TABLE B.13: POOL BOILING OF CFC-114 ON A 40 FPI TUBE WITH A SATURATION TEMPERATURE OF 2°C AND AN OIL CONCENTRATION OF 3%

h_o (W/m^2K)	Heat Flux (W/m^2)	Energy Transfer (Watts)	LMTD (^oC)	ΔT (^oC)	h_i (W/m^2K)	Reynolds Number	U_o (W/m^2K)
6.27E+03	3.54E+04	1.77E+03	1.11E+01	5.54E+00	8.21E+03	1.43E+04	3.23E+03
5.27E+03	2.99E+04	1.50E+03	1.08E+01	5.43E+00	7.28E+03	1.22E+04	2.79E+03
4.76E+03	2.52E+04	1.27E+03	1.04E+01	5.19E+00	6.24E+03	1.01E+04	2.46E+03
4.14E+03	2.01E+04	1.01E+03	9.68E+00	4.86E+00	5.21E+03	7.97E+03	2.10E+03
3.49E+03	1.50E+04	7.52E+02	8.81E+00	4.42E+00	4.13E+03	5.90E+03	1.72E+03

TABLE B.14: POOL BOILING OF HFC-236EA ON A 40 FPI TUBE WITH A SATURATION TEMPERATURE OF 2°C AND AN OIL CONCENTRATION OF 3%

h_o (W/m^2K)	Heat Flux (W/m^2)	Energy Transfer (Watts)	LMTD (^oC)	ΔT (^oC)	h_i (W/m^2K)	Reynolds Number	U_o (W/m^2K)
4.60E+03	3.47E+04	1.74E+03	1.27E+01	6.38E+00	8.41E+03	1.50E+04	2.75E+03
4.22E+03	2.99E+04	1.50E+03	1.21E+01	6.09E+00	7.41E+03	1.27E+04	2.48E+03
3.89E+03	2.49E+04	1.25E+03	1.13E+01	5.66E+00	6.34E+03	1.04E+04	2.22E+03
3.50E+03	2.00E+04	1.00E+03	1.05E+01	5.24E+00	5.25E+03	8.10E+03	1.93E+03
3.03E+03	1.50E+04	7.52E+02	9.47E+00	4.75E+00	4.13E+03	5.94E+03	1.60E+03

APPENDIX C

TUBE SPECIFICATIONS

The tables shown below summarize the exact geometry of each tube that was tested. All tubes had a nominal outer diameter of 19.1 mm and length of 838.2 mm. Units are presented in both the SI and English formats.

TABLE C.1: TUBE SPECIFICATIONS IN SI UNITS

tube	fin count (fins/m)	D_o nominal (mm)	D_i nominal (mm)	D_r (mm)	fin height (mm)	A_o nominal (m^2/m)	A_o actual (m^2/m)	A_i nominal (m^2/m)
plain	-	19.4	17.3	19.4	-	0.0512	0.0512	0.0456
26 fpi	1024	18.8	14.3	15.9	1.45	0.0588	0.195	0.0448
40 fpi	1575	18.8	15.6	17.1	0.86	0.0593	0.197	0.0488

TABLE C.2: TUBE SPECIFICATIONS IN ENGLISH UNITS

tube	fin count (fins/in.)	D_o nominal (in.)	D_i nominal (in.)	D_r (in.)	fin height (in.)	A_o nominal ($in.^2/in.$)	A_o actual ($in.^2/in.$)	A_i nominal ($in.^2/in.$)
plain	-	0.764	0.681	0.764	-	0.168	0.168	0.150
26 fpi	26	0.739	0.563	0.625	0.057	0.193	0.640	0.147
40 fpi	40	0.743	0.613	0.675	0.034	0.195	0.645	0.160

APPENDIX D

REFRIGERANT PROPERTIES

The following tables contain information for the thermodynamic and transport properties of CFC-114 [61]and HFC-236ea [62]. The property information is for saturated liquid and saturated vapor. Values are presented only in the testing range for pool boiling and condensation, which are $2^{o}C$ and $40^{o}C$, respectively.

TABLE D.1: PROPERTY DATA FOR CFC-114

Temperature (°C)	Pressure (kPa)	Enthalpy (kJ/kg)	Specific Heat (kJ/kg K)	Viscosity (mPa s)	Thermal Conductivity (W/m K)	
0.0	87.78	333.10	0.680	10.48	-	V
0.0	87.78	200.00	0.931	491.0	0.0704	L
2.0	94.96	334.28	0.683	10.57	-	V
2.0	94.96	201.91	0.933	478.1	0.0700	L
4.0	102.59	335.46	0.685	10.66	-	V
4.0	102.59	203.82	0.935	465.5	0.0695	L
38.0	320.26	355.39	0.731	12.00	-	V
38.0	320.26	237.24	0.979	299.2	0.0616	L
40.0	339.41	356.55	0.735	12.08	-	V
40.0	339.41	239.26	0.983	291.8	0.0611	L
42.0	359.41	357.70	0.739	12.16	-	V
42.0	359.41	241.28	0.987	284.6	0.0606	L

TABLE D.2: PROPERTY DATA FOR HFC-236EA

Temperature (°C)	Pressure (kPa)	Enthalpy (kJ/kg)	Specific Heat (kJ/kg K)	Viscosity (mPa s)	Thermal Conductivity (W/m K)	
0.0	78.30	366.2	0.809	10.18	-	V
0.0	78.30	200.0	1.160	584.2	0.0809	L
2.0	85.24	367.6	0.814	10.26	-	V
2.0	85.24	202.4	1.164	565.9	0.0804	L
4.0	92.65	369.0	0.820	10.35	-	V
4.0	92.65	204.7	1.168	548.3	0.0784	L
38.0	316.1	392.6	0.930	11.83	-	V
38.0	316.1	246.2	1.250	334.3	0.0672	L
40.0	336.5	393.9	0.938	11.92	-	V
40.0	336.5	248.8	1.256	325.3	0.0666	L
42.0	357.9	395.3	0.945	12.02	-	V
42.0	357.9	251.3	1.262	316.5	0.0659	L

TECHNICAL REPORT DATA
(Please read Instructions on the reverse before completing)

1. REPORT NO.	2.	3. RECIPIENT'S ACCESSION NO.
EPA-600/R-96-070		

4. TITLE AND SUBTITLE	5. REPORT DATE
Heat Transfer Evaluation of HFC-236ea and CFC-114 in Condensation and Evaporation	June 1996
	6. PERFORMING ORGANIZATION CODE

7. AUTHOR(S)	8. PERFORMING ORGANIZATION REPORT NO.
W. W. Huebsch and M. B. Pate	

9. PERFORMING ORGANIZATION NAME AND ADDRESS	10. PROGRAM ELEMENT NO.
Iowa State University 2088 H. M. Black Engineering Building Ames, Iowa 50011-2160	11. CONTRACT/GRANT NO. CR820755-01-4

12. SPONSORING AGENCY NAME AND ADDRESS	13. TYPE OF REPORT AND PERIOD COVERED
EPA, Office of Research and Development **Air Pollution Prevention and Control Division** **Research Triangle Park, NC 27711**	Final; 10/92-3/95
	14. SPONSORING AGENCY CODE **EPA/600/13**

15. SUPPLEMENTARY NOTES APPCD project officer is Theodore G. Brna, Mail Drop 63, 919/541-2683.

16. ABSTRACT The report gives results of a heat transfer evaluation of the refrigerants hexafluoropropane (HFC-236ea) and 1,1,2,2-dichloro-tetrafluoroethane (CFC-114). (NOTE: With the mandatory phase-out of chlorofluorocarbons (CFCs), as dictated by the Montreal Protocol and the Clean Air Act Amendments, it is imperative for the Navy to find a replacement for CFC-114 that is environmentally safe and possesses similar performance characteristics. Currently, one of the leading candidates to replace CFC-114 is HFC-236ea.) This research focuses on comparing the refrigerants not only in condensation and pool boiling, but also with various tube surfaces. The test facility used in this study was initially used for spray evaporation testing; however, it was redesigned and modified for use with condensation, pool boiling, or spray evaporation testing. During condensation, the rig was capable of producing saturated or superheated vapor. During pool boiling or spray evaporation, the test facility was capable of testing pure refrigerants or refrigerant/lubricant mixtures. The test facility is described in detail in the full report. The two refrigerants produced similar performance characteristics in condensing vapor on integral-fin tubes, so that the transition to HFC-236ea should be accomplished without major modifications to existing condensers.

17. KEY WORDS AND DOCUMENT ANALYSIS

a. DESCRIPTORS	b. IDENTIFIERS/OPEN ENDED TERMS	c. COSATI Field/Group
Pollution	Pollution Control	13B
Refrigerants	Stationary Sources	13A
Halohydrocarbons	Chlorofluorocarbons	07C
Condensing	Hydrofluorocarbons	07D
Spraying	Pool Boiling	13H, 07A
Evaporation	Tube Surfaces	

18. DISTRIBUTION STATEMENT	19. SECURITY CLASS *(This Report)*	21. NO. OF PAGES
Release to Public	**Unclassified**	140
	20. SECURITY CLASS *(This page)* **Unclassified**	22. PRICE

EPA Form 2220-1 (9-73)